Analysis of admissible steady-state fracture processes in discrete lattice structures

Nikolai Gorbushin

A thesis presented for the degree of
Doctor of Philosophy

Aberystwyth University
2017

Declaration

This work has not previously been accepted in substance for any degree and is not being concurrently submitted in candidature for any degree.

Signed ..... (candidate)

Date .....

Statement 1

This thesis is the result of my own investigations, except where otherwise stated. Other sources are acknowledged by footnotes giving explicit references. A bibliography is appended.

Signed ..... (candidate)

Date .....

Statement 2

I hereby give consent for my thesis, if accepted, to be available for photocopying and for inter-library loan, and for the title and summary to be made available to outside organisations.

Signed ..... (candidate)

Date .....

Acknowledgments

First of all I would like to thank my supervisor Prof. Gennady Mishuris for his invaluable help and support. It has been a great pleasure to obtain the scientific experience through his guidance, fruitful discussions with him and inheritance of his research experience. I was extremely lucky to be supervised by him.

I acknowledge support from the EU project CERMAT-2 (PITN-GA-2013-606878) that gave me a chance to carry out my research and attend numerous workshops, scientific schools and conferences. Moreover, I express my gratitude to the staff of Department of Mathematics at Aberystwyth University for creating a friendly environment which allowed me to enjoy the research process.

I appreciate the support and friendship of Gennaro Vitucci, Daria Andreeva and Francesca Zaccagnino. Without them the overall experience of this period, with no doubts, would not be as admirable as it was.

My special thanks go to Mariia Romanova who could always cheer me up at hard times, was very understanding and inspired for the personal development. These years were accompanied with challenges that would be impossible to overcome without her.

I am also very thankful to my mother and brother for their belief in me and being supportive. I can not imagine even to have an opportunity of doing a PhD without their help.

Abstract

The purpose of this work is to study physically possible crack propagation at constant velocity inside a discrete solid by means of theoretical analysis supported by numerical simulations.

Analytical solutions are delivered for fracture problems in one-dimensional chains, a double chain and square lattices. Evaluation of obtained solutions required implementation of numerical algorithms for computation of integral transforms. Consideration of one-dimensional cases, namely a simple chain of oscillators and a chain of masses with non-local interactions, allowed to examine the validity of derived formulae by a complementary computer simulation of a corresponding dynamic system. Starting from simple models, the analysis of physically admissible and forbidden fracture regimes has been performed. The analytical predictions of possible steady states found a good agreement with a purely numerical scheme.

The work discusses the advantages of different approaches to study steady-state failure processes: either with energetic or load characteristics. These attributes of fracture mechanics are shown to be efficient for quantifying global predictions, e.g. a choice a particular loading condition for achieving a certain value of a crack speed. However, it was demonstrated that derivation of these characteristics is not enough and consideration of the displacement or stress fields should be performed.

The results on chains with non-local interactions between the oscillators illustrated the features of failure at micro-level. Namely, different combi-

nations of microscopic parameters, that result in the same bulk quantities, reflect different patterns of crack propagation in discrete solids.

A problem of a separation a double chain compounded by two chains with different properties shows the peculiarities of parameters mismatch. Particularly, it was established that, contrary to quasi-static problems, a steady-state separation is necessarily caused by forces, applied to each chain, of different values. Furthermore, distinct material parameters of chains give a chance for the observation of the supersonic fracture of the structure.

Increasing the problem dimension from chains to lattices, several new features emerged. For instance, the behaviour of displacements along a crack path changes. Moreover, the admissibility analysis is expanded to the consideration of possible fracture behind a crack tip. The outcomes predict crack propagation regimes with high energy release rates be accompanied by snapping of the springs on the faces of the original moving crack. The evaluation of displacement field in the direction orthogonal to a crack path is also presented. The contrast in material properties in anisotropic lattices and mismatch of material properties in dissimilar lattices unveiled different scenarios of admissible regimes.

Furthermore, the question of the choice of a particular fracture criterion is addressed. Two history-dependent criteria are compared to the classical one of threshold elongation for linear bonds. The results show that steady-state regimes can be reached in the low subsonic crack speed range which can not be according to the classical criterion. Repercussions in terms of load and crack opening versus velocity are explained in details. Once known the steady-state regimes of fracture propagation, a procedure for applying history-dependent criteria emerges as not restricted to the two examined ones and opens the way to different and more complex problems.

Contents

Chapter 1

Introduction

1.1 Literature review

The study of the integrity of solids under mechanical load has a long-standing history. The extensive analysis of the analytical results, developed by means of various mathematical techniques, made it possible to observe the stress concentrations in solids and detect the most dangerous spots where breakage may happen. The breakthrough work done by Griffiths [34] gave a new turn in the study of solids and the field of fracture mechanics started to be established. It was shown that a crack does not start to grow unless a critical load is applied which is determined by a proposed fracture criterion. This criterion was formulated by means of energy and term *energy release rate* was introduced. Later, the criterion was reformulated in terms of stress fields by Irwin [41] and the concept *stress intensity factor* became widely used. This approach simplified the application of fracture mechanics to engineering problems [11]. Another contribution worth of mentioning was made by Rice [72] and Cherepanov [16] where a *path independent integral* was presented. This integral supports the introduction of an alternative fracture criterion which is equivalent to those already mentioned. The last technique found great applications in computational fracture mechanics.

The technological improvements and the complexity of natural fracture phenomena generated the development of analytical modelling. Consequently, the considerations of inertial effects were added to fracture processes and revealed new discoveries in this field. One of the most mathematically challenging problems appeared to be crack propagation problems in solids. The earliest research in this area was done by Yoffe [102]. She considered a straight crack propagation with a constant speed and determined associated stress fields. The major result showed that at high speeds the generated stresses may provide crack branching and, thus, cause crack instabilities. This observation has been noticed by a research community and various scenarios of straight crack propagation with a constant speed were proposed to study the specifics of this process [4, 9, 25]. The analysis has moved on to the consideration of cracks with a non-uniform speed [26, 46]. All these results and the other classical problems are published in manuscripts [10, 27]. Among all the other works related to the same topic, there are also theoretical results on the deviation of crack paths within their unsteady growth [20, 71, 99]. Therefore, much attention was focused on the understanding of crack instabilities that are spotted in experiments.

The experimental results on the fracture of solids clearly demonstrate the wave formations when a crack moves [18, 74]. The emanated waves from a crack tip form the so-called Mach cone, which is characterised with a well-pronounced front inclined at some angle to a crack path. This was explained analytically within the framework of fracture mechanics of continuous solids [74]. In other tests the fracture surface was studied and the correlations of its quality and crack speeds were pointed out [7, 40, 79]. It was possible to distinguish three major types of fracture surfaces: mirror, mist and hackle. Most of the mentioned experimental research referred to a brittle fracture of solids. The collection of experimental results, theoretical background and description of measuring techniques are well described in [23, 69, 89]. Evidence was also found of cracks that are faster than Rayleigh

speed of material [73]. The researchers in this field underlined the need for the development of an apparatus for treating the micro-level effects that are responsible for crack instabilities. This is a sphere where discrete models of solids are effective for further understanding of fracture phenomenon.

Among the application of discrete models in fracture the works on crack propagation in graphene layers can be mentioned [94, 100]. The detachment of long protein chains can be analysed by means of discrete models and optimisation can be performed [37, 52]. Moreover, the development of computational techniques allowed to perform simulations of solids to study microlevel aspects of fracture [1, 76] where a solid is presented by its atomic structure.

Theoretical works on crack propagation in structured media have revealed various phenomena that are not observable when considering the cracks in an elastic continuum. A one-dimensional model of a lattice fracture demonstrated that the force required to cause fracture of the lattice exceeds the force that is able to break a single element of a lattice [90]. Such phenomenon is called *lattice trapping*. This peculiarity indicates that such trapping can cause the establishment of non-linear effects at a crack tip before the fracture is observed. Lattice trapping is detected in molecular dynamic simulations of solids at microlevel [6, 44, 87], experiments on silicon lattices [21, 36], and is also important for production of adhesive surfaces [30, 96].

The study of cracks in lattices without consideration of the inertia terms [39, 90] has progressed in the analysis of steady-state fault propagation in mass-spring structures. The pioneering works of Slepyan [47, 86] presented the solution of dynamic fracture problems with lattice structures. The introduction of crack movement, eventually, was challenging in obtaining the final solution, in comparison with static problems, and required the application of such sophisticated mathematical techniques as the Wiener-Hopf method [28, 45, 61]. The main outcomes of the works showed that the crack propagation in a discrete structure is accompanied by a ration of

elastic waves from a crack tip. The fully comprehensive study is reflected in book [85].

The proposed solution methods by Slepyan appeared to be extremely efficient in examining various fracture problems and capable of explaining various related phenomena [43, 51, 85]. In particular, apart from explaining trapping in various lattice structures [19, 85], it was also instrumental in recognizing the role of the wave dissipation mechanism in fracture mechanics [49, 81, 85], in the description of a crack propagation in discrete and structural waveguides [12, 15, 53] and the analysis of the phase transitions and bistable structures [17, 91, 92, 93]. The method is equally valuable for structures of distinct geometries, fracture modes, for both open cracks and bridge cracks [56], homogeneous and inhomogeneous structures [55, 57, 60]. Although most of the works so far have been concerned with the structures constructed as masses linked by elastic springs, structures where the links are elastic beams have been recently analysed [59, 77]. The work [78] presents collection of various applications of the technique with a wide explanation of computations involved.

The approach suggested by Slepyan, supplemented by extensive numerical simulations and experimental analysis, has allowed explanation of dynamic fracture phenomena in continuous materials such as crack propagation instability and fast crack branching [24, 29, 51]. Some "forbidden regimes" have also been identified, explaining the instability of crack propagation for low crack speed, while the admissible regimes corresponding to possible steady-state crack propagation have been discussed for various (both rectangular and triangular) lattices [5, 32, 51, 64] with moderate and fast speeds. Moreover, for the fast propagating crack, a branching phenomenon appears as a result of possible breakage of the links lying not on the crack line ahead. Other phenomena recently discovered and explained include clustering and forerunning regimes, as observed in differing lattice structures [3, 32, 59]. Recently, the lattice structure approach has been used to model the complex

phenomenon of hydraulic fracture [50].

Several researchers addressed a question whether the steady-state regime of crack propagation can be observed at all. The answer to that question is positive and it is supported by numerous experimental results [23, 42, 70, 80]. The molecular dynamic simulations also detect the possibility of steady-states [1, 13, 14, 38]. Furthermore, numerical simulations on cellular and lattice structures [48, 51, 57, 59] as well as elastic media [63, 101] show that the steady-state regimes can be indeed reached. However, the validity of the solution found using the analytical models always should be always verified via both numerical simulations and experimentation as said solution is always obtained under the assumption of the existence of the steady-state regime. A real solution of the problem may be different to that predicted steady-state case, for example, the regular cluster propagation regime discovered numerically [57] and proved later analytically [84] is a simple but illuminating alternative.

1.2 Motivation

In spite of the fact that the aforementioned models describe a variety of fracture events, there are unfortunately open questions that remain unaddressed. Thus, most of the research to date considers steady-state crack propagation in discrete media appearing as the result of the actions of very limited types of external loading: displacements on the boundaries, constant energy fluxes and feeding waves from infinity. Varying the choices for the loading parameters can lead to different outcomes. Even for a static problem in a lattice structure loaded by both external and internal forces, a kind of material softening behaviour has been predicted [58]. It is clear that for dynamic problems, which are essentially non-linear, there are complex behaviours, and that each load configuration should be considered separately.

First of all, a crack propagation in a simple chain structure is studied.

The fracture results from an applied force moving with a constant speed and amplitude. We analyse the impact of the loading parameters (force magnitude and velocity of the force location) on the fracture process (character of the crack propagation, whether it approaches the steady-state regime predicted by theory, etc.). It is shown that transient regimes may approach the same steady-state quite differently depending on the combination of loading parameters. We compare the advantages of describing the results by dependences of energy release rate and force on crack speed.

Another concern of the work is to study the sensitivity of various combinations of microlevel parameters that lead to the same macroscopic properties, such as Young's modulus or speed of sound. The adjustment of a simple chain model was done by introduction of non-local interactions between the oscillators. Such discrete media can be related to some non-linear elastic theories [22, 68, 75, 88]. Also, the introduction of non-local interactions for treating phase transitions revealed some differences in comparison with conventional models [91, 92, 93]. The focus in this work is on the influence of such modification on fracture characteristics of structures. The works on this field are presented in [31, 32] and will be reproduced herein.

The extension of a simple chain model is then performed by consideration of a double chain of oscillators. Two simple chains of oscillators with different properties are linked together with linear springs. This model allows to study the consequences of parameters mismatch in bi-materials in the framework of fracture mechanics. Moreover, such formulation allows to perform a complementary numerical simulation for comparison of obtained predictions.

Previously considered models, supported by numerical simulation, provide the guarantee for the developed procedures and techniques. Also, although mentioned one-dimensional models benefit to the understanding the basic phenomena of a crack propagation in discrete media, there is a certain interest in lattice models. The achievements on lattice structures are

shown in [83, 23]. However, in this work we are interested in the analysis of physically admissible steady-state regimes and also distribution of displacement fields,- two aspects that are usually missing in the theoretical analysis. This investigation is performed for in anisotropic and bi-material square-cell lattices.

The final remark touches the choice of a fracture condition for prediction of failure of a solid. Griffith's criterion is formulated in terms of energetic considerations and can be adapted for a maximum elongation in mass-spring models. In this case it appears to be rate-independent. Alternatively, one can choose non-instantaneous fracture criteria which do not influence elastic properties but incorporate additional failure parameters. The examples of such criteria include the incubation time [66] and the Tuler-Butcher criteria [95]. The former permits the prediction of the stress level at the fracture moment for the all variety of loading pulses with different intensities and shapes [97]. Moreover, the incubation time approach has shown reliable in different branches of mechanics and physics, such as dynamic fracture of rocks and concretes, dynamic yielding of metals, acoustic ultrasonic cavitation of liquids, etc. [35, 65]. The Tuler-Butcher criterion possible to characterise fracture caused by damage accumulation [95]. The criterion has found fruitful application in analysing spallation, impact loading, thermal shock caused fracture in rocks, glass, aluminum, copper [8, 33, 98]. Thus, this work reports a study on prediction of steady-state regimes when non-conventional criteria are set.

1.3 Structure of the thesis

Chapter 2 presents the results of fracture processes in one-dimensional cases. In section 2.1 the one-dimensional fracture problem of a chain is considered where the main notations, the solution derivation and numerical algorithms are explained in details. The phenomenon of lattice trapping is demonstrated

for the case of static problem in section 2.1.1 and the dynamical case is studied throughout section 2.1.2. The theoretical results are compared with the ones achieved by purely numerical simulations of the problem in section 2.1.5. The following section 2.2 shows the effects of non-local interactions where only dynamical case is analysed. The double chain problem is discussed in section 2.3 which finishes the illustration of features of one-dimensional models in question.

Chapter 3 explores mode III fracture in square-cell lattices. The analytical solution for the problem concerning an anisotropic lattice and its outcomes are demonstrated in section 3.1. The dissimilar lattice problem is discussed in section 3.2 where the mismatch in material properties is analysed. There are some specifics of these problem in comparison with one-dimensional analogues. These features are mentioned within a chapter.

Chapter 4 presents the examination of various dynamic fracture criteria. The analysis extensively uses the results achieved previously. The technique of implementation of different fracture conditions for steady-state fracture problems is demonstrated and possible changes are shown as well.

The conclusion given in Chapter 4.4 summarises the achievements of the work and presents the final remarks.

Finally, the explanation of implemented numerical algorithms for Cauchy-type integrals and Fourier transforms is given in appendices.

Some of definitions and derivations are repeated throughout the work for convenience of the reader.

Chapter 2

Chain Problems

2.1 Simple chain

2.1.1 Static problem

We consider a chain attached to a rigid substrate depicted in Fig. 2.1. Taking into an account the symmetry of the problem, the equations for studying the problem have the following form:

$$\begin{gathered} c_1(u_2 - u_1) + F = 0, \\ c_1(u_{n+1} + u_{n-1} - 2u_n) = 0, \quad 1 < n < n_*, \\ c_1(u_{n+1} + u_{n-1} - 2u_n) - c_2 u_n = 0, \quad n \geq n_*, \end{gathered} \tag{2.1}$$

c_1 is the stiffness of the springs between oscillators and a rigid foundation, c_2 is the spring constant of the links between neighbouring oscillators, F is the magnitude of an external force, n_* is the position of the crack tip, u_n is a vertical displacement of an oscillator with index n.

The fracture criterion is taken in terms of critical strain at the crack tip $n = n_*$ and stated on the displacement of the oscillator at the tip. More specifically, the fracture criterion is:

$$u_{n_*} = u_c \tag{2.2}$$

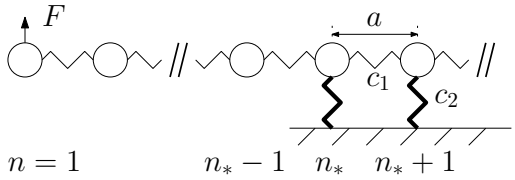

Figure 2.1: Oscillators connected together between each other in a chain by linear springs of stiffness c_1 (normal lines). The chain is partially attached to a rigid substrate by springs of stiffness c_2 (thick lines). The crack position is defined by an oscillator with index n_*. The force F is applied out of plane to the upper row and in to the plane on the lower oscillator.

We are going to search for the load that is high enough to cause the fracture. In this case we deal with the threshold force F. We are also interested in the effect of the anisotropy of the structure. Let us define the parameter that characterises it:

$$\mu = \frac{c_2}{c_1} \tag{2.3}$$

The solution of the problem (2.1) for $n \geq n_*$ can be written as:

$$u_n = \lambda^{(n-n_*)} u_c, \quad n \geq n_*, \tag{2.4}$$

where the introduced constant should satisfy condition $|\lambda| < 1$ in order to obtain a solution decaying at infinity. Straightforward substitution of (2.4) into the final equation of (2.1) and cancellation of common multipliers gives the equation on λ:

$$\lambda^2 - (2+\mu)\lambda + 1 = 0$$

This equation has two roots:

$$\lambda_{1,2} = \frac{(2+\mu) \pm \sqrt{(2+\mu)^2 - 4}}{2}$$
$$= \frac{(\sqrt{4+\mu} \pm \sqrt{\mu})^2}{(\sqrt{4+\mu} - \sqrt{\mu})(\sqrt{4+\mu} + \sqrt{\mu})} = \frac{\sqrt{4+\mu} \pm \sqrt{\mu}}{\sqrt{4+\mu} \mp \sqrt{\mu}}.$$

Among them we need to choose the only one that complements the requirement $|\lambda| < 1$ which is:

$$\lambda = \frac{\sqrt{4+\mu} - \sqrt{\mu}}{\sqrt{4+\mu} + \sqrt{\mu}}. \tag{2.5}$$

The displacements u_n of the remaining part of the chain, $1 < n < n_*$, can be expressed through the linear dependence on n:

$$u_n = \frac{F}{c_1}(n_* - n) + u_c, \quad 1 < n < n_*. \tag{2.6}$$

This form of solution follows from the specific type of the system of equations given by (2.1).

The relation between u_c and F is still needed to be found. For that one needs to consider the equation for $n = n_*$ from the set (2.1). Utilising the obtained relations (2.4) and (2.6) the equation at $n = n_*$ gives:

$$(\lambda - 1)u_c + \frac{F}{c_1} - \mu u_c = 0.$$

Finally, the relation between the load and a critical displacement is:

$$\frac{F}{F_0} = \frac{1 + \mu - \lambda}{\mu}, \quad F_0 = c_2 u_c, \tag{2.7}$$

where F_0 is a static force required to cause fracture in a mechanical system compounded by one mass attached to a rigid substrate by spring of stiffness c_2.

The final expression of the displacements:

$$\frac{u_n}{u_c} = \begin{cases} \lambda^{n-n_*}, & n \geq n_*, \\ (1 + \mu - \lambda)(n_* - n) + 1, & 1 < n < n_*. \end{cases} \tag{2.8}$$

Formulae (2.5), (2.7) and (2.8) fully solve the problem. In Fig. 2.2 one can see computed displacements u_n according to derived analytical expressions for different values of μ. With increase of μ there is a tendency in increase

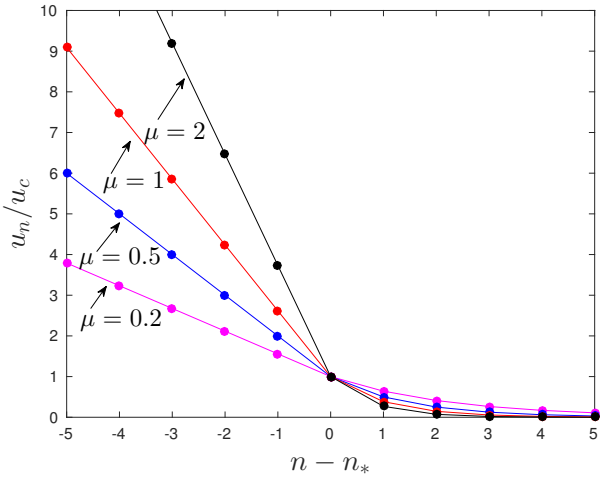

Figure 2.2: Displacements of masses u_n according to (2.8) for different values of contrast μ.

of inclination angle in the broken part of the structure, $n < n_*$, and decrease in magnitude of displacements for μ.

One of the major quantities in fracture mechanics is the energy release rate. This quantity is equal to the change in potential energy with an increase of crack length with opposite sign. In this case the change in potential energy is equal to half of external work done on the path from u_{n_*} to u_{n_*-1}. Thus, using the relations (2.1) and (2.8) for $n \leq n_*$, *global energy release rate* G for a half of the structure, i.e. one chain only, is equal:

$$G = \frac{1}{2} F \frac{u_{n_*-1} - u_{n_*}}{a} = \frac{F^2}{2ac_1} = \frac{c_2 u_c^2}{2ac_1} \frac{F^2}{c_2 u_c^2} = \mu \frac{c_2 u_c^2}{2a} \left(\frac{F}{F_0} \right)^2$$

The factor $1/a$ appears in order to highlight the unit crack length extension. The amount of energy that is released by the fracture of one spring only is equal to a stored elastic energy in the spring right before the fracture divided by a. Alternatively, the change of potential energy may be considered in a mass-spring system, similarly as for quantity F_0. This energy change is

referred as *local energy release rate* G_0 and can be expressed as:

$$G_0 = \frac{c_2 u_c^2}{2a}.$$

Finally, with the help of (2.7) we find the ratio of global energy release rate, G, and local energy release rate, G_0, to be:

$$\frac{G_0}{G} = \frac{\mu}{(1+\mu-\lambda)^2}, \quad G_0 = \frac{c_2 u_c^2}{2a}, \tag{2.9}$$

where the expression for λ is given by (2.5).

The plots of ratio G_0/G and normalised force as functions of contrast μ are shown in Fig. 2.3a) and Fig. 2.3b). There is clearly a monotonic dependence of G_0/G and F_0/F on the contrast μ.

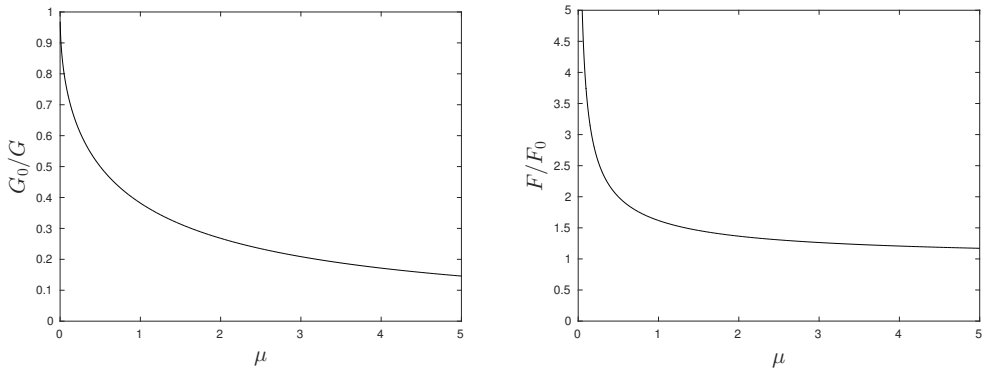

a) b)

Figure 2.3: a) Energy release rates ratio G_0/G as a function of μ according to (2.9), b) Force ratio F_0/F as function of μ according to (2.7).

The fact that $G_0/G < 1$, or $F/F_0 > 1$, for any choice of μ demonstrates the phenomenon called lattice trapping [90]. This phenomenon states that the energy spent on fracture that happens in the discrete mechanical system is greater the the energy spent on the fracture of one of its elements. With the reference to a problem under consideration this means that the force needed

to cause fracture in a chain is greater than the force that causes fracture in a simple structure of two masses and springs.

With these observations for the static case it is interesting to turn to the dynamic problem. However, the dynamic fracture of chain turned out to be far more complicated and required an incorporation of Wiener-Hopf method. The first analytical results were constructed by Slepyan [86].

2.1.2 Dynamic problem

2.1.2.1 Problem formulation

The dynamic problem of fault propagation is now considered. We consider a chain attached to a rigid substrate shown in Fig. 2.4. Such a problem formulation also corresponds to a problem of a symmetric double chain subjected to mode III fracture. The crack tip is defined by the index $n_* = n_*(t)$ and its movement is caused by an applied force of magnitude F at position $n_f = n_f(t)$.

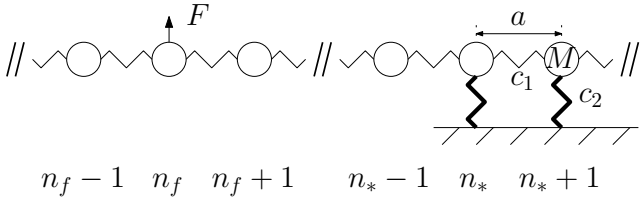

Figure 2.4: Chain of oscillators with equal masses M connected together by linear springs of stiffness c_1 (normal lines) and to the rigid foundation with springs of stiffness c_2 (thick lines). The crack position is defined by an oscillator with index n_*. The force is F and n_f is its position. The vertical springs of stiffness c_2 sequentially break as the crack moves. a is an equilibrium distance between the oscillators.

The linearised equations of motion of such a system take the form:

$$\begin{aligned} M\ddot{u}_n(t) &= c_1(u_{n+1}(t) + u_{n-1}(t) - 2u_n(t)) + F\delta_{nn_f}, \quad n < n_*, \\ M\ddot{u}_n(t) &= c_1(u_{n+1}(t) + u_{n-1}(t) - 2u_n(t)) - c_2u_n(t), \quad n \geq n_*, \end{aligned} \tag{2.10}$$

where M is the mass of an oscillator, c_2 is the stiffness of the springs that break while the crack propagates, c_1 is the spring constant of the links between neighbouring oscillators, F is the magnitude of an external force, $n_* = n_*(t)$ is the position of the crack tip, n_f is the location of the applied force, $u_n(t)$ is the vertical displacement of an oscillator with index n. The Kronecker delta is written as δ_{nm}.

The initial conditions for the problem are set to be homogeneous:

$$u_n(0) = 0, \quad \dot{u}_n(0) = 0, \quad \forall n. \tag{2.11}$$

We assume that no waves can come from infinity towards a crack tip, i.e. we choose appropriate radiation conditions at infinity. We extensively use the method developed by Slepyan and his co-authors [3, 59, 83, 84, 85].

In the presented configuration, we assume that the crack propagates from the left to the right. The displacement at the crack tip is subjected to a deformation fracture criterion given in the following form:

$$\begin{aligned} u_{n_*}(t_*) &= u_c, \\ u_n(t) &< u_c, \quad n > n_*(t), \end{aligned} \tag{2.12}$$

where u_c is a constant, t_* is a fracture time. The second condition is consistent with the assumption that the crack tip can be uniquely defined by index n_*.

We allow the location of the force n_f to vary according to the following rule:

$$n_f(t) = n_f(0) + \frac{v_f}{a}t, \quad v_f = const. \tag{2.13}$$

In further analysis, $v_f = 0$ corresponds to a fixed load, $v_f > 0$ indicates that the force is moving toward the crack tip, $v_f < 0$ that the force is moving in the opposite direction.

The contrast in elastic properties remains to be defined as μ:

$$\mu = \frac{c_2}{c_1}.$$

At this point it is convenient to turn to Bloch-Floquet analysis of the structure, i.e. study the acoustic properties of the structure.

2.1.2.2 Dispersion relations

Firstly, let us separately study the intact and broken parts of structure shown in in Fig. 2.5a) and Fig. 2.5b).

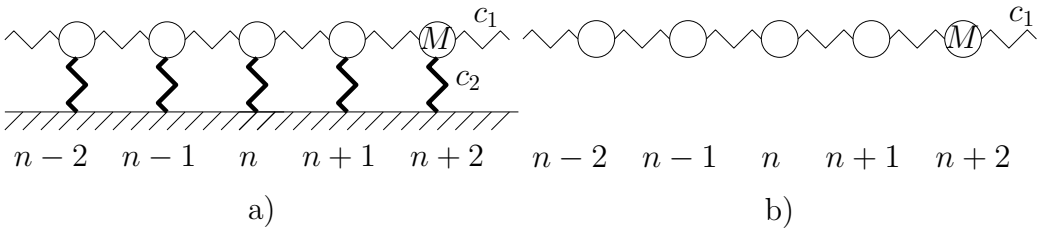

Figure 2.5: Two separate infinite chains of oscillators which have the same structure as : a) Intact part of chain with crack, b) Broken part of chain with crack.

The equations of motion for configuration in Fig. 2.5a) are:

$$M\ddot{u}_n^{(1)}(t) = c_1(u_{n+2}^{(1)}(t) + u_{n-2}^{(1)}(t) - 2u_n^{(1)}(t)) - c_2 u_n^{(1)}(t), \tag{2.14}$$

whereas the configuration in Fig. 2.5b) is described by:

$$M\ddot{u}_n^{(2)}(t) = c_1(u_{n+2}^{(2)}(t) + u_{n-2}^{(2)}(t) - 2u_n^{(2)}(t)). \tag{2.15}$$

One can search for the solution of these problems in the form:

$$u_n^{(j)}(t) = u_0^{(j)} e^{i(kn+\omega t)}, \quad j = 1, 2, \tag{2.16}$$

where k is a dimensionless wave number, ω is a frequency and $u_0^{(j)} = const \neq 0, j = 1, 2$. Plugging the solution $u^{(j)}$ from (2.16) into the equations (2.14)

one may find that it should be $\omega(k) = \omega_1(k)$ with:

$$\omega_1^2(k) = 4v_c^2 \sin^2\left(\frac{k}{2}\right) + \omega_0^2, \quad v_c^2 = \frac{c_1}{M}, \quad \omega_0^2 = \frac{c_2}{M}. \tag{2.17}$$

Similarly, the configuration in Fig. 2.5b) has the solution of the form (2.16) if $\omega(k) = \omega_2(k)$ where:

$$\omega_2^2(k) = 4v_c^2 \sin^2\left(\frac{k}{2}\right). \tag{2.18}$$

Relations (2.17) and (2.18) characterise the possible scenarios of wave propagation and turn out to be useful for the construction of the solution to the initial problem of crack movement.

We now turn to study the steady-state regime.

2.1.2.3 Steady-state crack propagation

We search for the solution of the problem in a steady-state regime that naturally requires some assumptions for derivation of the final formulae. For the moment, let us assume that at some moment in time the crack speed stabilizes and the crack moves periodically. This means that every breakage occurs within a certain time step and that the deformation picture of the entire structure remains (in the moving reference frame coinciding with the crack tip at the moment of breakage) the same at these moments as compared with the equivalent picture at the moment of the previous breakage. In the proceeding analysis we define the time of the beginning of this process as $t = 0$ and may define the crack speed as v.

The model provides a parameter for the critical value of the crack speed v which is defined by the value of a speed of sound v_c of the broken part of the structure:

$$v < v_c = \sqrt{\frac{c_2}{M}}a. \tag{2.19}$$

This limitation follows from the evidence that the load is applied far away behind a crack tip (from the left to it as shown in Fig. 2.4) and has to

continuously provide the energy supply for the crack propagation. It remains valid as long as the force remains situated in the broken part of a chain. In the case where the load moves faster then the crack tip, this condition is guaranteed by the computational time frame.

In the following analysis we normalise the velocities by the equilibrium distance between the oscillators:

$$\tilde{v} = \frac{v}{a}, \quad \tilde{v}_c = \frac{v_c}{a}, \quad \tilde{v}_f = \frac{v_f}{a}. \tag{2.20}$$

Hence, the units of the speed quantities become $[T^{-1}]$. Following [85], this allows us to introduce a change of variables:

$$\eta = n - n_*(t), \quad n_*(t) = n_f(0) + n_0 + vt, \tag{2.21}$$

where $n_0 = n_*(0) - n_f(0)$ is the distance between the crack tip and the force location at the beginning of the steady-state motion, v is the respective speed of the moving coordinate system whose origin coincides with the position of the crack tip at moments when breakages occur. The limitation on the values of crack speed v is given in (2.19). We assume it is a known parameter whose value remains to be determined by further analysis.

Let us introduce new function $u(\eta, t)$:

$$u_n(t) = u(\eta, t), \tag{2.22}$$

which depends on two continuous independent variables for any fixed value of n. In the moving coordinate system, the equations of motion (2.10) for the new function is written in the form:

$$\begin{aligned} M\left(\frac{\partial^2}{\partial t^2} - 2v\frac{\partial^2}{\partial t \partial \eta} + v^2\frac{\partial^2}{\partial \eta^2}\right) u(\eta, t) = c_1(u(\eta+1, t) + u(\eta-1, t) - 2u(\eta, t)) \\ -c_2 u(\eta, t)H(\eta) + F\delta(\eta + n_0 + (v - v_f)t), \end{aligned} \tag{2.23}$$

where $H(\eta)$ is the Heaviside step function, and $\delta(\eta)$ is the Dirac delta function. As we changed variables in (2.21), we also modify the derivative with

respect to time, which has been incorporated into (2.23). The initial conditions (2.11) for this new formulation become:

$$u(\eta,t)=f_0(\eta),\quad \left(\frac{\partial}{\partial t}-v\frac{\partial}{\partial \eta}\right)u(\eta,t)=g_0(\eta),\quad t=0. \tag{2.24}$$

Here, $f_0(\eta)$ and $g_0(\eta)$ are unknown functions. Although they are important for the description of transient problem, they have no impact on the final expressions of the steady-state solution, which is explicitly shown below in section 2.1.2.6. The fracture criterion in (2.12) for the steady-state regime becomes:

$$\begin{aligned} u(0)&=u_c,\\ u(\eta)&<u_c,\quad \eta>0. \end{aligned} \tag{2.25}$$

2.1.2.4 Reduction of the transient problem to the Wiener-Hopf problem

The solution of problem (2.23) can be achieved by means of Fourier and Laplace transforms. Recall the properties of Fourier transform for an arbitrary function $f(\eta)$ and its Fourier transform $\hat{f}(k)$:

$$\int_{-\infty}^{\infty} f(\eta)e^{ik\eta}d\eta=\hat{f}(k)\Longrightarrow \int_{-\infty}^{\infty} f(\eta\pm q_0)e^{ik\eta}d\eta=\hat{f}(k)e^{\mp iq_0k},$$
$$\int_{-\infty}^{\infty} \delta(\eta+q_0)e^{ik\eta}d\eta=e^{-ikq_0},$$

with $q_0=const.$ Keeping these properties in mind we consequently apply Fourier and Laplace transforms to (2.23) and get:

$$\begin{aligned} &\left[(s+ikv)^2+\omega_1^2(k)\right]U^+(k,s)+\left[(s+ikv)^2+\omega_2^2(k)\right]U^-(k,s)\\ &\qquad=\frac{Fe^{-ikn_0}}{M}\frac{1}{s+ik(v-v_f)}+H_0(k), \end{aligned} \tag{2.26}$$

where the last term $H_0(k)$ encapsulates the initial conditions in (2.24) and notations of dispersion relations (2.17) and (2.18) were utilised.

The unknown complex valued functions $U^{\pm}(k,s)$ are analytic in the respective half-planes $\pm\Im k > 0$ for any $s > 0$, and defined as:

$$\begin{aligned} U(k,s) &= \int_0^\infty \left[\int_{-\infty}^\infty u(\eta,t)e^{ik\eta}d\eta\right] e^{-st}dt = U^+(k,s) + U^-(k,s), \\ U^{\pm}(k,s) &= \int_0^\infty \left[\int_{-\infty}^\infty u(\eta,t)H(\pm\eta)e^{ik\eta}d\eta\right] e^{-st}dt. \end{aligned} \tag{2.27}$$

Equation (2.26) can be written in the form of the inhomogeneous Wiener-Hopf equation by division by term $(s+ikv)^2 + \omega_2^2(k)$:

$$\begin{aligned} &L(k,s)U^+(k,s) + U^-(k,s) \\ &= \frac{Fe^{-ikn_0}}{M}\frac{1}{s+ik(v-v_f)}\frac{1}{(s+ikv)^2+\omega_2^2(k)} + \frac{H_0(k)}{(s+ikv)^2+\omega_2^2(k)}. \end{aligned} \tag{2.28}$$

with kernel function $L(k,s)$:

$$L(k,s) = \frac{(s+ikv)^2+\omega_1^2(k)}{(s+ikv)^2+\omega_2^2(k)}. \tag{2.29}$$

One can directly check that for any $s > 0$, this function has no zeros along the real axis, $k \in \mathbb{R}$, and possesses the following properties:

$$\begin{aligned} &L(k,s) = \overline{L(-k,s)}, \\ &|L(k,s)| = |L(-k,s)|, \quad \mathrm{Arg}L(k,s) = -\mathrm{Arg}L(-k,s), \quad s > 0, k \in \mathbb{R}. \end{aligned} \tag{2.30}$$

As a result, the kernel has zero index (winding number) [85] and is estimated at infinity by the following:

$$L(k,s) = 1 - \frac{\omega_0^2}{k^2v^2} + O(k^{-4}), \quad k \to \infty. \tag{2.31}$$

Utilizing (2.30) and (2.31), $L(k,s)$ can be factorised by means of the Cauchy-type integral:

$$\begin{aligned} L(k,s) &= L^+(k,s)L^-(k,s), \\ L^{\pm}(k,s) &= \exp\left(\pm\frac{1}{2\pi i}\int_{-\infty}^\infty \frac{\mathrm{Log}L(\xi,s)}{\xi-k}\,d\xi\right), \quad \pm\Im k > 0. \end{aligned} \tag{2.32}$$

Function Log$k$ is a complex logarithm which is:

$$\mathrm{Log}k = \log|k| + i\mathrm{Arg}k,$$

where $\log|k|$ is a real logarithm and Arg$k$ is an argument function. Concerning (2.32), the Wiener-Hopf equation (2.28) reduces to:

$$L^+(k,s)U^+(k,s) + \frac{1}{L^-(k,s)}U^-(k,s) = T(k,s). \tag{2.33}$$

The right-hand side of the last equation is:

$$\begin{aligned} T(k,s) = \frac{Fe^{-ikn_0}}{M}\frac{1}{s+ik(v-v_f)}\frac{1}{[(s+ikv)^2+\omega_2^2(k)]L^-(k,s)} \\ + \frac{H_0(k)}{[(s+ikv)^2+\omega_2^2(k)]L^-(k,s)}. \end{aligned} \tag{2.34}$$

Taking $T(k,s)$ as the sum of the "plus" and "minus" function, we can solve this Wiener-Hopf equation for any fixed value of the variable s. Then, inverting both transforms, it is possible to analyse the transient regime of the fracture propagating with a constant speed, v. This, however, is rather a computationally challenging task.

Our main interest in the problem considered is to evaluate a possible steady-state solution $u(\eta)$, that is the limit of the function $u(\eta,t)$ as $t\to\infty$:

$$u(\eta) = \lim_{t\to\infty} u(\eta,t) = \lim_{s\to 0} s\int_0^\infty u(\eta,t)e^{-st}\,dt. \tag{2.35}$$

Here, the second relation follows from the finite value theorem for Laplace transform [62], where we assume that the limits in (2.35) exist. In this case, we need to multiply the equation (2.33) by $s\to 0+$. Comment (2.35) is reflected on the integral transforms as follows:

$$\begin{aligned} U(k) = \int_{-\infty}^{\infty} u(\eta)e^{ik\eta}d\eta, \\ U(k) = \lim_{s\to 0+} sU(k,s), \quad U^{\pm}(k) = \lim_{s\to 0+} sU^{\pm}(k,s). \end{aligned} \tag{2.36}$$

The kernel function becomes:

$$\begin{aligned} L(k,s) &= \frac{(s+ikv)^2+\omega_1^2(k)}{(s+ikv)^2+\omega_2^2(k)}, \\ L(k) &= \lim_{s\to 0+} L(k,s) = \frac{(0+ikv)^2+\omega_1^2(k)}{(0+ikv)^2+\omega_2^2(k)}. \end{aligned} \tag{2.37}$$

The expressions $(0 \pm ikv)$ should be understood as follows:

$$(0 \pm ikv) = \lim_{s\to 0+} (s \pm ikv). \tag{2.38}$$

Limit $sT(k,s), s \to 0+$ is still needed to be carefully studied.

2.1.2.5 Dispersion relations and the kernel function of the problem

The kernel function of the problem $L(k,s)$ and its steady-state limit $L(k)$ are given by (2.37). The objective here is to analyse the function $L(k)$ and its singularities, bearing in mind the properties of the function $L(k,s)$.

From the definition of $L(k)$ it is clear that its real zeros and poles are intersection points of $\omega_1^2(k)$ and $\omega_2^2(k)$, as seen in (2.37), with the function $(vk)^2$, respectively. The plots of the dispersion relationships are presented in Fig. 2.6 for several crack speeds.

Since $\omega_{1,2}^2(k)$ and $(vk)^2$ are even functions of k, it is sufficient to search for the positive roots of the equations $\omega_{1,2}(k) - vk = 0$. For the fixed crack speed v let us define:

$$\begin{aligned} z_j > 0: &\quad \omega_1(z_j) - vz_j = 0, \quad j = 1,\dots,Z, \\ p_j > 0: &\quad \omega_2(p_j) - vp_j = 0, \quad j = 1,\dots,P, \end{aligned} \tag{2.39}$$

where P and Z are integers which represent the total numbers of positive zeros and poles of function $L(k)$, respectively. There is also a root at the point $k = 0$ in the function $\omega_2(k)$:

$$\omega_2(0) = 0, \tag{2.40}$$

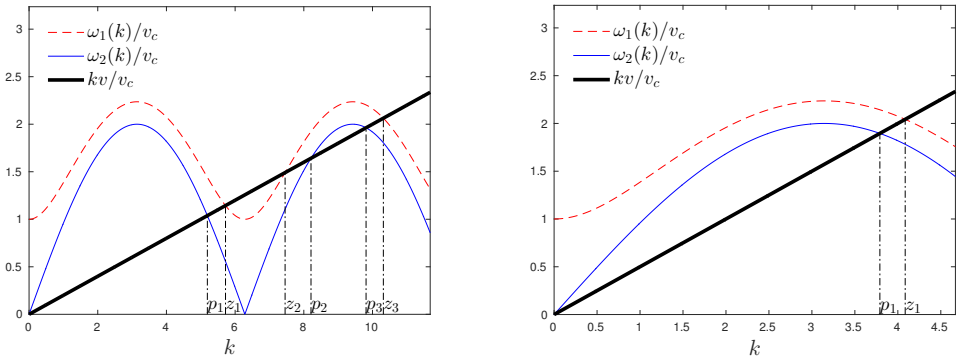

a) b)

Figure 2.6: Dispersion diagram of a chain for several crack speeds for the contrast in elastic properties $\mu = 1$: a) $v = 0.2v_c$, b) $v = 0.3v_c$. The dispersion relationships $\omega_1(k)$ (see (2.17)) and $\omega_2(k)$ (see (2.18)) correspond to an intact region of a chain and a broken one, respectively.

By using the definition of $L(k,s)$, we can analyse the behaviour of the function $L(k)$ at its zeros and poles, as $k \to 0$:

$$\begin{aligned} (s+ikv)^2 + \omega_1^2(k) &\sim (v_c^2 - v^2)(k - z^+(s))(k - z^-(s)), \quad k \to 0, \\ (s+ikv)^2 + \omega_2^2(k) &\sim (v_c^2 - v^2)(k - p^+(s))(k - p^-(s)), \quad k \to 0, \end{aligned} \tag{2.41}$$

where

$$z^{\pm}(s) = \frac{-isv \mp i\sqrt{\omega_0^2(v_c^2 - v^2) + v_c^2 s^2}}{v_c^2 - v^2}, \quad p^{\pm}(s) = \frac{\mp is}{v_c \mp v}. \tag{2.42}$$

We can also find that:

$$z^{\pm}(s) = \frac{\mp i\omega_0}{\sqrt{v_c^2 - v^2}} + O(s), \quad s \to 0. \tag{2.43}$$

Thus, function $L(k)$ has the zeros and poles defined in (2.39). The asymptotic relations hold (with the terms $s(k - z_i)$ or $s(k - p_i)$ omitted due to the limit

$s \to 0$):

$$\begin{aligned}(s+ikv)^2+\omega_1^2(k) &= (2z_iv-is)((\omega_1'(z_i)-v)(k-z_i)+is)\\ &\quad +O((k-z_i)^2), \quad k\to z_i,\\ (s+ikv)^2+\omega_2^2(k) &= (2p_iv-is)((\omega_2'(p_i)-v)(k-p_i)+is)\\ &\quad +O((k-p_i)^2), \quad k\to p_i.\end{aligned} \tag{2.44}$$

Functions $L^{\pm}(k)$ in (2.32) should be free of zeros and poles in $\pm\Im k>0$, respectively. Hence, apart from finding the roots along the real axis when $s\to 0+$, it is also necessary to know which half-plane they belong to. It is possible to find the roots of (2.44) within the leading terms of asymptotic, i.e. to consider equations:

$$(\omega_1'(z_i)-v)(k-z_i)+is=0, \quad (\omega_1'(p_i)-v)(k-p_i)+is=0.$$

The last equations reveal that if $\omega_{1,2}'(z_i)>v$ then the corresponding root goes to " $+$ " function and if $\omega_{1,2}'(z_i)<v$ it, on the contrary, belongs to " $-$ " function. Thus, from the continuity of functions $\omega_{1,2}(k)$ we conclude that the function $L^+(k,s)$ contains zeros and poles of even index, i.e. $z_{2j}, p_{2j}, j=1,2,...$, whereas the function $L^-(k,s)$ contains zeroes and poles of odd index, i.e. $z_{2j-1}, p_{2j-1}, j=1,2,....$

The asymptotic relationships for the functions $L^{\pm}(k,s)$ follow from (2.32) and (2.42):

$$L^{\pm}(k,s)\sim R^{\pm 1}\frac{k-z^{\pm}(s)}{k-p^{\pm}(s)}, \quad k\to 0, \quad s\to 0, \tag{2.45}$$

where constant R is expressed by means of function $L(k)$ as:

$$R=\exp\left(\frac{1}{\pi}\int_0^{\infty}\frac{\mathrm{Arg}L(k)}{k}dk\right).$$

This constant is found to be important for the further investigations and it will be recalled later. We write the asymptotic behaviour of $L^-(k,s)$ at

positive zeros and poles as:

$$\begin{aligned} L^-(k,s) &= V_j^-((2z_{2j-1}v - is)((\omega_1'(z_{2j-1}) - v)(k - z_{2j-1}) + is)) \\ &\quad + O((k - z_{2j-1})^2), \quad k \to z_{2j-1} \\ L^-(k,s) &= \frac{W_j^-}{(2p_{2j-1}v - is)((\omega_1'(z_{pj-1}) - v)(k - z_{pj-1}) + is)} \\ &\quad + O((k - p_{2j-1})^2), \quad k \to p_{2j-1}, \end{aligned} \tag{2.46}$$

where V_j^-, W_j^- are some constants which can be explicitly expressed through the factorisation of function $L(k)$.

2.1.2.6 Analysis of right-hand side of (2.34) in a limit $s \to 0+$

The first term in the expression for $T(k,s)$ in (2.34) multiplied by s is given as:

$$\frac{F}{M}\frac{s}{s + ik(v - v_f)}\frac{e^{-ikn_0}}{[(s + ikv)^2 + \omega_2^2(k)]L^-(k,s)}. \tag{2.47}$$

The key point to notice here is that the only non-zero values of this function, in the limit $s \to 0+$, are associated with the zeros of the denominator of the last fraction:

$$\begin{gathered} \left[(s + ikv)^2 + \omega_2^2(k)\right] L^-(k.s) \to 0, \quad k = z^-(s), p^+(s), z_{2j-1}, p_{2j}, \\ j = 1, 2, ..., \quad s \to 0 + . \end{gathered} \tag{2.48}$$

Now, let us consider the additional limit $k \to 0$:

$$\begin{gathered} \frac{e^{-ikn_0}}{[(s + ikv)^2 + \omega_2^2(k)]\, L^-(k,s)} \sim -\frac{R}{v_c^2 - v^2}\frac{1}{z^-(s)}\frac{1}{k - p^+(s)}, \\ k \to 0,\ s \to 0. \end{gathered} \tag{2.49}$$

The product of the middle fraction of (2.47) and the term $1/(k - p^+(s))$ from (2.49) gives:

$$\frac{s}{s + ik(v - v_f)}\frac{1}{k - p^+(s)} \sim \frac{1}{i(v - v_f)}\frac{s}{p^+(s) - \frac{is}{(v - v_f)}}\left[\frac{1}{k - p^+(s)} - \frac{1}{k - \frac{is}{(v - v_f)}}\right].$$

We can then use expression for $p^+(s)$ from (2.42) to obtain:

$$\frac{1}{i(v-v_f)}\frac{s}{p^+(s)-\frac{is}{(v-v_f)}}=\frac{v_c-v}{v_c-v_f}.$$

The last expression does not depend on s and is equal to zero only when $v=v_c$. We finally get:

$$\frac{s}{s+ik(v-v_f)}\frac{1}{k-p^+(s)}=\frac{v_c-v}{v_c-v_f}\left[\frac{1}{k+i0}-\frac{1}{k-i0}\right]+O(s),\quad s\to 0+, \tag{2.50}$$

where we used the notations for a limit from (2.38). Expression (2.50) is valid for $v_f<v$ but as long as the location of the force remains behind the crack tip this suitable for our purposes. It should be also stressed that in the case $v=v_f$ the factorisation should be accomplished differently. Indeed, in this case the fraction $s/(s+ik(v-v_f))=1$, which leads to certain changes in the analysis, e.g. in (2.50). However, the obtained results support the analysis of the solution and extract the relations in question.

We shall now consider the limits $k\to z_{2j-1}$, as mentioned in (2.48):

$$\begin{aligned}\frac{e^{-ikn_0}}{[(s+ikv)^2+\omega_2^2(k)]\,L^-(k)}&=\frac{\hat{V}_j^-e^{-in_0z_{2j-1}}}{(\omega_1'(z_{2j-1})-v)(k-z_{2j-1})+is}\\&\quad+O(1),\quad k\to z_{2j-1},\\ \hat{V}_j^-=\frac{1}{[(s+iz_{2j-1}v)^2+\omega_2^2(z_{2j-1})]}&\frac{1}{V_j^-(2z_{2j-1}v-is)}=O(s),\quad s\to 0.\end{aligned} \tag{2.51}$$

We note that the product of the middle fraction of (2.47) and the factor in the last expression is:

$$\begin{aligned}&\frac{s}{s+ik(v-v_f)}\frac{1}{(\omega_1'(z_{2j-1})-v)(k-z_{2j-1})+is}\\ &\sim\frac{1}{i(v-v_f)(\omega_1'(z_{2j-1})-v)}\frac{s}{z_{2j-1}-\frac{is}{(\omega_1'(z_{2j-1})-v)}-\frac{is}{v-v_f}}\\ &\quad\times\left[\frac{1}{k-z_{2j-1}+\frac{is}{(\omega_1'(z_{2j-1})-v)}}-\frac{1}{k-\frac{is}{v-v_f}}\right].\end{aligned} \tag{2.52}$$

In this case, the factor in front of the square brackets is:

$$\frac{s}{z_{2j-1} - \frac{is}{(\omega_1'(z_{2j-1})-v)} - \frac{is}{v}} = o(s), \quad s \to 0. \tag{2.53}$$

In other words, there is no contribution from the points $k = z_{2j-1}$ to the expression (2.47) in the limit $s \to 0$. The same reasoning applies to the limit $k \to p_{2j}$ which are also roots of function in (2.48).

We can observe that function $H_0(k, s)$ in (2.34) comes from the initial conditions of the original problem, does not contain any singularities, and that:

$$s\frac{H_0(k,s)}{[(s+ikv)^2 + \omega_2^2(k)]L^-(k,s)} = o(s), \quad s \to 0. \tag{2.54}$$

Thus, using the expressions from (2.42) and (2.43) and the reasoning associated with the above functions in (2.47) and (2.54) we conclude that the function $sT(k, s)$ of equation (2.34) weakly converges:

$$\begin{aligned} sT(k,s) &= \frac{C}{0-ik} + \frac{C}{0+ik} + O(s), \quad s \to 0, \\ C &= \frac{F}{M}\frac{v_c - v}{v_c - v_f}\frac{R}{\sqrt{\omega_0^2(v_c^2 - v^2)}}, \end{aligned} \tag{2.55}$$

where the quantity ω_0^2 is defined in (2.17).

2.1.2.7 Evaluation of the limiting steady-state regime

To find the steady-state solution, we multiply the Wiener-Hopf equation (2.33) by s and pass it to the limit $s \to 0+$. The resulting equation is gained with the notations in (2.36), (2.29) and derivations of the previous section summarized in (2.17). We get:

$$L^+(k)U^+(k) + \frac{1}{L^-(k)}U^-(k) = \frac{C}{0-ik} + \frac{C}{0+ik}, \tag{2.56}$$

where constant C is given in (2.55).

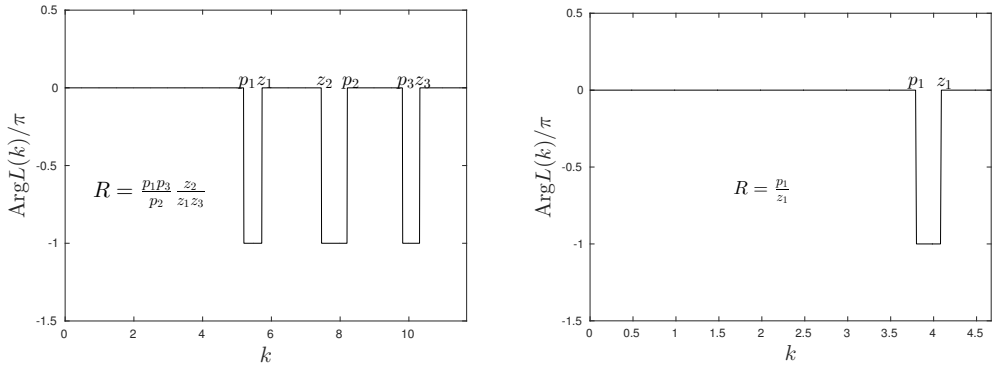

a) b)

Figure 2.7: Function $\mathrm{Arg}L(k)$ for the contrast in elastic properties $\mu = 1$: a) $v = 0.2v_c$, b) $v = 0.5v_c$. The way to calculate function R in (2.57) is shown for the presented cases.

The auxiliary parameter R in the last expression is related to the energy balance of the system and plays a crucial role in the further analysis:

$$R = R(v) = \exp\left(\frac{1}{\pi}\int_0^\infty \frac{\mathrm{Arg}L(k)}{k}\,dk\right). \tag{2.57}$$

One can notice that the integration in (2.57) is taken along the real axis which makes the evaluation of the integral easy [83]. Indeed, for $k \in \mathbb{R}$ function $L(k)$ is real valued and its argument jumps between values 0 and $-\pi$. The plots of function $\mathrm{Arg}L(k)$ for two values $v = 0.2v_c$ and $v = 0.5v_c$ are shown in Fig. 2.7.

The jumps of $\mathrm{Arg}L(k)$ happen exactly at poles and zeros of function $L(k)$, given by the roots in (2.39), and are strongly related to dispersion properties (see Fig. 2.6). The computation of R for particular v is reduced to a root finding procedure and its values for $v = 0.2v_c$ and $v = 0.5v_c$ are shown on the plots in Fig. 2.7a) and Fig. 2.7b), respectively.

Taylor expansion of expression of factors $L^{\pm}(k)$ in (2.32) at infinity gives:

$$L^{\pm}(k) = 1 \pm i\frac{Q}{k} + O\left(\frac{1}{k^2}\right), \quad k \to \infty, \quad Q = \frac{1}{\pi}\int\limits_0^{\infty} \log|L(k)|\, dk. \tag{2.58}$$

The asymptotics of $L^{\pm}(k)$ are estimated to be:

$$\begin{gathered} L^{\pm}(k) = \frac{\omega_0}{\sqrt{v_c^2 - v^2}} \frac{R^{\pm 1}}{0 \mp ik} \left(1 + (0 \mp ik)S\right) + O(k), \quad k \to 0, \\ S = \frac{1}{\pi}\int\limits_0^{\infty} \frac{\log|L(k)|}{k^2}\, dk. \end{gathered} \tag{2.59}$$

Let us observe that the displacement field is expected to be continuous in the vicinity of the crack tip $\eta = 0$ and, hence, that the asymptotics must at least satisfy $U^{\pm} = O(k^{-1})$, $k \to \infty$. The last estimate, together with (2.58) allows us to solve the Wiener-Hopf equation (2.56) by utilising Liouville's theorem:

$$U^{+}(k) = \frac{C}{0 - ik}\frac{1}{L^{+}(k)}, \quad U^{-}(k) = \frac{C}{0 + ik}L^{-}(k). \tag{2.60}$$

In turn, from (2.58) and (2.59), it follows that:

$$\begin{gathered} U^{\pm}(k) = \pm\frac{Ci}{k}\left(1 - \frac{Qi}{k}\right) + O\left(\frac{1}{k^3}\right), \quad k \to \infty, \\ U^{+}(k) = \frac{C}{\omega_0 R}\sqrt{v_c^2 - v^2} + o(1), \quad k \to 0, \\ U^{-}(k) = \frac{\omega_0 C}{R}\frac{1}{\sqrt{v_c^2 - v^2}}\left(\frac{1}{(0 + ik)^2} + \frac{S}{0 + ik}\right) + O(1), \quad k \to 0. \end{gathered} \tag{2.61}$$

The sought for steady-state solution $u(\eta)$, in terms of the inverse Fourier transform, takes the form:

$$u(\eta) = \frac{1}{2\pi}\int_{-\infty}^{\infty} U^{\pm}(k)e^{-ik\eta}\, dk, \quad \pm\eta > 0. \tag{2.62}$$

Asymptotic estimates (2.61), the Abel-Tauber type theorem (Theorem A.5 in [67]) and Cauchy's residue theorem allow us to obtain the asymptotic

behaviour of the solution $u(\eta)$:

$$\begin{aligned} u(\eta) &= C(1 - Q\eta) + O(\eta^2), \quad \eta \to 0, \\ u(\eta) &= -\frac{C}{R}\frac{\omega_0}{\sqrt{v_c^2 - v^2}}(\eta - S) + O(1), \quad \eta \to -\infty. \end{aligned} \tag{2.63}$$

We note that the value of the constant part of the leading term of $(2.63)_2$, as $\eta \to -\infty$, defines the inclination angle of the destroyed part of the structure between the crack tip and the position of the force. Furthermore, estimate $(2.61)_3$ suggests that there might be oscillations (reflected waves) in the limit $\eta \to \infty$ and that they are included in the $O(1)$ term of $(2.63)_2$.

The application of fracture condition (2.25) to $(2.63)_2$ implies that:

$$C = u_c, \tag{2.64}$$

and, in light of (2.55), this last result gives the relationship between the loading parameters, F, v_f, the geometry of the problem, and the steady-state crack speed, v:

$$\frac{F}{F_0} = \frac{v_c}{\omega_0 R}\frac{v_c - v_f}{v_c - v}\sqrt{\frac{v_c^2 - v^2}{v_c^2}}, \quad F_0 = c_2 u_c, \tag{2.65}$$

where, as in the case of static problem, F_0 is a static force needed to detach an oscillator linked to a rigid substrate by spring of stiffness c_2. Relation (2.65) suggests that, for two different pairs of loading parameters $F^{(1)}, v_f^{(1)}$ and $F^{(2)}, v_f^{(2)}$ leading to the same steady-state speed, the following is valid:

$$\frac{F^{(1)}}{F^{(2)}} = \frac{v_c - v_f^{(1)}}{v_c - v_f^{(2)}}. \tag{2.66}$$

Even though the formal relations for the solution $u(\eta)$ are governed their numerical treatment remains a challenging task. The technique used for its evaluation is presented in a separate section.

2.1.3 Factorisation of function $L(k)$ and associated analysis

2.1.3.1 Factorisation of function $L(k)$

Let us consider the following representation of function $L(k)$:

$$L(k) = \frac{(0+ikv)^2 + \omega_1^2(k)}{(0+ikv)^2 + \omega_2^2(k)} = L_0(k)l(k), \quad l(k) = l^+(k)l^-(k), \tag{2.67}$$

where dispersion relations $\omega_{1,2}(k)$ are given in (2.17) and (2.18), respectively. Functions $l^{\pm}(k)$ are defined as follows:

$$\begin{aligned} l^+(k) &= \frac{(p_0 - ik)^{d+1}}{0-ik} \frac{\prod_{j=1}^{Z'}(0 - i(k - z_{2j}))(0 - i(k + z_{2j}))}{\prod_{j=1}^{P'}(0 - i(k - p_{2j}))(0 - i(k + p_{2j}))}, \\ l^-(k) &= \frac{(p_0 + ik)^{d+1}}{0+ik} \frac{\prod_{j=1}^{Z'}(0 + i(k - z_{2j-1}))(0 + i(k + z_{2j-1}))}{\prod_{j=1}^{P'}(0 + i(k - p_{2j-1}))(0 + i(k + p_{2j-1}))}, \\ d &= P - Z, \quad Z' = \left\lceil \frac{Z+1}{2} \right\rceil, \quad P' = \left\lceil \frac{P+1}{2} \right\rceil. \end{aligned} \tag{2.68}$$

Recall that Z is the number of real, positive poles p_j of function $L(k)$ in the limit $s \to 0+$ (positive roots of equation $\omega_1(k) - vk = 0$) whereas P is the number of real, positive zeros z_j of function $L(k)$ (positive roots of equation $\omega_2(k) - vk = 0$). The corresponding notations appeared in (2.39). Symbol $\lceil x \rceil$ stands for the ceiling of a number x.

The first fractions in $l^{\pm}(k)$ appear in order to take into an account the pole at $k = 0$ of function $L(k)$ and also to keep the necessary asymptotic of functions $l^{\pm}(k)$. The real constant $p_0 > 0$ is chosen in such a way that the condition $L_0(0) = 1$ is satisfied when $s \to 0+$, or explicitly:

$$p_0 = \left(\frac{\omega_0^2}{v_c^2 - v^2} \frac{\prod_{j=1}^{P} p_j^2}{\prod_{j=1}^{Z} z_j^2} \right)^{\frac{1}{2d+2}}. \tag{2.69}$$

Expressions $(0 \pm ik) = \lim(s \pm ik), s \to 0+$ as was previously highlighted by (2.38). For the numerical implementations the expression $(s \pm ik)$ and value $s = 10^{-13}$ was set to produce the computations. This value was found to be small enough to get efficient results.

The function $|L_0(k)| \to 0$ as $k \to \infty$ and has zero index. Moreover, while the inverting the Fourier transform, we keep the variable $k \in \mathbb{R}$. So, we can factorize $L_0(k)$ by means of Cauchy-type integral from (2.32) but bearing in mind also Sokhotski–Plemelj theorem, which reveals:

$$L_0^{\pm}(k) = \sqrt{L_0(k)} \exp\left(\pm \frac{1}{2\pi i} \text{V.P.} \int_{-\infty}^{\infty} \frac{\text{Log} L_0(\xi)}{\xi - k} \, d\xi \right), \quad \Im k \to 0, \tag{2.70}$$

where V.P. stands for the Cauchy principal value. Notice that for $k \in \mathbb{R}$ the arguments of function $L(k)$ and $l(k)$ coincide. This circumstance leads to the fact that $\text{Arg} L_0(k) = 0$, $k \in \mathbb{R}$, which simplifies the integration. The final factorization of function $L(k)$ can be expressed via $l^{\pm}(k)$ and $L^{0\pm}(k)$:

$$L(k) = L^+(k) L^-(k), \quad L^{\pm}(k) = l^{\pm}(k) L_0^{\pm}(k). \tag{2.71}$$

We also note that functions $l^{\pm}(k), L_0(k)$ possess the same properties as function $L(k)$, i.e.:

$$l^{\pm}(-k) = \overline{l^{\pm}(k)}, \quad L_0^{\pm}(-k) = \overline{L_0^{\pm}(k)}, \quad k \in \mathbb{R}. \tag{2.72}$$

2.1.3.2 Asymptotic behaviour of functions at infinity

Let us study the asymptotic behaviour of functions which we use in the calculations. We start with the behaviour of functions at infinity, i.e. $k \to \infty$, where $k \in \mathbb{R}$.

The terms of order $O(s)$ are omitted and not mentioned from now on as the limiting case $s \to 0+$ is under investigation. Besides, the choice for computations $s = 10^{-13}$ makes such terms irrelevant.

1. Let us study behaviour of functions $l^{\pm}(k), l(k)$ in a limit $s \to 0+$.

   For some term in numerator of $l^{\pm}k$ containing an arbitrary zero z_i we have:

   $$(0 \pm i(k + z_i))(0 \pm i(k - z_i)) = -k^2 \left(1 - \frac{z_i^2}{k^2}\right).$$

   Whereas for the a denominator of $l^{\pm}(k)$ having a term with any pole p_i the following expansion holds:

   $$\frac{1}{(0 \pm i(k + p_i))(0 \pm i(k - p_i))} = -\frac{1}{k^2}\left(1 + \frac{p_i^2}{k^2}\right) + O\left(\frac{1}{k^4}\right), \quad k \to \infty.$$

   The remaining term in $l^{\pm}(k)$ is expanded as:

   $$\frac{(p_0 \pm ik)}{0 \pm ik}(p_0 \pm ik)^d$$
   $$= (-1)^{d/2} k^d \left(1 \pm \frac{ip_0}{k}\right)\left[1 \mp \frac{ip_0 d}{k} - \frac{p_0 d(d-1)}{2k^2} + O\left(\frac{1}{k^4}\right)\right], \quad k \to \infty.$$

   Referring to the expressions of functions $l^{\pm}(k)$ we, finally, obtain:

$$
\begin{gathered}
l^{\pm}(k) = 1 + \frac{a_1^{\pm}}{k} + \frac{a_2^{\pm}}{k^2} + O\left(\frac{1}{k^2}\right), \quad k \to \infty, \\
a_1^{+} = i(p_0 + dp_0), \quad a_2^{+} = \sum_{j=1}^{P'} p_{2j}^2 - \sum_{j=1}^{Z'} z_{2j}^2, \\
a_1^{-} = -i(p_0 + dp_0), \quad a_1^{-} = \sum_{j=1}^{P'} p_{2j-1}^2 - \sum_{j=1}^{Z'} z_{2j-1}^2.
\end{gathered}
\tag{2.73}
$$

Function $l(k)$ from (2.67) is then behave as follows:

$$
l(k) = 1 + \frac{a_2^{+} + a_2^{-} + a_1^{+} a_1^{-}}{k^2} + O\left(\frac{1}{k^3}\right), \quad k \to \infty, \tag{2.74}
$$

where the property $a_1^{+} + a_1^{-} = 0$ was utilised.

2. We can turn to the derivation of asymptotic behaviour of function $L_0(k)$. The estimated behaviour of function $L(k)$ in (2.31) and function $l(k)$ in (2.74) allows to find the asymptotic behaviour of function $L_0(k)$ introduced in (2.67):

$$
L_0(k) = \left[1 - \frac{\omega_0^2}{k^2 v^2}\right] \left[1 + \frac{a_2^{+} + a_2^{-} + a_1^{+} a_1^{-}}{k^2}\right]^{-1} + O\left(\frac{1}{k^3}\right), \quad k \to \infty.
$$

Final expression for is written as:

$$
\begin{gathered}
L_0(k) = 1 + \frac{f_0}{k^2} + O\left(\frac{1}{k^3}\right), \quad k \to \infty, \\
f_0 = -\frac{\omega_0^2}{v^2} - (a_2^{+} + a_2^{-} + a_1^{+} a_1^{-}),
\end{gathered}
\tag{2.75}
$$

where coefficients $a_1^{\pm}, a_2^{\pm}$ are given in (2.73). With (2.75) it is useful to write the expression for $\log |L_0(k)|$ at $k \to \infty$:

$$
\log |L_0(k)| = \frac{f_0}{k^2} + O\left(\frac{1}{k^4}\right), \quad k \to \infty. \tag{2.76}
$$

The term $O(k^{-4})$ follows from the properties (2.72), which lead function $|L_0(k)|$ to be even for real values of k.

3. Now we turn to functions $L_{0\pm}(k)$ in (2.70). The integral in that expression can be estimated as:

$$\begin{aligned}
&\exp\left(\pm\frac{1}{2\pi i}\int\limits_{-\infty}^{\infty}\frac{\mathrm{Log}L_0(\xi)}{\xi-k}\,d\xi\right)\\
&=\exp\left(\mp\frac{1}{2\pi k i}\int\limits_{-\infty}^{\infty}\mathrm{Log}L_0(\xi)\,d\xi+O\left(\frac{1}{k^3}\right)\right)\\
&=1\pm\frac{i}{k}Q_0-\frac{1}{k^2}\frac{Q_0^2}{2}+O\left(\frac{1}{k^3}\right),\quad k\to\infty.
\end{aligned}$$

The function $|L_0(k)|$ is even and $\log|L_0(k)|=O(k^{-2}), k\to\pm\infty$. The function $\mathrm{Arg}L_0(k)$ is odd and the integral from this function vanishes. Moreover, this function annihilates for real k. From the expression (2.70),(2.75) and $\Im k\to 0$ we gain:

$$\begin{aligned}
L_0^{\pm}(k)&=1\pm\frac{i}{k}Q_0+\frac{f_0-Q_0^2}{2}\frac{1}{k^2}+O\left(\frac{1}{k^3}\right),\quad k\to\infty,\\
Q_0&=\frac{1}{\pi}\int\limits_0^{\infty}\log|L_0(k)|\,dk.
\end{aligned}\tag{2.77}$$

The calculation of Q_0 is done similarly to the computations of Cauchy-type integral in (2.77). Such a procedure is demonstrated in the corresponding section. Briefly, the function $\log|L_0(k)|$ is regular for $k\in\mathbb{R}$ and it is approximated by splines on the interval $(0,A)$, where A is large enough. On the remaining part of the interval, (A,∞), we integrate the function that approximates $\ln|L_0(k)|$ asymptotically at infinity. The asymptotic behaviour of $\ln|L_0(k)|$ is presented by (2.76).

4. The expressions for the functions $U^{\pm}(k)$ can be found in (2.60). From all the previously derived expressions for $l^{\pm}(k)$ and $L_0^{\pm}(k)$ we can now obtain the asymptotic behaviour of the functions $U^{\pm}(k)$. The factorisation (2.71) and (2.73), (2.77) lead to:

$$U^{\pm}(k) = \pm\frac{u_c i}{k}\left(1 - \frac{Q_0 i \pm a_1^{\pm}}{k}\right) + O\left(\frac{1}{k^3}\right), \quad k \to \infty, \tag{2.78}$$

where constants $a_1^{\pm}$ are given in (2.73) and Q_0 is shown in (2.77). The behaviour of Fourier transform (2.78) in turn determine the behaviour of the original function $u(\eta)$:

$$u(\eta) = u_c(1 - (Q_0 + p_0)\eta) + O(\eta^2), \quad \eta \to 0, \tag{2.79}$$

where the presentations for $a_1^{\pm}$ in (2.73) have been used. The constant p_0 is shown in (2.69).

2.1.3.3 Asymptotic behaviour of functions at zero

Analogous analysis of the functions can be performed to study their behaviour at the points $k = 0$ and $k \in \mathbb{R}$. We also omit terms $O(s)$ as it was done in previously.

1. First we start again with functions $l_{\pm}(k), l(k)$. The terms that compound these functions are expanded as:

$$(0 \pm i(k + z_i))(0 \pm i(k - z_i)) = z_i^2\left(1 - \frac{k^2}{z_i^2}\right),$$
$$\frac{1}{(0 \pm i(k + p_i))(0 \pm i(k - p_i))} = \frac{1}{p_i^2}\left(1 + \frac{k^2}{p_i^2}\right) + O(k^2), \quad k \to 0.$$

The remaining terms in the expressions of $l^{\pm}(k)$ at the vicinity of $k = 0$ give:

$$\frac{(p_0 \pm ik)^{d+1}}{(0 \pm ik)} = \frac{p_0^{d+1}}{ik}\left(\pm 1 + \frac{1}{p_0}k\right)\left(1 \pm \frac{id}{p_0}k - \frac{d(d-1)}{2p_0^2}k^2 + O(k^3)\right)$$
$$= \frac{ip_0^{d+1}}{k}\left(\mp 1 - \frac{i(d+1)}{p_0}k \pm \frac{d(d+1)}{2p_0^2}k^2 + O(k^3)\right), \quad k \to 0.$$

Finally, we obtain the expression for $l^{\pm}(k)$:

$$
\begin{gathered}
l^{\pm}(k) = \frac{1}{k}\left(\alpha_1^{\pm} + \alpha_2^{\pm} k + \alpha_3^{\pm} k^2 + O(k^3)\right), \quad k \to 0, \\
\alpha_1^{+} = i p_0^{d+1} \frac{\prod\limits_{j=1}^{Z'} z_{2j}^2}{\prod\limits_{j=1}^{P'} p_{2j}^2}, \quad \alpha_2^{+} = -i \frac{\alpha_1^{+}(d+1)}{p_0}, \\
\alpha_3^{+} = \alpha_1^{+}\left[\sum_{j=1}^{P'} \frac{1}{p_{2j}^2} - \sum_{j=1}^{Z'} \frac{1}{z_{2j}^2} - \frac{d(d+1)}{2p_0^2}\right], \\
\alpha_1^{-} = -i p_0^{d+1} \frac{\prod\limits_{j=1}^{Z'} z_{2j-1}^2}{\prod\limits_{j=1}^{P'} p_{2j-1}^2}, \quad \alpha_2^{-} = i \frac{\alpha_1^{-}(d+1)}{p_0}, \\
\alpha_3^{-} = \alpha_1^{-}\left[\sum_{j=1}^{P'} \frac{1}{p_{2j-1}^2} - \sum_{j=1}^{Z'} \frac{1}{z_{2j-1}^2} - \frac{d(d+1)}{2p_0^2}\right].
\end{gathered}
\tag{2.80}
$$

From the last expression we can easily obtain an asymptotic behaviour of function $l(k)$ from (2.67):

$$
l(k) = \frac{\alpha_1^{+}\alpha_1^{-}}{k^2} + (\alpha_1^{+}\alpha_3^{-} + \alpha_1^{-}\alpha_1^{+} + \alpha_2^{+}\alpha_2^{-}) + O(k^2), \quad k \to 0. \tag{2.81}
$$

In the last expression the fact that $l(k)$ is an even function for real k was used. Specifically, this property gives the following relations between the coefficients in (2.80):

$$
\alpha_1^{+}\alpha_2^{-} + \alpha_1^{-}\alpha_2^{+} = 0.
$$

2. In order to study behaviour of function $L(k)$ we write it down explicitly:

$$
L(k) = 1 + \frac{\omega_0^2}{(0 + ikv)^2 + 4v_c^2 \sin\left(\frac{k}{2}\right)}, \quad \mu = \frac{\omega_0^2}{v_c^2}.
$$

After Taylor expansion of function $\sin(k/2)$ at the vicinity of point $k = 0$ we get:

$$\begin{aligned} L(k) &= \frac{\delta_1}{k^2} + 1 + \delta_2 + \delta_3 k^2 + O(k^3), \quad , k \to 0, \\ \delta_1 &= \frac{\omega_0^2}{v_c^2 - v^2}, \quad \delta_2 = \frac{\delta_1^2}{12\mu}, \quad \delta_3 = \frac{\delta_1 \delta_2}{12\mu} - \frac{\delta_1^2}{360\mu}. \end{aligned} \tag{2.82}$$

The estimated asymptotic behaviours of function $l(k)$ and $L(k)$ allow to obtain an expression for function $L_0(k)$:

$$\begin{aligned} L_0(k) = \frac{L(k)}{l(k)} &= 1 + \gamma_1 k^2 + \gamma_2 k^4 + O(k^6), \quad k \to 0, \\ \gamma_1 &= \frac{1 + \delta_2 - (\alpha_1^+ \alpha_3^- + \alpha_1^- \alpha_3^+ + \alpha_2^+ \alpha_2^-)}{\alpha_1^+ \alpha_1^-}, \\ \gamma_2 &= \frac{\delta_3 - \gamma_1 (\alpha_1^+ \alpha_3^- + \alpha_1^- \alpha_3^+ + \alpha_2^+ \alpha_2^-)}{\alpha_1^+ \alpha_1^-}, \end{aligned} \tag{2.83}$$

where coefficients $\alpha_1^\pm, \alpha_2^\pm, \alpha_3^\pm$ are given in (2.80) and coefficients δ_2, δ_3 can be found in (2.82). In (2.83) we used the fact that function $L_0(k)$ is even for $k \in \mathbb{R}$ and $L_0(0)$. The former implies that:

$$\frac{\delta_1}{\alpha_1 \beta_1} = 1.$$

Then, the behaviour of $\log |L_0(k)|$ is:

$$\log |L_0(k)| = \gamma_1 k^2 + (\gamma_2 - \frac{1}{2}\gamma_1) k^4 + O(k^4), \quad k \to 0. \tag{2.84}$$

3. We switch to the analysis of functions $L_0^\pm(k)$ (remember that $\mathrm{Arg} L_0(k) = 0, k \in \mathbb{R}$). The integral in expression (2.70) gives:

$$\exp\left(\pm \frac{1}{2\pi i} \int_{-\infty}^{\infty} \frac{\mathrm{Log} L_0(\xi)}{\xi - k} \, d\xi \right) = 1 \mp i S_0 k - \frac{S_0^2}{2} k^2 + O\left(k^3\right), \quad k \to 0.$$

Thus, with the help of (2.83), we obtain:

$$\begin{aligned} L_0^{\pm}(k) &= 1 \mp iS_0k + \frac{\gamma_1 - S_0^2}{2}k^2 + O(k^3), \quad k \to 0, \\ S_0 &= \frac{1}{\pi}\int_0^{\infty} \frac{\log|L_0(k)|}{k^2}\, dk. \end{aligned} \tag{2.85}$$

The computations of S_0 are performed in the same way as for the constant Q_0 from (2.77) which is described below that expression.

4. The final purpose of the analysis behaviour of the previous functions was to achieve an asymptotic behaviour of function $U^-(k)$ in (2.60). This function, in contrary to $U^+(k)$, possesses a singularity at $k = 0$ which causes computational challenge. To obtain the asymptotic behaviour of $U^-(k)$ expressions (2.73) and (2.77) are used. The result is:

$$\begin{aligned} U^-(k) &= \frac{\Delta_1}{(0+ik)^2} + \frac{\Delta_2}{(0+ik)} + \Delta_3 + O(k), \quad k \to 0 \\ \Delta_1 &= i\alpha_1^- u_c, \quad \Delta_2 = u_c(\alpha_2^- + i\alpha_1^- S_0), \\ \Delta_3 &= -iu_c\left(\alpha_3^- + \beta_1\frac{\gamma_1 - S_0^2}{2} + iS_0\alpha_2^-\right). \end{aligned} \tag{2.86}$$

Here, coefficients $\alpha_1^-, \alpha_2^-, \alpha_3^-$ are from (2.80), γ_1 and S_0 are given in (2.83) and (2.85), respectively. The term $(0+ik)$ was used in order to highlight that the root lies slightly above the real line.

2.1.3.4 Asymptotic behaviour of functions at finite non-zero singular points

From (2.60), the singular points of function $U^+(k)$ are located at the zeros of function $L^+(k)$, whereas the singularities of $U^+(k)$ are at poles of $L^-(k)$. The definition of functions $U^+(k)$ and the presentation of $L^{\pm}(k)$ in (2.71) through functions $l^{\pm}(k)$ and $L_0^{\pm}(k)$ in (2.68) and (2.70), respectively:

$$U^+(k) \sim \frac{W_j^+}{0 - i(k - z_{2j})}, \quad k \to z_{2j}, \quad j = 1, 2, ..., Z',$$
$$W_j^+ = \frac{(-1)^{d+1}}{2(p_0 - iz_{2j})^{d+1}} \frac{\prod\limits_{j'=1}^{P'}(z_{2j}^2 - p_{2j'}^2)}{\prod\limits_{j'=1,\, j' \neq j}^{Z'}(z_{2j}^2 - z_{2j'}^2)} \frac{C}{(0 - iz_{2j})L_0^+(z_{2j'})}. \tag{2.87}$$

In addition to this, the expression for the asymptotic behaviour of function $U_-(k)$ in the vicinity of its real poles is obtained:

$$U^-(k) \sim \frac{W_j^-}{0 + i(k - p_{2j-1})}, \quad k \to p_{2j-1}, \quad j = 1, 2, ..., P'$$
$$W_j^- = \frac{(-1)^{d+1}(p_0 - ip_{2j-1})^{d+1}}{2p_{2j-1}^2} \frac{\prod\limits_{j'=1}^{Z'}(p_{2j-1}^2 - z_{2j'-1}^2)}{\prod\limits_{j'=1,\, j' \neq j}^{P'}(p_{2j-1}^2 - p_{2j'-1}^2)} \frac{CL_0^-(p_{2j-1})}{0 + ip_{2j-1}}. \tag{2.88}$$

The properties of function $L(k)$ and its factors in (2.72) lead to the fact that $U(-k) = \overline{U(k)}, k \in \mathbb{R}$ which, in turn, provides:

$$U^+(k) \sim \frac{\overline{W_j^+}}{0 - i(k + z_{2j})}, \quad k \to -z_{2j}, \quad j = 1, 2, ..., Z',$$
$$U^-(k) \sim \frac{\overline{W_j^-}}{0 + i(k + p_{2j-1})}, \quad k \to -p_{2j-1}, \quad j = 1, 2, ..., P'.$$

For the further analysis it is better to operate with polar representation of quantities $W_j^\pm$, thus we introduce the notations:

$$\begin{aligned} \rho_j^+ &= \left|W_j^+\right|, \quad \beta_j^+ = \mathrm{Arg}\left(W_j^+\right), \quad j = 1, 2, ..., P', \\ \rho_j^- &= \left|W_j^-\right|, \quad \beta_j^- = \mathrm{Arg}\left(W_j^-\right), \quad j = 1, 2, ..., Z'. \end{aligned} \tag{2.89}$$

2.1.3.5 Solution representation

The solution of the problem in terms of Fourier transform is defined as:

$$u(\eta) = \frac{1}{2\pi} \int_{-\infty}^{\infty} \left[U^+(k) + U^-(k) \right] e^{-ik\eta} \, dk.$$

Firstly, we notice that for $\eta > 0$ the integration along the real line can be substituted with the contour integration along the path displayed in Fig. 2.8a). Notice that the contour lie in the half-plane $\Im k < 0$ where $U^-(k)$ is analytic. Hence, the integral along this contour of the function $U^-(k) \exp(-ik\eta)$ is zero. Moreover, due to Jordan's lemma from complex analysis the integral containing $U^-(k)$ vanishes along the semi-circle when its radius tends to infinity. Thus, we obtain:

$$\frac{1}{2\pi} \int_{-\infty}^{\infty} U^-(k) e^{-ik\eta} \, dk = 0, \quad \eta > 0.$$

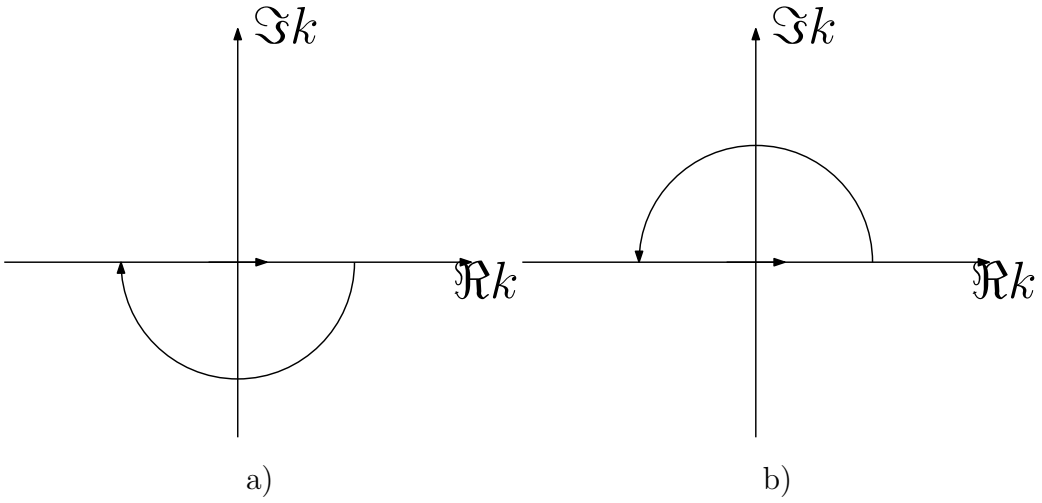

Figure 2.8: a) Contour of integration for $\eta > 0$ and $\Im k < 0$, b) Contour of integration for $\eta < 0$ and $\Im k > 0$.

Following the same reasoning we get:

$$u(\eta) = \frac{1}{2\pi} \int_{-\infty}^{\infty} U^{\pm}(k) e^{-ik\eta} \, dk, \quad \pm\eta > 0.$$

Let us subtract all the singularities that functions $U^{\pm}(k)$ have along the real line:

$$\begin{aligned}\hat{U}^{+}(k) &= U^{+}(k) - \sum_{j=1}^{Z'} \left[\frac{W_j^{+}}{0 - i(k - z_{2j})} + \frac{\overline{W_j^{+}}}{0 - i(k + z_{2j})} \right], \\ \hat{U}^{-}(k) &= U^{-}(k) - \sum_{j=1}^{P'} \left[\frac{W_j^{-}}{0 - i(k - p_{2j-1})} + \frac{\overline{W_j^{-}}}{0 - i(k + p_{2j-1})} \right] \\ &\quad - \frac{\Delta_1}{(0 + ik)^2} - \frac{\Delta_2}{0 + ik},\end{aligned} \tag{2.90}$$

where constants $W_j^{\pm}$ can be found in (2.87) and (2.88), the coefficients $\Delta_{1,2}$ are presented in (2.86). The functions $\hat{U}^{\pm}(k)$ are free of singularities along the real line and the numerical algorithms for their evaluation may be applied. The application of residue theorem for the singular terms in (2.90) and using the respective contours give:

$$u(\eta) = \frac{1}{2\pi} \int_{-\infty}^{\infty} \hat{U}^{+}(k) e^{-ik\eta}\, dk + \sum_{j=1}^{Z'} \left[W_j^{+} e^{-iz_{2j}\eta} + \overline{W_j^{+}} e^{iz_{2j}\eta} \right], \quad \eta > 0$$

$$u(\eta) = \frac{1}{2\pi} \int_{-\infty}^{\infty} \hat{U}^{-}(k) e^{-ik\eta}\, dk - \Delta_1 \eta + \Delta_2$$

$$+ \sum_{j=1}^{P'} \left[W_j^{-} e^{-ip_{2j-1}\eta} + \overline{W_j^{-}} e^{ip_{2j-1}\eta} \right], \quad \eta < 0.$$

Notice that due to the properties in(2.72) functions $\hat{U}^{\pm}(k)$ possess the same properties. The final expression for the displacement field with the use of notations in (2.89) is:

$$u(\eta) = \frac{1}{\pi}\Re\left(\int_0^\infty \hat{U}^+(k)e^{-ik\eta}\,dk\right) + 2\sum_{j=1}^{Z'}\rho_j^+\cos\left(z_{2j}\eta - \beta_j^+\right), \quad \eta > 0$$
$$u(\eta) = \frac{1}{\pi}\Re\left(\int_0^\infty \hat{U}^-(k)e^{-ik\eta}\,dk\right) - \Delta_1\eta + \Delta_2$$
$$+2\sum_{j=1}^{P'}\rho_j^-\cos\left(p_{2j-1}\eta - \beta_j^-\right), \quad \eta < 0. \tag{2.91}$$

It was this expression that was used for the computations of the displacement fields and the analysis of the problem. The way the integrals were evaluated is shown in Appendix A.2.

2.1.4 Analysis of the analytical solution

The solution of the problem, $u(\eta)$, is given in terms of the inverse Fourier transform and can be evaluated when a certain crack speed is specified. To illustrate the results, the displacements for the chosen crack speeds are shown in Fig. 2.9 for different values of $\mu = c_2/c_1$.

In Fig. 2.9a), we see that for $v = 0.2v_c$, the second part of fracture condition $(2.25)_2$ is violated for $\mu = 1, 2$, whereas for $v = 0.5v_c$ in Fig. 2.9b) it is fulfilled for every shown case of contrast μ.

Following this observation, we can examine the displacement field ahead of the crack tip for every chosen value of v and check the validity of the condition $(2.25)_2$. A similar analysis was performed for a triangular cell lattice in [43]. In accordance with fracture condition (2.25), the obtained solutions can be divided into two groups:

- An obtained solution represents an **admissible regime** if the fracture condition $(2.25)_2$ is fulfilled. This regime is fully consistent with the set of assumptions corresponding to the steady-state regime with the given crack speed, v.

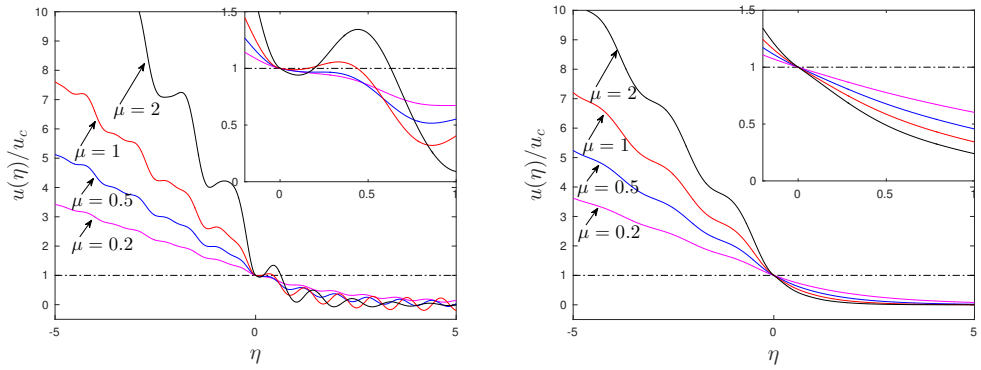

Figure 2.9: Displacement field $u(\eta)$ for different values of contrast μ and different choices of crack speed: a) $v = 0.2v_c$, b) $v = 0.5v_c$. The inserts show a zoom of the displacement profile in the neighbourhood of the crack tip. The dash-dot line shows the level of displacement $u(\eta) = u_c$.

- If condition $(2.25)_2$ is violated, the steady-state propagation regime with speed v is **forbidden**.

Forbidden regimes contain many diverse behaviours, which include clustering [3] and forerunning [82] (also known as a mother-daughter crack mechanism [29]) can be named.

We now analyse the energetic aspect of the considered problem. Similarly to the case of static chain problem we introduce local and global energy release rates (ERR) [85]. As previously, the local ERR, denoted by G_0, corresponds to the potential energy stored in a spring pre-fracture multiplied by the crack speed. Meanwhile, the global ERR, G, characterises the change in energy of the whole structure as the crack moves. The computation of G can be performed similarly to [54]. The contribution to the change of energy is supported by the work rate of the remote force at $\eta \to -\infty$ and growth of kinetic and potential energies in the broken part of the chain. Thus, the calculation of G is also similar to the one for the static case shown in

section 2.1.1.

We need to keep the leading term of the asymptotic behaviour of $u(\eta)$ at $\eta \to -\infty$ from (2.63):

$$u(\eta) \sim -\frac{u_c}{R}\frac{\omega_0}{\sqrt{v_c^2 - v^2}}\eta, \quad \eta \to -\infty.$$

The energy release rate is then:

$$G = \frac{1}{a}\left[\frac{c_1}{v}\left(u(\eta-1) - u(\eta)\right)\frac{du}{dt} - \frac{c_1}{2}\left(u(\eta-1) - u(\eta)\right)^2 - \frac{M}{2}\left(\frac{du}{dt}\right)^2\right],$$

where the first term in the parenthesis stands for the work rate of the remote force, the second and third terms are the potential and kinetic energies, respectively. In the last expression the asymptotic behaviour of function $u(\eta)$ at $\eta \to -\infty$ should be used and $d/dt = -vd/d\eta$ for the steady state. Using notations for v_c and ω_0 from (2.17), we get:

$$\begin{aligned} G &= \frac{1}{a}\left[\frac{M\omega_0^2 u_c^2}{R^2}\frac{v_c^2}{v_c^2 - v^2} - \frac{M\omega_0^2 u_c^2}{2R^2}\frac{v_c^2}{v_c^2 - v^2} - \frac{M\omega_0^2 u_c^2}{2R^2}\frac{v^2}{v_c^2 - v^2}\right] \\ &= \frac{c_2 u_c^2}{2a}\frac{1}{R^2}. \end{aligned}$$

Hence, the ratio between local ERR G_0 and global ERR G is represented by parameter R, as defined in (2.57), which is is also supported by works [85, 86]:

$$\frac{G_0}{G} = R^2, \quad G_0 = \frac{c_2 u_c^2}{2a}. \tag{2.92}$$

We notice that this ratio does not explicitly depend on the loading parameters, and that it was shown in [85] that this relation is valid for similar types of loads, such as those constant amplitude, that lead to a steady-state crack propagation. The related parameter to R^2 is a universal function of a crack tip that appears in problems of the dynamic fracture of continuum solids [25, 26, 27].

The respective plots of energy release rate ratio are presented in Fig. 2.10a) for different values of contrast in material properties: $\mu =$

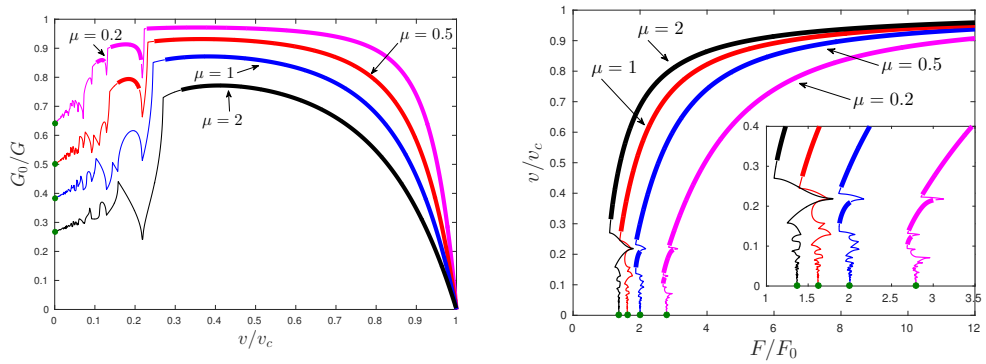

a) b)

Figure 2.10: Admissible (thick lines) and forbidden (normal lines) regimes of crack propagation in terms of a) dependence of the ERR ratio G_0/G on the normalised crack speed v/v_c for different μ. Values at $v/v_c = 0$ are computed by (2.9), b) dependence of normalised crack speed v/v_c on normalised force F/F_0 for different μ. Values at $v/v_c = 0$ are computed by (2.7) and displayed by green markers. The insert shows the zoom of region of low crack speeds and displayed by green markers.

$0.2, 0.5, 1, 2$. The dependence of normalised force F/F_0 is shown in Fig. 2.10b) for the same set of parameters μ. The limiting values of such dependences at $v/v_c \to 0$ are calculated by formulae (2.9) and (2.7) for G_0/G and F/F_0, respectively.

It should be stressed that similar plots of G_0/G for various structures and loading conditions appear in various papers [3, 43, 51, 86]. A common feature of these studies is that G_0/G usually possesses a smooth maximum within the intermediate values of v/v_c. The oscillating behaviour of this dependence for low values of v/v_c may make an impression that the stable steady-state crack propagation does not appear in this range. However, a full analysis of the solution reveals that there are physically relevant (admissible) regimes for small values of v/v_c which is vividly seen for the cases of $\mu = 0.2, 0.5$.

The non-monotonicity of G_0/G may create an ambiguity in choosing certain loading conditions. Indeed, it can happen, looking at the plots of G_0/G in Fig. 2.10a), that one value of G_0/G correspond to multiple values of crack speed. This trouble is partially resolved by means of plots in Fig. 2.10b) when the crack speed is presented as a function of the force magnitude. The most of admissible regimes now are characterised by monotonic dependence between v/v_c and F/F_0.

From the analysis of displacement and plots in Fig. 2.10, we can also conclude that change in the parameter μ leads to qualitative changes with respect to the number of intervals of admissible regimes. Specifically, there are three distinct intervals for the case $\mu = 0.2$, two for the case $\mu = 0.5$, and only one for the remaining cases. Interestingly, there is still non-uniqueness in determination of crack speed for $\mu = 0.2, 0.5$ at low crack speeds. The insert in Fig. 2.10b) demonstrates the small intersection of admissible regimes for these μ and, thus, it is not clear which one is actually realised by application of a certain force.

This raises a question: in reality, which value for the crack speed is evident on such an occasion? The theoretical and numerical study of the spontaneous destruction of a discrete structure [3] has already shown that some regimes of stable crack propagation surely exist, at least for a structure with pronounced anisotropy in its mechanical properties.

2.1.5 Numerical simulations

2.1.5.1 Numerical set up

We consider the structure that is defined by the number N of oscillators in Fig. 2.11 where all the mechanical quantities are also shown. This configuration is distinguished by the in Fig. 2.4 only by its finite length. Thus, we keep all the notations the same as those used in Section 2.1.2.

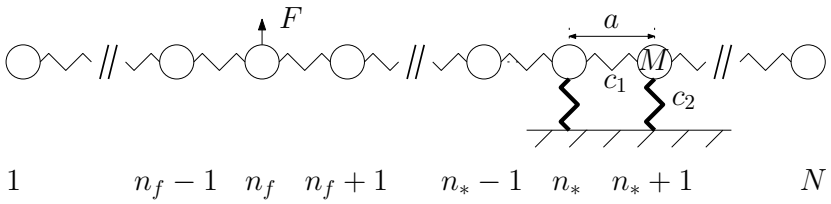

Figure 2.11: Finite chain of oscillators with the same notations used in Section 2.1.2.

The equations of motion of such a system take the form:

$$\begin{aligned} M\ddot{u}_n(t) &= c_2(u_{n+1}(t) + u_{n-1}(t) - 2u_n(t)) + F\delta_{nn_f}, \quad 1 < n < n^*, \\ M\ddot{u}_n(t) &= c_2(u_{n+1}(t) + u_{n-1}(t) - 2u_n(t)) - c_1 u_n(t), \quad n_* \leq n < N. \end{aligned} \tag{2.93}$$

The initial conditions for the problem are set to be homogeneous:

$$u_n(t) = 0, \quad \dot{u}_n(t) = 0, \quad t = 0, \quad 1 \leq n \leq N. \tag{2.94}$$

The numerical simulations also require boundary conditions to be stated as well. For the clamped ends the equations at the ends of a chain are:

$$u_1(t) = u_N(t) = 0, \quad t > 0.$$

Free ends boundary conditions can be set as:

$$u_2(t) - u_1(t) = u_{N-1}(t) - u_N(t) = 0, \quad t > 0.$$

However, we are interested in the analysis of a solution close to a crack tip with established propagation regime. For the choice of a reasonably large number of N oscillators the displacements of oscillators close to a crack tip do not depend on the stated boundary conditions. The effects of boundary conditions in one particular case are shown explicitly later in section 2.1.5.3.

In the presented configuration, we assume that the crack propagates from the left to the right. In order to observe the steady-state regime the following fracture condition should be satisfied:

$$\begin{aligned} u_{n_*}(t_*) &= u_c, \\ u_n(t) &< u_c, \quad n > n_*(t), \end{aligned} \tag{2.95}$$

where u_c is a constant and the second condition is consistent with the assumption that the crack tip can be uniquely defined by index n_*.

We allow the location of the force n_f to vary according to the following rule:

$$n_f(t) = n_f(0) + v_f t, \quad v_f = const. \tag{2.96}$$

For the computations we need to have integer values for $n_f(t)$, and thus choose the ceiling of this number. We also trialled using the floor of $n_f(t)$ or its more general rounding, but the change did not seem sensitive in the prediction of the steady-state crack speed. In further analysis, $v_f = 0$ corresponds to a fixed load, $v_f > 0$ indicates that the force is moving toward the crack tip, $v_f < 0$ that the force is moving in the opposite direction. In this numerical analysis the same normalisation (2.20) is taken.

In the case where the load moves faster then the crack tip the computational time frame is chosen in such a way that calculations stop when the force appears ahead of a crack tip. Such occasions have not been considered in the proposed analytical model and, therefore, appear beyond the scope of interest. We demonstrate that there is a wide time frame where steady-state is realised.

The numerical simulation is performed by running series of iterations. Let us define t_*^j as the time of the j-th fracture event at the point $n = n_*^i(t_*^j)$. The j-th iteration then has the following steps:

1. Once condition $(2.95)_1$ is fulfilled, the relevant solution for moment t_*^j is archived for all values of n:

$$u_n^j = u_n(t_*^j), \quad w_n^j = \dot{u}_n(t_*^j). \tag{2.97}$$

2. The spring of stiffness c_1 of the oscillator with index $n_*^j(t_*^j)$ is removed, and for the next iterations we choose $n_*^{j+1}(t) = n_*^j(t_*^j) + 1$. We also check condition $(2.95)_2$ to hold at any time, but in the cases considered it was always fulfilled.

3. System (2.93) is solved again, using the previously stored values u_n^j, w_n^j from (2.97) as initial conditions.

All computations are done within the Matlab R2015b environment. The geometrical settings of the structure used in the computations in this section are summarised in Table 2.1.

	$\mathbb{S}_1$	$\mathbb{S}_2$	$\mathbb{S}_3$	$\mathbb{S}_4$
Total number of oscillators, N	4000	4000	4000	8000
Total number of breakages, I	1000	1000	1000	1000
Initial crack tip position, $n_*(0)$	2000	2000	2000	2000
Initial force position, $n_f(0)$	1000	1500	1900	1000

Table 2.1: Geometrical settings of the structure on Fig. 2.11 used in the computations.

The chosen sets of the parameters, $\mathbb{S}_j$, guarantee that the fracture process exhibits stable and well developed behaviour for a sufficiently long time, thus allowing us to study its properties. Comparing results for sets $\mathbb{S}_1$ (shorter structure) and $\mathbb{S}_4$ (longer structure) allows us make some conclusions on the influence of the distance between the initial crack tip (and the point where the force is applied) and the left hand side of the structure. We check the impact of the initial force position $n_f(0)$ on the results with respect to configurations $\mathbb{S}_1$, $\mathbb{S}_2$ and $\mathbb{S}_3$, where the distance decreases with each respective set. We do not employ damping in the numerical computations, but control the overall time in the process before the fracture is affected by the reflected waves approaching the crack tip from the left-hand side and right-hand side of the structure. As mentioned earlier, we will also investigate the influence of the boundary conditions at the ends of the structure.

The following choices for physical parameters remain unchanged through-

out all the simulations:

$$c_1 = 1[F/L], \quad M = 1[M], \quad a = 1[L], \quad u_c = 1[L],$$

while the other quantities are determined as previously:

$$\mu = \frac{c_2}{c_1}, \quad F_0 = c_1 \mu u_c.$$

Henceforth, we omit the units in given quantities, assuming them to be appropriate in form.

2.1.5.2 Calculation of the crack speed

In this section we describe the data analysis used throughout the thesis to extract the physical and geometrical properties of the process (crack speed, displacement profiles, etc.) This analysis provides enough confidence to allow us to make conclusions and explain the basic peculiarities of the process. In particular, it establishes a proven link between the results obtained numerically from the discrete structure and those evaluated analytically from the corresponding continuous structure.

One of the most important parameters describing the fracture process is the instantaneous speed of the propagating crack, $v(t)$, which takes discrete values since the structure itself is discrete. Assuming that the crack tip moves by breaking of preceding springs only, i.e. without any breakage being detected ahead, we define an instantaneous crack speed (normalised by the equilibrium length a as in (2.20)) in the following way:

$$v(t_*^j) = \frac{n_*(t_*^{j+1}) - n_*(t_*^j)}{t_*^{j+1} - t_*^j}. \tag{2.98}$$

Here, j is the number of the latest breakage in the fracture process. In order to compare the analytical result for the steady-state speed, v, which is a constant value for the given geometrical and physical parameters, with the results of the numerical simulations, we need to have an equivalent definition for this quantity, supplemented by a quantitative estimate of the latter.

We may accept the mean value, $\bar{v}$, of the instantaneous speed, $v(t_*)$, as a possible numerical definition of the limiting steady state crack speed, v. With this in mind, we consider the set of the data starting from the m-th breakage of the link with index $j = n_*(0) + m$, where the remaining part of the fracture process is computed up to the final point $j = n_*(0) + I$, and the instantaneous speed $v(t_*)$ demonstrates a regular oscillatory behaviour with a small amplitude.

$$\bar{v} = \frac{1}{I-m} \sum_{j=m}^{I-1} v(t_*^j). \tag{2.99}$$

We also may calculate the sample standard deviation $\sigma(v)$, to have some quantitative measure providing an insight into the accuracy of the chosen assumption:

$$\sigma(v) = \sqrt{\frac{1}{I-m-1} \sum_{j=m}^{I-1} \Big(v(t_*^j) - \bar{v}\Big)^2}. \tag{2.100}$$

An alternative method for estimating the crack speed from the numerical analysis would be to use the average speed on the same interval:

$$v_a = \frac{n_*(t_*^I) - n_*(t_*^m)}{t_*^I - t_*^m}, \tag{2.101}$$

where the difference between the values of $\bar{v}$ and v_a serves as an additional accuracy measure.

We now analyse the consequences of particular choices for the geometrical parameters when computing the crack speed from the numerical data. A typical plot for the instantaneous speed, $v(t_*)$, can be seen in Fig. 2.12a), where the typical sample set of the data is one where the oscillations of $v(t_*)$ become regular. This set of data is later used for evaluation of the steady-state crack speed from the numerical data.

The geometrical configuration used in this example corresponds to set $\mathbb{S}_1$ from Table 2.1, where $\mu = 2$, $F = 2.5F_0$ and $v_f = 0.3v_c$. At both ends of the structure, free boundary conditions are prescribed. It is clear that the

instantaneous speed is not a constant but has a clear tendency to approach some limiting value with time as the fracture process develops.

The profile of the entire structure at a certain moment of the fracture event is shown in Fig. 2.12b). We can observe that the displacements behind the crack tip do not form the pure inclined straight line that is seen when examining the global picture in the insert of Fig. 2.12b). This discrepancy is caused by the reflection of waves from the crack tip back to the source. It can be also seen that the amplitude of these waves is much larger than those transmitted into the structure on the crack line ahead (if those exist at all, which is not obvious on the presented scale).

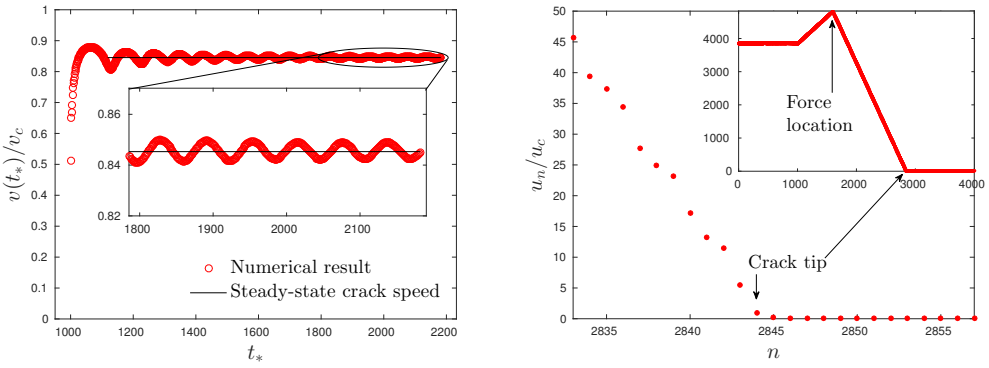

a) b)

Figure 2.12: Results of the computations for geometrical setting $\mathbb{S}_1$ of Table 2.1, where $\mu = 2$, $F = 2.5F_0$ and $v_f = 0.3v_c$. Free edge boundary conditions are prescribed at the structure ends: Fig. 2.12a) – The instantaneous crack speed $v(t_*)/v_c$ given by (2.98). The insert highlights the final stage of the computations, Fig. 2.12b) – The displacements profile of the oscillators close to the crack tip at time $t_* \approx 2000$, taken from the middle of the region shown in the insert, during the well established regime shown in in Fig. 2.12a).

Different strategies can be employed to numerically evaluate the steady-

state crack propagation speed from the computations. In Table 2.2 we present results obtained from three sets of samples (differing by length of the observation time or the length of the fractured structure) for the same structure $\mathbb{S}_1$. The shortest period ($m = 300$) seems the most appropriate choice when analysing computations done in accordance with equations (2.99), (2.100) and (2.101), but it is difficult to make a stronger justification. To illustrate this point, the speed of the steady-state propagation computed via the analytical formula derived in the next section is $v = 0.8457 v_c$ (compare with the values in Table 2.2). For a reason which will become clear later we will use the largest data set ($m = 100$), that contains practically the entire fracture regime except its initial stage. While sacrificing a little accuracy in the steady-state speed evaluation we can guarantee in this way not to miss any essential features of the process when the oscillatory behaviour changes (for other sets of the material parameters).

Starting point	Sample length	$\bar{v}/v_c$	v_a/v_c	$\sigma(v)/v_c$
$m = 100$	$I - m = 900$	0.8452	0.8453	0.0079
$m = 200$	$I - m = 800$	0.8458	0.8459	0.0051
$m = 300$	$I - m = 700$	0.8456	0.8456	0.0042

Table 2.2: Evaluation of the predicted steady-state crack speed using the formulae (2.99), (2.100) and (2.101) and the standard deviation of this value, $\sigma(v)$, for the data presented in Fig. 2.12a).

Another direct conclusion from this preliminary analysis is that the difference between the mean value, $\bar{v}$, and the average value, v_a, of the crack speed is definitely smaller than the accuracy of the computations, bearing in mind its sensitivity with respect to the choice of sample set. For this reason, from now on we report only the mean values, $\bar{v}$, defined numerically by (2.99).

In the next subsection we discuss the effects of the choice of geometrical configuration from Table 2.1 and its impact on the evaluation of the major

process parameters.

2.1.5.3 Effect of values of the geometrical and physical parameters

Firstly, we analyse the impact of the prescribed boundary conditions at the ends of the structure on the numerical results. We consider two options: free ends and clamped end conditions. The results for the displacement field close to a crack tip and for the entire structure are shown in Fig. 2.13 for the same geometrical setting, $\mathbb{S}_1$, and $\mu = 2$, $F = 2.5F_0$, $v_f = 0.3v_c$ at time $t_* \approx 2000$. We observe that, for the chosen numbers of oscillators and iterations, the boundary conditions do not have an effect on the results for the displacement field close to a crack tip, nor those for the crack speed. The predictions for the inclination slope behind the crack tip are also not affected.

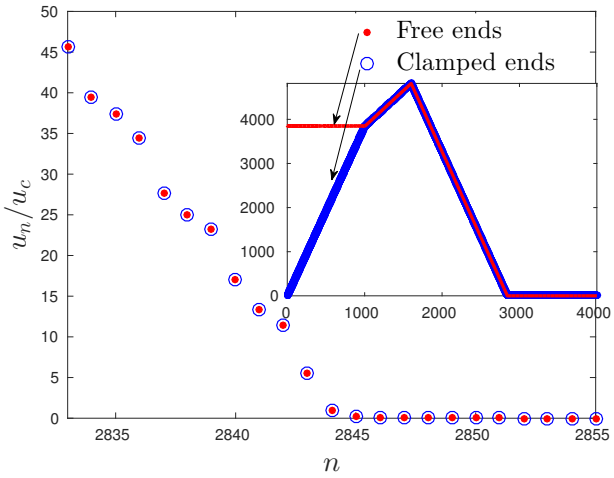

Figure 2.13: Displacement of the oscillators close to a crack tip for two different boundary conditions, given the configuration $\mathbb{S}_1$ from Table 2.1 and $\mu = 2$,$F = 2.5F_0$, $v_f = 0.3v_c$ at time $t_* \approx 2000$. The insert shows the displacement of the whole chain. The red colour corresponds to free ends, while blue corresponds to clamped ends.

The response to the boundary conditions may, however, be noticed if the crack speed is sufficiently slow and the reflected wave reaches the crack tip in the chosen time frame ($I = 1000$ fracture events). This can be avoided by an increase in the number of oscillators in the structure, for example from the number in set $\mathbb{S}_1$ to that in set $\mathbb{S}_4$, both given in Table 2.1. In order to demonstrate this effect, we choose the alternative values for the material parameters: $\mu = 0.5$, $F = 2F_0$ and $v_f = 0$, leading to a lower steady-state crack speed. The ensuing results are shown in Fig. 2.14.

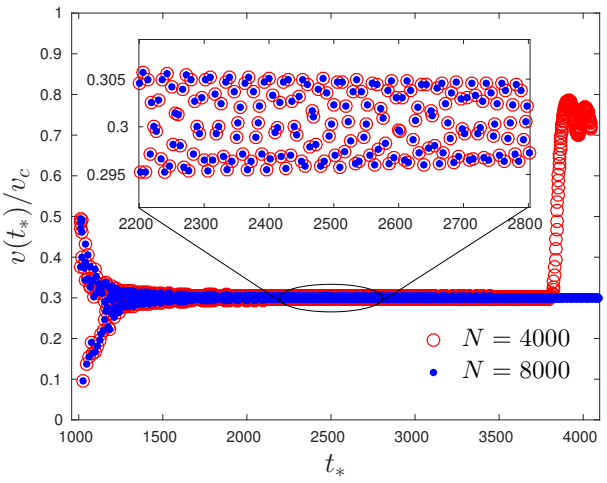

Figure 2.14: The Instantaneous crack speed $v(t_*)/v_c$, given by (2.98), for different total number of oscillators N, where $\mu = 0.5$, $F = 2F_0$ and $v_f = 0$. The results for the set of geometrical parameters shown in red correspond to structure $\mathbb{S}_1$, while in blue correspond to structure $\mathbb{S}_4$.

Note that the only difference between the configurations $\mathbb{S}_1$ and $\mathbb{S}_4$ is a much longer tail in the second case ($N = 8000$ instead of the original $N = 4000$). In the figure, we can see that for both the shown cases there is an established quasi steady-state region. However, for a shorter chain where $N = 4000$, the instantaneous crack speed speed experiences a jump at $t_* \approx 3800$. This event indicates the arrival of the reflected wave from

the left-hand end of the structure. Despite this phenomenon, the results $v(t_*)$, established before this event, are identical for different N, within the accuracy of the evaluation.

Finally, we present the effects of different initial distances between the force position $n_f(0)$ and the crack tip $n_*(0)$. We choose the same physical configuration as in the previous subsection, that is $\mu = 2$, $F = 2.5F_0$, $v_f = 0.3v_c$, and different geometrical configurations $\mathbb{S}_1$, $\mathbb{S}_2$ and $\mathbb{S}_3$, which give: $n_*(0) = 1000$ when we set $n_f(0) = 1500$ and $n_f(0) = 1900$, respectively. The results are shown in Fig. 2.15a). We can see that the respective steady-state crack speeds calculated from (2.99) are $\bar{v} = 0.8456v_c$, $\bar{v} = 0.846v_c$, $\bar{v} = 0.8453v_c$. These calculated values of $\bar{v}$ remain within the chosen accuracy up to the third decimal place. As expected, the fracture process starts earlier for the smaller initial distance between the crack tip and the force position. Moreover, it seems from the computation that the amplitude of the variation of the instantaneous speed, $v_*(t)$, decreases much faster here than in the other two cases, $n_f(0) = 1500$ and $n_f(0) = 1000$.

This suggests that we can set the initial force location sufficiently close to the crack tip to achieve fast convergence to the desired steady-state regime and so obtain a more accurate result. However, we avoid this scenario in the computations for the following simple reason: in the case of a small force moving faster than the crack tip itself, the time interval may become insufficiently long for the cause of making a confident conclusion on the convergence of the process.

As a result of this analysis, and similarly to the case in which we discussed the length of the data sample used in further evaluations, we use configuration $\mathbb{S}_1$ in further computations. This configuration is, in a sense, worse in comparison to the others when judged on the convergence rate of the fracture process to the steady-state regime. However, since the distance between the crack tip and the load is sufficiently large, it provides more confidence that the analysed phenomena has been properly captured even if we have slightly

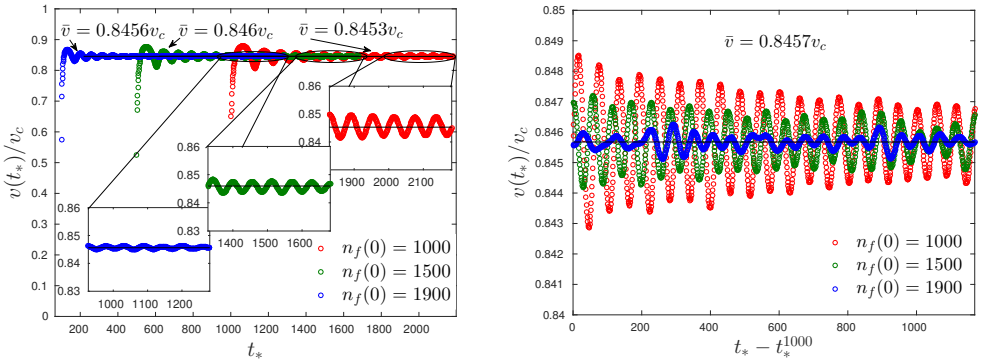

a) b)

Figure 2.15: The Instantaneous crack speed $v(t_*)/v_c$, given by (2.98), for different initial positions of force $n_f(0)$, where $\mu = 2$, $F = 2.5F_0$ and $v_f = 0.3v_c$. a) The first $I = 1000$ breakages, where the inserts show the final stages of the computations. The steady-state crack speeds estimated by (2.99) are also shown, and are presented by solid straight lines. b) The continuation of the computations after the 1000th breakage. The estimation of the steady-state crack speed is the same for all the presented cases.

sacrificed some accuracy and efficiency in the computations.

Finally, in Fig. 2.15b) we analyse the convergence of the fracture process to a pure steady-state regime, continuing the iterations beyond the chosen limit $I = 1000$. Fortunately in this case, unlike in the example presented in Fig. 2.14, no response from reflected waves deforms the physical picture. We present the corresponding results , starting from the differing moments in time when the fracture processes reach the same link $j = n_*(0) + I$. We may conclude that the processes slowly converge, while the computations for the steady-state crack speed using formula (2.99) using the respective data sample give the consistent value $\bar{v} = 0.8457v_c$ which coincides with that predicted analytically.

From the computations performed in this section, we observe that, for

appropriately chosen geometrical parameters, the instantaneous crack speed, $v(t_*)$, stabilises and begins to oscillate about some central value with decreasing amplitude. Even though the full process is not steady-state and, generally speaking, is represented by a transient regime, we can numerically evaluate the average of the crack speed, $\bar{v}$, and assess the accuracy of the computations. The computations may, however, be time consuming if we want to examine the process for a wide range of structural parameters.

2.1.5.4 Comparison of force-speed relations

The results of the numerical evaluation of the steady-state crack speed using equation (2.99) in the case $\mu = 2$ in comparison with the theoretical ones produced from the equation (2.65) are summarised in Fig. 2.16a). Supplementary results showing the standard deviation, calculated using (2.100) are given in Fig. 2.16b).

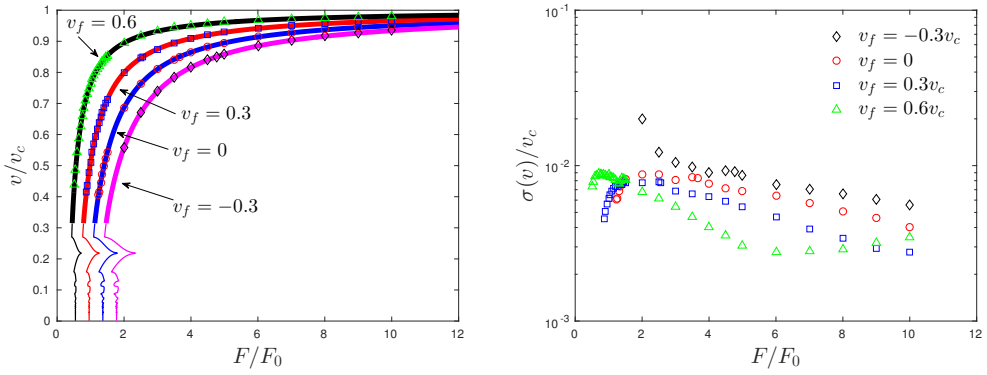

a) b)

Figure 2.16: a) Dependence of the steady-state crack speed for different force magnitude, F, and values $v_f/v_c = -0.3, 0, 0.3, 0.6$ in case $\mu = 2$. Markers correspond to the results from the numerical simulations, as computed by (2.99), whereas the solid lines are the calculations made by formula (2.65). b) presents the standard deviation according to (2.100).

Selecting different strengths of the force, F, and velocity of its location, v_f, we attempt to cover the entire interval of the admissible regime shown in Fig. 2.10 for this case. Numerical results are depicted by markers while their theoretical equivalents are presented by solid lines. Different speeds for the applied force are also considered ($v_f/v_c = -0.3, 0, 0.3, 0.6$).

The results presented in Fig. 2.16a) clearly illustrate that the steady-state regimes predicted by the analytical formulae (2.65) have been attained by the proposed numerical simulations. The results both qualitatively and quantitatively agree within the accuracy estimated by the analysis.

Interestingly, by reducing the speed of the force location, v_f, we were able to cover a wider region on the energy-speed diagram. However, this strategy has a clear limit as the standard deviation, $\sigma(v)$, demonstrates the opposite behaviour, as is clearly seen from Table 2.1, where in the case of $v_f = -0.3v_c$ we observe a dramatic increase in the standard deviation with reduction in F when using the standard geometrical configuration $\mathbb{S}_1$. For lesser values of the force, we could not identify a clear tendency in the crack propagation regime. This, in turn, makes it impossible to provide a justified comparison between the numerical simulations, indicating that the theory requires another analysis.

Selecting different parameters from Table 2.1 was unhelpful in the identification of a limiting steady-state regime. An optimal choice is to consider a fixed force position. In addition to the previous arguments, this would eliminate possible small perturbations related to the movement of the force in the numerical simulation.

The minimum achieved steady-state crack speed that we can prove without any doubt did not not become significantly smaller than the global minimum of G_0/G dependence in Fig. 2.10a), which is observed at $v_* = 0.409v_c$ for $v_f = 0$. On the other hand, the performed theoretical analysis showed a wider range of crack speeds in the admissible region. This observation implies that it may be necessary to take the loading history prior to the steady-state

regime into account. More precisely, we should probably take into account how the system reached the value of G_0/G in Fig. 2.10a). Moreover, in order to check whether there is anything particular about the global minima of G_0/G we performed simulations for several choices of μ and results come further in this section.

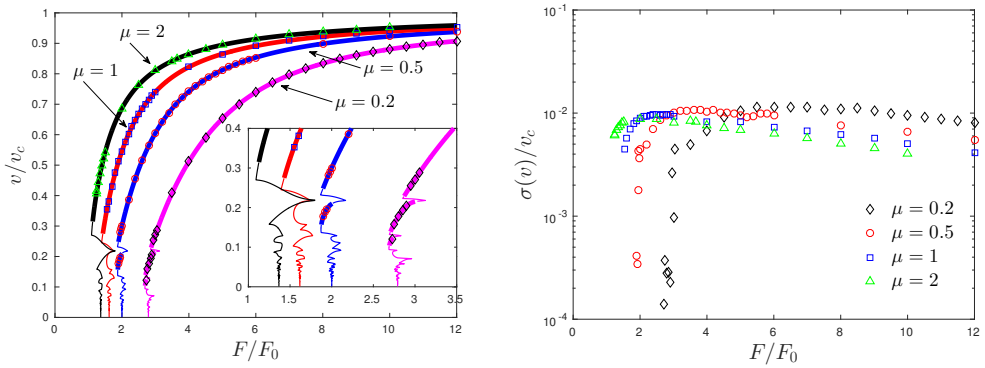

a) b)

Figure 2.17: The results of the numerical simulations in the case of $v_f = 0$ and several choices of c_1: a) Estimations of the steady-state crack speed, where the markers correspond to the calculated values from (2.99) whereas the solid lines are the calculations made by formula (2.65). The thick and normal lines correspond to the admissible and forbidden regimes, respectively. The insert shows zoom of low crack speed region. c) Standard deviation from (2.100) of the estimates of the steady-state crack speed.

In this work we have also varied the spring stiffness c_2 describing the contraction properties of the horizontal and vertical springs. Hence, the value μ was changed. It has been highlighted in Section 2.1.4 that a change in μ led to qualitative changes in the admissible regimes. In Fig. 2.17 we present the results of the evaluation of the steady-state crack speed, v, from the respective numerical simulations as compared with the corresponding analytical data. Here we use the loading-speed relationship instead of the energy-speed

diagram, as the former is characterised by a one-to-one relationship in most of the cases considered.

The simulations show that in the case of a weak interface it is always possible to reach a steady-state regime at low crack speeds. Thus, it is also possible to obtain crack speeds which are less then those of maximizers of G_0/G.

However, for two cases when the vertical links are much weaker than the horisontal ones ($\mu = 0.2$ and $\mu = 0.5$) there exist intervals in the admissible regimes that do not reflect the uniqueness in determination of crack speed. The last can be clearly seen in the insert of Fig. 2.17a). The numerical results presented on this figure were achieved using parameter set $\mathbb{S}_3$ from Table 2.1. With a high level of confidence, the simulations showed that the solutions develop steady-state propagating regimes from few possible predicted admissible steady-state regimes (compare Fig. 2.17a)). However, we have not been unable to identify any rule explaining which regime is preferred, and why. Thus, this question remains open.

2.1.5.5 Comparison of displacement fields

Finally, we point out some particular examples of the displacement profiles from the numerical simulations and compare them with their analytical equivalents. These are shown in Fig. 2.18 and were chosen to illustrate the features of the radiating waves from the moving crack tip. The curves demonstrate the trajectory of a chosen mass that moves from right to left. In the case where $\mu = 0.5$, $F = 1.9F_0$, the waves appearing behind and ahead of the crack tip are observed, while in the second case $\mu = 2$, $F = 1.25F_0$, only waves behind the crack tip were initiated. Both computations were made with a fixed force position ($v_f = 0$). As it is seen from the presented plots, there is a good agreement between the predicted theoretically displacements and those attained by means of numerics. Thus, the comparison of displacement can be treated as an additional marker of a steady-state regime.

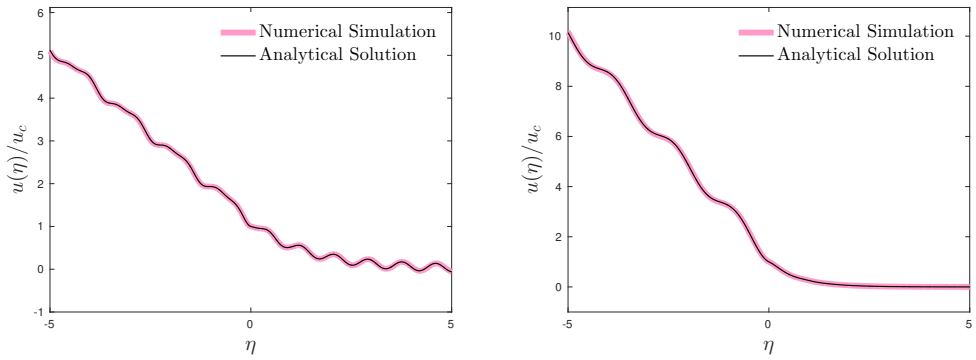

a) b)

Figure 2.18: The comparison of displacement fields for a fixed load ($v_f = 0$): a) $\mu = 0.5$, $F = 1.9F_0$, $v = 0.178v_c$, b) $\mu = 2$, $F = 1.25F_0$, $v = 0.414v_c$.

2.2 Chain with non-local interactions

2.2.1 Problem formulation

Let us consider a discrete model with non-local interactions represented by a chain of masses and analyse the crack propagation in the structure presented in Fig. 2.19. Additionally to the notations that were utilised for a chain problem in Section 2.1.2 there is one parameter that captures non-local interactions. We add linear springs of stiffnesses c_3 between second neighbour interactions. The other quantities are the same: M is the mass, c_1 is the stiffness of the springs between oscillators and a rigid foundation, c_2 is the spring constant of the links between neighbouring oscillators, F is the magnitude of an external force, n_f is the position of the force, n_* is the position of the crack tip. The equilibrium distance between oscillators is a.

Linearised equations of motion for the mechanical system under consid-

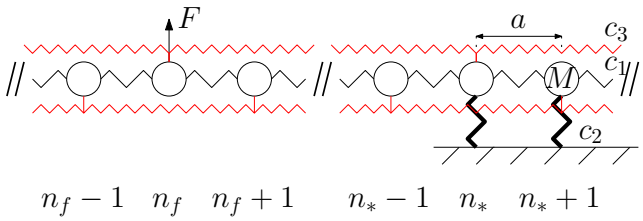

Figure 2.19: Chain of oscillators with equal masses M connected together by linear springs of stiffness c_1 (normal lines) and to the rigid foundation with springs of stiffness c_2 (thick lines). Non-local interactions are modelled by second-neighbour interactions with linear springs c_3 (red color). The crack position is defined by an oscillator with index n_*. The force F and n_f is its position. The vertical springs of stiffness c_2 consequently break as the crack moves. a is an equilibrium distance between the oscillators.

eration take the form:

$$\begin{aligned} M\frac{d^2u_n}{dt^2} &= c_3(u_{n+2} + u_{n-2} - 2u_n) + c_1(u_{n+1} + u_{n-1} - 2u_n) - c_2u_n, \quad n \geq n^*, \\ M\frac{d^2u_n}{dt^2} &= c_3(u_{n+2} + u_{n-2} - 2u_n) + c_1(u_{n+1} + u_{n-1} - 2u_n) - F\delta_{nn_f}, \quad n < n^*. \end{aligned} \tag{2.102}$$

The fracture criterion remains in the same form as in the previous sections: In the presented configuration, we assume that the crack propagates from the left to the right. The displacement at the crack tip is subjected to a deformation fracture criterion given in the following form:

$$\begin{aligned} u_{n_*}(t_*) &= u_c, \\ u_n(t) &< u_c, \quad n > n_*(t), \end{aligned} \tag{2.103}$$

where u_c is a constant, t_* is a fracture time. The second condition is consistent with the assumption that the crack tip can be uniquely defined by index n_*. The force position moves with a constant speed v_f:

$$n_f(t) = n_f(0) + \frac{v_f}{a}t, \quad v_f = const. \tag{2.104}$$

The contrasts in elastic properties are defined as:

$$\mu = \frac{c_2}{c_1 + 4c_3}, \quad \nu_1 = \frac{c_1}{c_1 + 4c_3}, \quad \nu_2 = \frac{c_3}{c_1 + 4c_3}. \tag{2.105}$$

The value of a critical speed is influenced by the introduced non-local interaction. It becomes:

$$v_c^2 = \frac{c_2 + 4c_3}{M}. \tag{2.106}$$

In the further analysis the normalisation of speeds is applied according to (2.20). For the further consideration of the problem it is useful to define the dispersion relations.

2.2.2 Dispersion relations

The analysis of the dispersion relations repeats the one in Section 2.1.2.2. However, the equations of motion should be changed in accordance with (2.102). The intact part of the chain in Fig. 2.19 far from a crack tip is described by the following equation:

$$M\ddot{u}_n^{(1)}(t) = c_3(u_{n+2} + u_{n-2} - 2u_n) + c_1(u_{n+1} + u_{n-1} - 2u_n) - c_2 u_n,$$

whereas the equations for the broken part of the chain far from a crack tip are:

$$M\ddot{u}_n^{(2)}(t) = c_1(u_{n+2}^{(2)}(t) + u_{n-2}^{(2)}(t) - 2u_n^{(2)}(t)).$$

The solution of these problems is sought in the form:

$$u_n^{(j)}(t) = u_0^{(j)} e^{i(kn + \omega_j t)}, \quad j = 1, 2,$$

where k is a dimensionless wave number, ω is a frequency and $u_0^{(j)} = const \neq 0, j = 1, 2$. Plugging the solution $u^{(j)}$ into the corresponding governing equations give:

$$\begin{gathered} \omega_1^2(k) = 4\nu_2 v_c^2 \sin(k) + 4\nu_1 v_c^2 \sin\left(\frac{k}{2}\right) + \omega_0^2, \quad \omega_0^2 = \frac{c_2}{M} \\ \omega_2^2(k) = 4\nu_2 v_c^2 \sin(k) + 4\nu_1 v_c^2 \sin\left(\frac{k}{2}\right), \end{gathered} \tag{2.107}$$

where μ, ν_1, ν_2 are contrasts from (2.105). The plots of dispersion relations are presented in Fig.2.20 for two sets of parameters. As it can be seen, there are some changes of dispersion diagrams. Hence, several peculiarities can be expected due to introduced non-local springs.

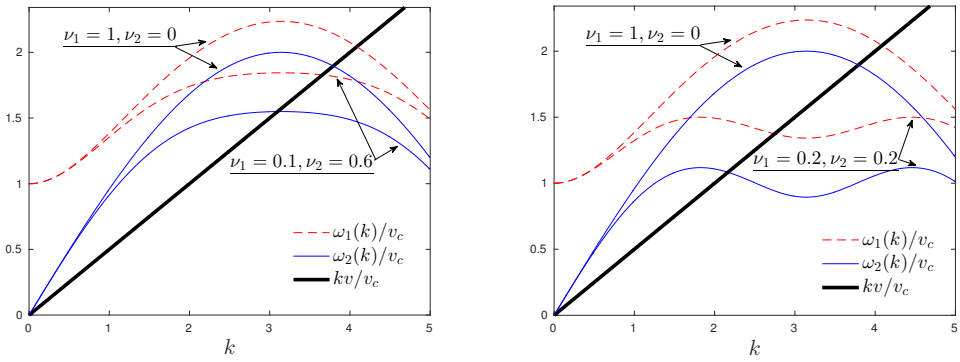

a) b)

Figure 2.20: Dispersion diagram of a chain with non-local interactions for different contrasts, $\mu = 1$ and $v = 0.5v_c$: a) comparison of classical case ($\nu_2 = 0$) and case $\nu_1 = 0.6, \nu_2 = 0.1$, b) comparison of classical case and case $\nu_1 = 0.2, \nu_2 = 0.2$. The dispersion relationships $\omega_{1,2}(k)$ are given in (2.107).

2.2.3 Solution of the problem

The scheme of the solution derivation is the same as in Section 2.1.2 and only the key-points are reproduced. We start with the assumption on the steady-state which allows to consider the problem in a moving frame with constant speed v (normalised by a as in (2.20)):

$$\eta = n - (n_*(0) + vt), \quad v < v_c. \tag{2.108}$$

With the introduced variable η equations of motion in (2.102) are modified:

$$\begin{aligned} M\left(\frac{\partial^2}{\partial t^2} - 2v\frac{\partial^2}{\partial t \partial \eta} + v^2\frac{\partial^2}{\partial \eta^2}\right)u(\eta,t) \\ = c_3(u(\eta+2,t) + u(\eta-2,t) - 2u(\eta,t)) \\ +c_1(u(\eta+1,t) + u(\eta-1,t) - 2u(\eta,t)) - c_2 u(\eta,t)H(\eta) \\ +F\delta(\eta + n_0 + (v-v_f)t), \end{aligned} \tag{2.109}$$

where $H(\eta)$ is the Heaviside function and $n_0 = n_f(0) - n_*(0)$. To obtain the solution to this reformulated problem we apply Fourier and Laplace transforms which leads to the equation:

$$\begin{aligned} L(k,s)U^+(k,s) + U^-(k,s) \\ = \frac{Fe^{-ikn_0}}{M}\frac{1}{s+ik(v-v_f)}\frac{1}{(s+ikv)^2+\omega_2^2(k)}, \end{aligned} \tag{2.110}$$

where:

$$U(k,s) = \int_0^\infty \left[\int_{-\infty}^\infty u(\eta,t)e^{ik\eta}d\eta\right] e^{-st}dt = U^+(k,s) + U^-(k,s),$$
$$U^\pm(k,s) = \int_0^\infty \left[\int_{-\infty}^\infty u(\eta,t)H(\pm\eta)e^{ik\eta}d\eta\right] e^{-st}dt.$$

The function $L(k,s)$ is defined:

$$L(k,s) = \frac{(s+ikv)^2+\omega_1^2(k)}{(s+ikv)^2+\omega_2^2(k)},$$

where $\omega_{1,2}(k)$ are presented in (2.107). From this point the analysis repeats the one given in Section 2.1.2. The limiting case for a steady-state regime provides the following kernel function:

$$L(k) = \frac{(0+ikv)^2+\omega_1^2(k)}{(0+ikv)^2+\omega_2^2(k)}. \tag{2.111}$$

Steady-state displacement $u(\eta)$ and its Fourier transform is:

$$u(\eta) = \lim_{t\to\infty} u(\eta,t), \quad U(k) = \int_{-\infty}^\infty u(\eta)e^{ik\eta}\,dk.$$

The solution of the corresponding Wiener-Hopf problem is:

$$U^+(k) = \frac{u_c}{0 - ik}\frac{1}{L^+(k)}, \quad U^-(k) = \frac{u_c}{0 + ik}L^-(k). \tag{2.112}$$

The function $L(k)$ has been factorised with the help of Cauchy-type integral in the same way as in (2.32). These factors have the following behaviour at infinity:

$$L^\pm = 1 \pm i\frac{Q}{k} + O\left(\frac{1}{k^2}\right), \quad k \to \infty, \quad Q = \frac{1}{\pi}\int_0^\infty \log|L(k)|\,dk, \tag{2.113}$$

and at zero:

$$\begin{gathered} L^\pm = \frac{\omega_0}{\sqrt{v_c^2 - v^2}}\frac{R^{\pm 1}}{0 \mp ik}(1 + (1 \mp ik)S) + O(k), \quad k \to 0, \\ R = \exp\left(\frac{1}{\pi}\int_0^\infty \frac{\mathrm{Arg}L(k)}{k}\,dk\right), \quad S = \frac{1}{\pi}\int_0^\infty \frac{\log|L(k)|}{k^2}\,dk. \end{gathered} \tag{2.114}$$

The displacement $u(\eta)$ can be defined in terms of the inverse Fourier transform:

$$u(\eta) = \frac{1}{2\pi}\int_{-\infty}^{\infty} U^\pm e^{-ik\eta}\,dk, \quad \pm\eta > 0. \tag{2.115}$$

The estimated behaviour of functions $L^\pm(k)$ in (2.113) and (2.114) with the known terms $U^\pm(k)$ give:

$$\begin{gathered} u(\eta) = u_c(1 - Q\eta) + O(\eta^2), \quad \eta \to 0, \\ u(\eta) = -\frac{u_c}{R}\frac{\omega_0}{\sqrt{v_c^2 - v^2}}(\eta - S) + O(1), \quad \eta \to -\infty. \end{gathered} \tag{2.116}$$

Again, the wave ahead of the crack tip can be expected for some values of crack speed. The relation between the loading parameters, F, v_f, the geometry of the problem, and the steady-state crack speed, v are remained in the form of (2.65):

$$\frac{F}{F_0} = \frac{v_c}{\omega_0 R}\frac{v_c - v_f}{v_c - v}\sqrt{\frac{v_c^2 - v^2}{v_c^2}}, \quad F_0 = c_2 u_c, \tag{2.117}$$

where v_c is a critical speed from (2.106), ω_0 is defined in (2.107) and R is shown in (2.114). The last parameter defines the energetic properties of the process. It defines the ratio of local energy release rate, G_0, and global energy release rate, G:

$$\frac{G_0}{G} = R^2, \quad G_0 = \frac{c_2 u_c^2}{2a}. \tag{2.118}$$

2.2.4 Note on the function behaviour

In the presented section the form of function $L(k)$ is the same as the one in the problem of a dynamic chain problem from Section 2.1.2. However, the dispersion relations $\omega_{1,2}(k)$ from (2.107) are different. Thus, the asymptotic behaviour of function $L(k)$ should be corrected accordingly. Despite of this fact it is only enough to update the behaviour of function $L(k)$ at zero. It becomes:

$$\begin{aligned} L(k) &= \frac{\delta_1}{k^2} + 1 + \delta_2 + \delta_3 k^2 + O(k^3), \quad k \to 0, \\ \delta_1 &= \frac{\omega_0^2}{v_c^2 - v^2}, \quad \delta_2 = \frac{\delta_1^2}{\mu}\left(\frac{4}{3}\nu_2 + \frac{1}{12}\nu_1\right), \\ \delta_3 &= \frac{\delta_1 \delta_2}{12\mu}\left(16\nu_2 + \nu_1\right) - \frac{\delta_1^2}{\mu}\left(\frac{8}{45}\nu_2 + \frac{1}{360}\nu_1\right). \end{aligned}$$

The contrasts μ, ν_1, ν_2 are given in (2.105) and the dispersion relations, related to the function $L(k)$, are found in (2.107). Then, with the notations in Section 2.1.3 everything keeps the same.

2.2.5 Solution analysis

The evaluation of displacement field was performed by means of developed and implemented algorithms shown in Section A.1 and Section A.2 from Appendix. In this section the investigation of effects of introduced non-local interactions is performed. For the results presented in this section the value of critical speed v_c is kept to be same. In other words, by means of different

combinations of parameters ν_1 and ν_2 in (2.105) can provide the same value of v_c.

The results for the displacements are displayed. For such case the value of crack speed $v = 0.32v_c$ was chosen. This value is definitely belongs to the range of admissible regimes when there are only closest interactions ($\nu_2 = 0$). The plots are shown in Fig. 2.21 for $\mu = 0.5$ and $\mu = 1$.

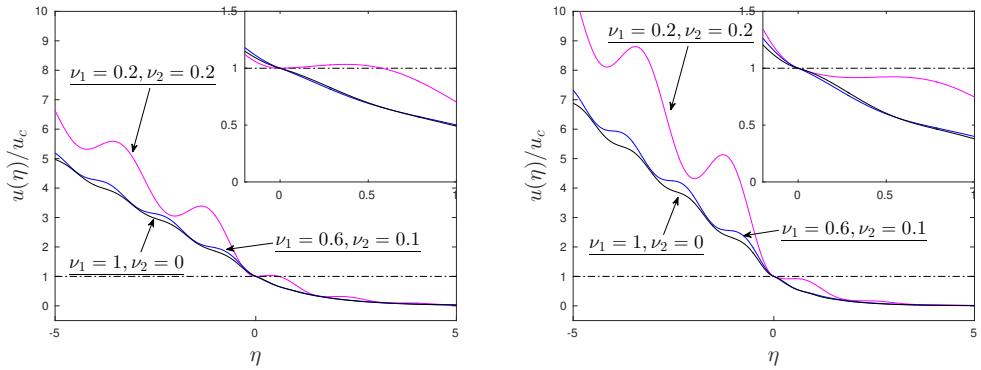

Figure 2.21: Displacement field $u_0(\eta)$ at $v = 0.32v_c$ and different values of contrasts from (2.105) : a) $\mu = 0.5$, b) $\mu = 1$. The inserts show a zoom of the displacement profile in the neighbourhood of the crack tip. The dash-dot line shows the level of displacement $u(\eta) = u_c$.

First thing to notice is that the inclination angle formed behind a crack tip is growing with an increase of μ. It can be seen by comparison of two plots in Fig. 2.21. This can be explained by the fact that the stored energy released just before fracture increases together with μ.

Next, the low values of ν_2 seems do not cause a great change in the displacement fields, at least for the presented examples. Indeed, the significant change in displacements is observed for significant stiffness of non-local interaction in comparison with the one of closest neighbour interactions.

Moreover, there is also an important qualitative difference. The value of

crack speed corresponds to an admissible regime for a case $\nu_2 = 0$ and for both $\mu = 0.5$ and $\mu = 1$. However, with the introduced strong non-local interactions this regime of crack propagation becomes forbidden as it is seen for a case $\nu_1 = \nu_2 = 0.2$ in Fig. 2.21a).

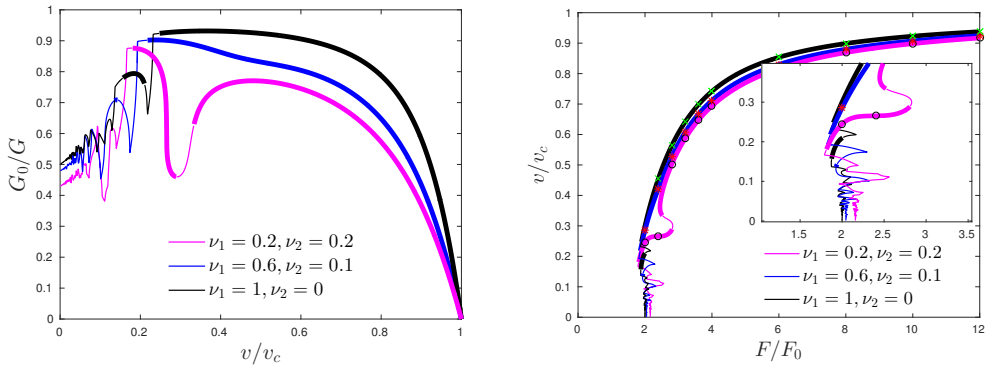

a) b)

Figure 2.22: Admissible (thick lines) and forbidden (normal lines) regimes of crack propagation for $\mu = 0.5$ and different parameters ν_1 and ν_2 in terms of a) dependence of the ERR ratio G_0/G on the normalised crack speed v/v_c ,b) dependence of normalised crack speed v/v_c on normalised force F/F_0. The insert shows the zoom of region of low crack speeds and the markers show the results from the numerical simulations.

At this point it is useful to switch to the analysis of the energy release rate and the force as functions of crack speed. These dependences are given in (2.117) and (2.118). For the demonstration of results value $v_f = 0$ has been chosen and most the attention is focused on the effect of the model parameters.

The displacement field was analysed for a range of values of the crack speeds. The solution was separated into two categories: admissible and forbidden regimes. Such investigation is made in the same way as it was done for a chain with local interactions only in Section 2.1.2. The numerical sim-

ulation has also been performed in the way similar to the one described in section 2.1.5 in order to validate the derived formulae.

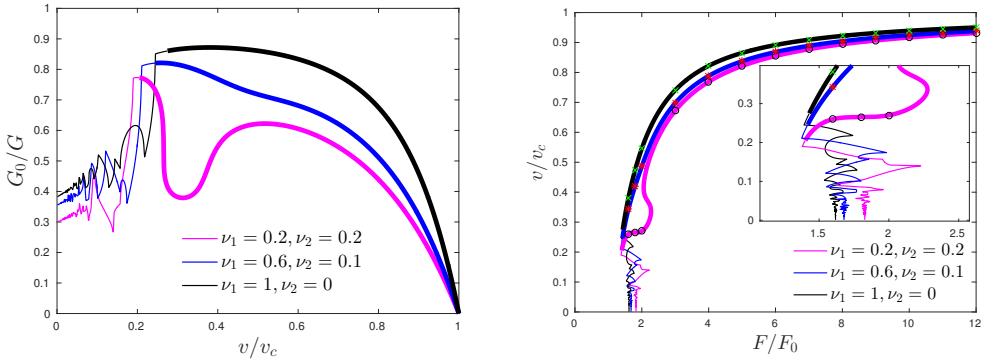

a) b)

Figure 2.23: Admissible (thick lines) and forbidden (normal lines) regimes of crack propagation for $\mu = 1$ and different parameters ν_1 and ν_2 in terms of a) dependence of the ERR ratio G_0/G on the normalised crack speed v/v_c, b) dependence of normalised crack speed v/v_c on normalised force F/F_0. The insert shows the zoom of region of low crack speeds and the markers show the results from the numerical simulations.

The dependences of G_0/G and F/F_0 on normalised crack speed are displayed in Fig. 2.22a) and Fig. 2.22b). Looking at the dependence of G_0/G it could be seen that there is a tendency in decrease of the values of this function with increase of ν_2. However, it is not observed within the whole interval of crack speed and mostly noticed within the intermediate values of v/v_c (see Fig. 2.22a)). Meanwhile, there is a clear trend in decrease of F/F_0 for a chosen v/v_c with increase of μ. The last argument can be spotted in Fig. 2.22b).

Additionally, the advance of non-local interaction is reflected on the behaviour of the dependences in Fig. 2.22. Particularly, for strong non-local interactions, $\nu_2 = 0.2$, there has been developed a drop in G_0/G with a

smooth minimum for intermediate values of crack speed which can be seen in Fig. 2.22a). This change in the behaviour of G_0/G adds to its non-monotonicity and, hence, to the uncertainty in the choice of established crack speed. This problem has been partly resolved by the plots of force-speed dependences for the case of local interactions. But it turns out that with strong non-local interactions the non-unique choice of crack speed remains to be a question. The last point is vividly seen in the insert of Fig. 2.22b).

The solution admissibility is also affected in a certain way with the change in stiffness of non-local springs. Firstly, with an increase of ν_2 the admissible regimes for small values of crack speed start to disappear. Indeed, the range of admissible crack speeds at $v \approx 0.2v_c$, that has been achieved with numerical simulations as well (see Section 2.1.5.4), considerably shrinks for case $\nu_1 = 0.6, \nu_2 = 0.1$ and vanishes for case $\nu_1 = 0.2, \nu_2 = 0.2$. This is also explicitly shown in the insert of Fig. 2.22b). Another drastic change in admissible regimes is that for $\nu_1 = 0.2, \nu_2 = 0.2$ the forbidden regimes come out for the intermediate range of values of crack speed. These forbidden regimes are located in the "valley" of G/G_0 in Fig. 2.22a).

The same analysis of the solution is performed for the case of $\mu = 1$, i.e. for the higher stiffness of springs that are subjected to failure. The plots for G_0/G and F_0/F are shown in Fig. 2.23. In these figure the same patterns concerning the change in ν_2 can be detected as for the case of $\mu = 0.5$.

The intervals of admissible and forbidden regimes for case $\mu = 1$ turn out to be different from case $\mu = 0.5$. The major contrast is that there are no admissible regimes at low crack speeds which is shown in Fig. 2.23b). The existed range of forbidden regimes in the intermediate values of crack speed for $\mu = 0.5, \nu_1 = \nu_2 = 0.2$ disappears in the case $\mu = 1$. But still the non-monotonic behaviour of F/F_0 within the admissible regimes remains. This suggests that the alternative analysis should be proposed to get determined dependences between loading parameters, model parameters and crack speed.

2.3 Dissimilar chain problem

2.3.1 Static problem.

In order to demonstrate the effect of lattice trapping it is useful to start with an analysis of a static problem. The solution to this problem is much easier to obtain then in the dynamic case. Hence, we consider a static problem of a fracture of double chain displayed in Fig.2.24.

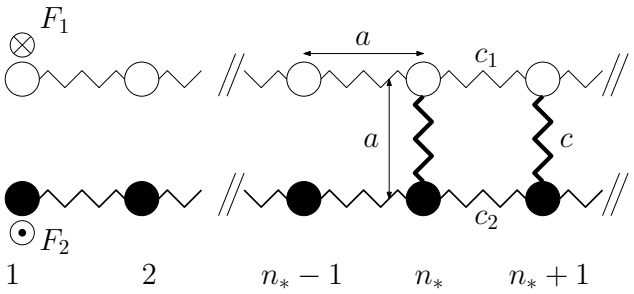

Figure 2.24: Double chain of dissimilar oscillators with c_1, c_2 being spring constants, respectively. Two chains are connected together by linear springs with stiffness c starting from oscillators with index n_* which represents a crack tip.

Here, c_1, c_2 - spring constants between the oscillators of the same kind, i.e. stiffnesses in horizontal directions. The oscillators in each chain are numbered with indices n. The masses with the same index $n \geq n_*$ are connected with each other by the linear springs of stiffness c. The external forces are defined F_1 and F_2. In spite of the necessary equilibrium condition which leads to $F_1 = F_2$, we derive that equality independently. It is handy to introduce the following notations for a problem description:

$$\mu_{1,2} = \frac{c}{c_{1,2}}, \quad \alpha = \mu_1 + \mu_2, \quad \beta = \mu_1 - \mu_2. \tag{2.119}$$

The displacements of the chains are defined u_n for a top chain and w_n. It is possible to split the analysis to the separate study of the broken and

intact parts. We start with the consideration of an intact part of a structure, $n \geq n_*$:

$$\begin{aligned} c_1(u_{n+1} + u_{n-1} - 2u_n) - c(u_n - w_n) = 0, \\ c_2(w_{n+1} + w_{n-1} - 2w_n) + c(u_n - w_n) = 0. \end{aligned} \quad n \geq n_*, \tag{2.120}$$

The solution of these equation can be, equivalently, presented for the linear combinations of u_n and w_n. For this, we consider functions ψ_n and ϕ_n given by relations:

$$\psi_n = u_n - w_n, \quad \phi_n = u_n + w_n. \tag{2.121}$$

Notice, that the function ψ_n describes the force in the springs of stiffness c between the corresponding masses for $n \geq n_*$ and crack opening for $n < n$. Equations (2.120) can be then presented in terms of ψ_n and ϕ_n:

$$\begin{aligned} \psi_{n+1} + \psi_{n-1} - (2 + \alpha)\psi_n = 0, \\ \phi_{n+1} + \phi_{n-1} - 2\phi_n = \beta\psi_n. \end{aligned} \quad n \geq n_* \tag{2.122}$$

At the crack tip, $n = n_*$, the fracture condition should be also imposed. In this case we set a deformational criterion:

$$\psi_{n_*} = \epsilon_c, \tag{2.123}$$

where ϵ_c is some material parameter that reflects toughness of a single element of a structure. Moreover, the solution is supposed to be zero at $n \to \infty$. The solutions of equations (2.122) are sought in the form:

$$\psi_n = \epsilon_c \lambda^{n-n_*}, \quad \phi_n = \epsilon_c \frac{\beta}{\alpha} \lambda^{n-n_*}, \quad n \geq n_*, \tag{2.124}$$

with factor $|\lambda| < 1$ in order to achieve the decaying solution at $n \to \infty$. The choice for ϕ_n in (2.124) reduces the equation for this function in (2.122) for the one of ψ_n. The substitution of these forms of solution (2.124) into (2.122) provides an equation for λ:

$$\lambda^2 - (2+\alpha)\lambda + 1 = 0.$$

The last equation has two roots. Between them only one should be taken that deliver a required condition on λ and support a decreasing displacement field at $n \to \infty$. This root is:

$$\lambda = \frac{\sqrt{4+\alpha} - \sqrt{\alpha}}{\sqrt{4+\alpha} + \sqrt{\alpha}}. \tag{2.125}$$

Now, the equations for the broken part of structure is given by:

$$\begin{aligned} &c_1(u_2 - u_1) + F_1 = 0, \quad c_2(w_2 - w_1) - F_2 = 0, \quad n = 1, \\ &c_1(u_{n+1} + u_{n-1} - 2u_n) = 0, \\ &c_1(w_{n+1} + w_{n-1} - 2w_n) = 0. \end{aligned} \quad 1 < n < n_*, \tag{2.126}$$

The solution can be written directly due to its special structure:

$$u_n = \frac{F_1}{c_1}(n_* - n) + u_0, \quad w_n = -\frac{F_2}{c_2}(n_* - n) + w_0, \quad 1 \le n < n_*,$$

where u_0, w_0 are the values of displacements at a crack tip. From this we conclude that:

$$\begin{aligned} \psi_n &= \left[\frac{F_1}{c_1} + \frac{F_2}{c_2}\right](n_* - n) + \epsilon_c, \\ \phi_n &= \left[\frac{F_1}{c_1} - \frac{F_2}{c_2}\right](n_* - n) + \epsilon_c \frac{\beta}{\alpha^2}, \end{aligned} \quad n < n_*. \tag{2.127}$$

Although the formal solution is derived, we still need to obtain the relations between the forces that cause the fracture and material properties. For that we consider the equations at $n = n_*$ which in terms of ψ_n and ϕ_n are:

$$\begin{aligned} (\psi_{n_*-1} - \psi_{n_*}) + (\psi_{n_*+1} - \psi_{n_*}) - \alpha\psi_{n_*} = 0, \\ (\phi_{n_*-1} - \phi_{n_*}) + (\phi_{n_*+1} - \phi_{n_*}) - \beta\psi_{n_*} = 0. \end{aligned}$$

Utilising the derived solutions in (2.124), (2.127) and the governing equation for λ we arrive at:

$$\frac{F_1}{c_1} + \frac{F_2}{c_2} = \epsilon_c\left(\frac{1}{\lambda} - 1\right), \quad \frac{F_1}{c_1} - \frac{F_2}{c_2} = \epsilon_c\frac{\beta}{\alpha}\left(\frac{1}{\lambda} - 1\right).$$

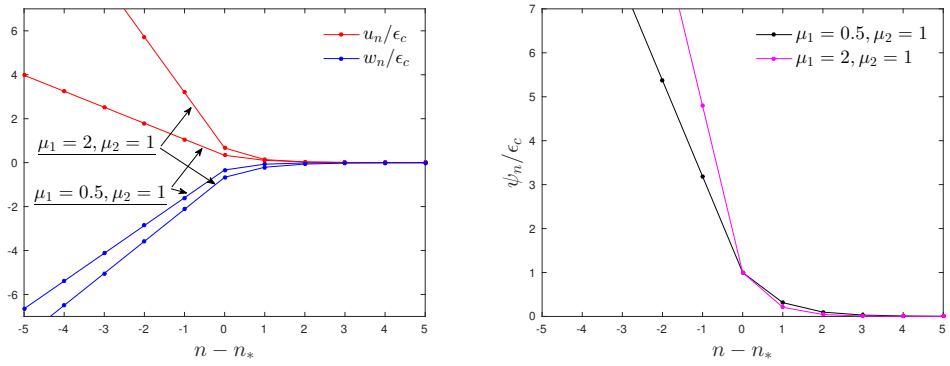

a) b)

Figure 2.25: a) Displacements of the chains for two sets of parameters, b) corresponding function ψ_n for the same sets of parameters.

The last set of equations finally allows to determine the dependences of forces:

$$\begin{gathered} F_1 = F_2 = F, \\ \frac{F}{F_0} = \frac{1}{\mu_1 + \mu_2}\left(\frac{1}{\lambda} - 1\right), \quad F_0 = c\epsilon_c. \end{gathered} \tag{2.128}$$

Here, F_0 is a static force required to break the structure compounded from the two masses connected by a spring of stiffness c. So, the relations (2.121), (2.124), (2.125), (2.127) and (2.128) solve the problem. The displacements for two particular cases are shown in Fig. 2.25.

Global energy release rate G can be computed by consideration of change in potential energy of the structure when the crack advances by a unite value length a. It is enough to consider the change in potential energy while a crack progresses, which is a difference between the work of forces on the change of displacements and elastic energies in the broken part of a structure. The energy release rate G, then, can be computed from the following equation:

$$G = \frac{1}{2a}F_1(u_{n_*-1} - u_{n_*}) - \frac{1}{2a}F_2(w_{n_*-1} - w_{n_*}) = \frac{F_1^2}{2ac_1} + \frac{F_2^2}{2ac_2}$$

The substitution of (2.128) into the last equation results in:

$$G = \frac{G_0}{\mu_1 + \mu_2}\left(\frac{1}{\lambda} - 1\right)^2, \quad G_0 = \frac{\epsilon_c^2 c}{2a}. \tag{2.129}$$

Quantity G_0 is the local energy release rate which is equal to the amount of the released energy when the failure of structure of two masses and spring of stiffness c happens related to a cell of size a. This quantity is adjacent two the one for the force F_0.

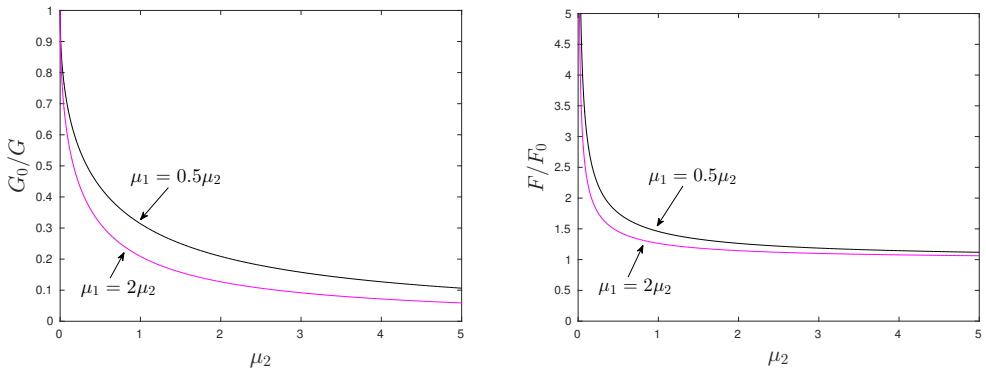

a) b)

Figure 2.26: a) Energy release rate ratio G_0/G for two sets of the parameters, b) force ratio F/F_0 for the same sets of parameters.

The plots for the ratios G_0/G and F/F_0 are presented in Fig. 2.26 for two sets of material parameters. The attention should be paid to the fact that for any set of parameters, not only those that were depicted, we observe $G_0/G < 1$ and $F/F_0 > 1$ which illustrates lattice trapping. Particularly, this effect demonstrates that in the force required to break such a discrete structure exceeds the force required to break its single element separately from the structure. That is a feature of a discrete model which is not observed in the analysis of continuum solids. It shows that at microlevel analysis of the material a special analysis is required. With this remark we turn to the

analysis of a steady-state crack movement and, consequently, the contribution of inertia.

2.3.2 Dynamic problem

Let us consider a structure of a double chain of dissimilar oscillators fig.2.27. The parameters of the model are: m_1, m_2 - masses of upper and lower chains, respectively, c_1, c_2 spring constants between the oscillators of the same sort. The oscillators in each chain are numbered with indices n. The masses with the same index $n \geq n_*$ are connected with each other by the linear springs of stiffness c. There are external forces F_1, F_2 applied to upper and lower chains, correspondingly.

$$\begin{aligned} m_1\frac{d^2u_n(t)}{dt^2} &= c_1(u_{n+1}(t)+u_{n-1}(t)-2u_n(t))+F_1\delta_{nn_1^f}, \\ m_2\frac{d^2w_n(t)}{dt^2} &= c_2(w_{n+1}(t)+w_{n-1}(t)-2w_n(t))-F_2\delta_{n_2^f}, \end{aligned} \qquad n<n^*,$$

$$\begin{aligned} m_1\frac{d^2u_n(t)}{dt^2} &= c_1(u_{n+1}(t)+u_{n-1}(t)-2u_n(t))+c(w_n(t)-u_n(t)), \\ m_2\frac{d^2w_n(t)}{dt^2} &= c_2(w_{n+1}(t)+w_{n-1}(t)-2w_n(t))+c(u_n(t)-w_n(t)), \end{aligned} \qquad n\geq n_*. \tag{2.130}$$

Note that without posing initial conditions, which appears to be the case of a steady-state process, the solution can be determined up to a random constant. The oscillators with index $n_* = n_*(t)$ represent a crack tip. The movement of the crack is a result of the breakage of the respective link $n_* = n_*(t)$ at the corresponding moment $t = t_*$ such that the following conditions are valid:

$$u_{n_*} - w_{n_*} = \epsilon_c, \quad u_n(t_*) - w_n(t_*) < \epsilon_c, \quad n > n_*, \tag{2.131}$$

where $\epsilon_c = const$ is a strength quantity of the springs of stiffness c. Both chains separately have characteristic speeds of sounds that limit the signal

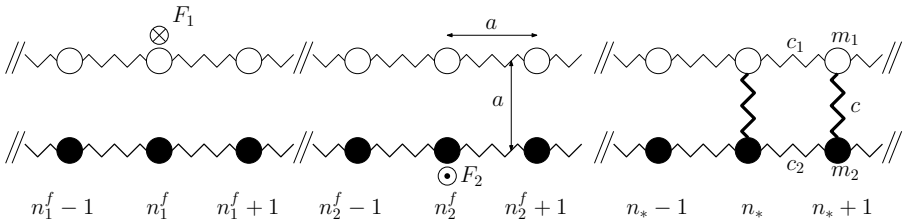

Figure 2.27: Double chain of dissimilar oscillators with c_1, c_2 being spring constants, m_1, m_2 being masses of oscillators from upper and lower chains, respectively. Two chains are connected together by linear springs with stiffness c starting from oscillators with index n_* which represents a crack tip.

propagation within the chains. Their values, normalised by equilibrium distance a, are:

$$v_j^2 = \frac{c_j}{m_j}, \quad j = 1, 2. \tag{2.132}$$

For a sake of convenience, we introduce following notations:

$$\beta_j^2 = \frac{c}{m_j} = \mu_j v_j^2, \quad j = 1, 2, \tag{2.133}$$

which involve the contrasts of spring constants in (2.119). The positions of the forces may change according to the following rules:

$$n_j^f(t) = v_j^f t, \quad j = 1, 2, \tag{2.134}$$

which should also be rounded to the integer number and $v_j^f, j = 1, 2$ are the velocities of top and bottom forces,respectively.

2.3.2.1 Formulation of the problem in terms of Fourier transform

We assume that starting from some moment of time a crack speed can be approximated by constant speed v. There are two quantities with respect to which there are differences in a crack propagation regimes:

$$\begin{gathered} v_c = \min\{v_1, v_2\}, \\ v_* = \frac{c_1 + c_2}{m_1 + m_2} = \frac{\beta_2^2}{\beta_1^2 + \beta_2^2} v_1^2 + \frac{\beta_1^2}{\beta_1^2 + \beta_2^2} v_2^2. \end{gathered} \tag{2.135}$$

The constant v_c reflects the crack speed when the changes of fracture processes can be detected. The other speed, v_*, equals to a speed of sound in the intact part of the structure in Fig. 2.27. Notice, that in the case $v_1 = v_2$ there is a limiting value of crack propagation, $v < v_c$, and $v_c = v_*$. Otherwise, the crack movement can exceed v_c. Also, $v_c < v_* < \max v_1, v_2$ which implies that various combinations of material properties and crack propagation regimes are expected within different values of crack speeds. The peculiarities of the problem are discussed further.

We study the steady-state solution and, for that reason, displacements $u_n(t), w_n(t)$ may be expressed as functions of the new variable:

$$\eta = n - n_*(t) = n - n_0 - vt, \tag{2.136}$$

where n_0 is a distance between the origin of laboratory coordinate system and a moving frame at time when the oscillations of a crack speed may be neglected. Variable η is assumed to be continuous. We assume that the displacement of the oscillators may be expressed as:

$$u_n(t) = u(\eta, t), \quad w_n(t) = w(\eta, t). \tag{2.137}$$

In this dynamic case it is also convenient to consider linear combinations of the displacements. Thus, we define:

$$\psi(\eta, t) = u(\eta, t) - w(\eta, t), \quad \phi(\eta, t) = u(\eta, t) + w(\eta, t). \tag{2.138}$$

Function $\psi(\eta, t)$ defines a crack opening at the broken part of the structure, $\eta < 0$, and it equals to an elongation of a spring between 2 chains in the intact part of the structure, $\eta > 0$. The stated fracture criterion becomes:

$$\psi(0, t) = \epsilon_c, \quad \psi(\eta, t) = \epsilon_c, \quad \eta > 0. \tag{2.139}$$

Moreover, we impose an additional condition to avoid a rigid body motion:

$$\frac{\partial}{\partial t}\phi(\eta, t) = 0, \quad t \to \infty. \tag{2.140}$$

For the steady-state crack motion the equations of motion (2.130) become:

$$\begin{gathered} m_1\left(\frac{\partial^2}{\partial t^2}-2v\frac{\partial^2}{\partial t\partial\eta}+v^2\frac{\partial^2}{\partial\eta^2}\right)u(\eta,t)= \\ c_1(u(\eta+1,t)+u(\eta-1,t)-2u(\eta),t) \\ -c(u(\eta,t)-w(\eta,t))H(\eta)+F_1\delta(\eta+n_2+(v-v_1^f)t), \\ m_2\left(\frac{\partial^2}{\partial t^2}-2v\frac{\partial^2}{\partial t\partial\eta}+v^2\frac{\partial^2}{\partial\eta^2}\right)w(\eta,t)= \\ c_2(w(\eta+1,t)+w(\eta-1,t)-2w(\eta),t) \\ +c(u(\eta,t)-w(\eta,t))H(\eta)-F_2\delta(\eta+n_1+(v-v_2^f)t), \end{gathered} \tag{2.141}$$

where $H(x)$ is the Heaviside step function, $\delta(x)$ is the Dirac delta function and $n_j, j=1,2$ are the distances between the crack tip and top and bottom forces, respectively, at the beginning of the steady-state motion. The consequent application of the Fourier transform and Laplace transform (with the terms from initial conditions being omitted as irrelevant in a limiting case $t\to\infty$):

$$\begin{aligned} \left[(s+ikv)^2+\omega_1^2(k)\right]U(k,s) &= -\beta_1^2\Psi^+(k,s)+\frac{F_1}{m_1}\frac{e^{-ikn_0}}{s+ik(v-v_1^f)}, \\ \left[(s+ikv)^2+\omega_2^2(k)\right]W(k,s) &= \beta_2^2\Psi^+(k,s)-\frac{F_2}{m_2}\frac{e^{-ikn_0}}{s+ik(v-v_2^f)}. \end{aligned} \tag{2.142}$$

The notations have been introduced:

$$\begin{aligned} U(k,s) &= \int_0^\infty\left(\int_{-\infty}^\infty u(\eta,t)e^{ik\eta}\,d\eta\right)e^{-st}\,dt, \\ W(k,s) &= \int_0^\infty\left(\int_{-\infty}^\infty w(\eta,t)e^{ik\eta}\,d\eta\right)e^{-st}\,dt, \\ \Psi(k,s) &= U(k,s)-W(k,s)=\Psi^+(k,s)+\Psi^-(k,s), \\ \Psi^\pm(k,s) &= \int_0^\infty\left(\int_{-\infty}^\infty \psi(\eta,t)H(\pm\eta)e^{ik\eta}\,d\eta\right)e^{-st}\,dt, \\ \Phi(k,s) &= U(k,s)+W(k,s). \end{aligned} \tag{2.143}$$

Functions $\omega_{1,2}(k)$ are defined as:

$$\omega_j^2(k) = 4v_j \sin^2\left(\frac{k}{2}\right), \quad j = 1, 2, \tag{2.144}$$

with $v_{1,2}^2$ being defined in (2.132). The combination of equations (2.142) reduces problem to the one of a Wiener-Hopf type for function $\Psi(k, s)$:

$$\begin{gathered}\Psi^-(k,s) + L(k,s)\Psi^+(k,s) = \\ \frac{F_1}{im_1(v - v_1^f)} \frac{e^{-ikn_1}}{k - f_1^-} \frac{1}{(s + ikv)^2 + \omega_1^2(k)} \\ + \frac{F_2}{im_2(v - v_2^f)} \frac{e^{-ikn_2}}{k - f_2^-} \frac{1}{(s + ikv)^2 + \omega_2^2(k)}, \\ f_1^- = \frac{is}{v - v_1^f}, \quad f_2^- = \frac{is}{v - v_2^f}.\end{gathered} \tag{2.145}$$

The kernel function $L(k, s)$ is defined as follows:

$$L(k,s) = 1 + \frac{\beta_1^2}{(s + ikv)^2 + \omega_1^2(k)} + \frac{\beta_2^2}{(s + ikv)^2 + \omega_2^2(k)} \tag{2.146}$$

Here, the parameters $v_{1,2}^2$ and $\beta_{1,2}^2$ are introduced in (2.133) and (2.132), respectively. The complementary equation for $\Phi(k, s)$ is:

$$\begin{gathered}\Phi(k,s) = -M(k,s)\Psi^+(k,s) \\ + \frac{F_1}{im_1(v - v_1^f)} \frac{e^{-ikn_1}}{k - f_1^-} \frac{1}{(s + ikv)^2 + \omega_1^2} \\ - \frac{F_2}{im_2(v - v_2^f)} \frac{e^{-ikn_2}}{k - f_2^-} \frac{1}{(s + ikv)^2 + \omega_2^2},\end{gathered} \tag{2.147}$$

where function $M(k, s)$ is:

$$M(k,s) = \frac{\beta_1^2}{(s + ikv)^2 + \omega_1^2(k)} - \frac{\beta_2^2}{(s + ikv)^2 + \omega_2^2(k)} \tag{2.148}$$

In the present analysis we are interested in the steady-state regime which is, presumably, achieved at $t \to \infty$. Thus, we can reformulate the problem

in terms of Fourier transform only. For that, we multiply equations (2.147) by s and pass it to limit $s \to 0+$. All the functions become to be defined by a single parameter k:

$$\begin{aligned} U(k) = \lim_{s\to 0+} sU(k,s), \quad W(k) = \lim_{s\to 0+} sW(k,s), \\ \Psi^{\pm}(k) = \lim_{s\to 0+} s\Psi^{\pm}(k,s), \quad \Phi^{\pm}(k) = \lim_{s\to 0+} s\Phi^{\pm}(k,s) \end{aligned} \tag{2.149}$$

Function $L(k,s)$ and function $M(k,s)$ become:

$$\begin{aligned} L(k) = \lim_{s\to 0+} L(k,s) = 1 + \frac{\beta_1^2}{(0+ikv)^2+\omega_1^2(k)} + \frac{\beta_2^2}{(0+ikv)^2+\omega_2^2(k)}, \\ M(k) = \lim_{s\to 0+} M(k,s) = \frac{\beta_1^2}{(0+ikv)^2+\omega_1^2(k)} - \frac{\beta_2^2}{(0+ikv)^2+\omega_2^2(k)}. \end{aligned} \tag{2.150}$$

From now we keep the notations $(0 \pm ik)$ which are understood as:

$$(0 \pm ik) = \lim_{s\to 0+} (s + ik) \tag{2.151}$$

Due to these arguments displacements and, hence, their combinations become functions of a single parameter η. The fracture condition that has to be checked at the steady-state is:

$$\psi(0) = \epsilon_c, \quad \psi(\eta) = \epsilon_c, \quad \eta > 0. \tag{2.152}$$

At the same time condition (2.140) is still has to be satisfied.

2.3.2.2 Modification of (2.145)

We start with consideration of equation (2.145). This equation has a standard form for an application of Wiener-Hopf technique. We point out that function $L(k,s)$ in (2.146) possesses following properties:

$$\begin{aligned} |L(k,s)| = |L(-k,s)|, \quad \mathrm{Arg}L(k,s) = -\mathrm{Arg}L(-k,s), \quad k \in \mathbb{R}, \\ L(k,s) = 1 + O\left(\frac{1}{k^2}\right), \quad k \to \infty. \end{aligned} \tag{2.153}$$

We also notice that the index of this function (winding number) is zero. All these arguments allow to factorise function $L(k,s)$ by means of Cauchy-type integral:

$$\begin{gathered} L(k,s) = L^+(k,s)L^-(k,s), \\ L^\pm(k,s) = \exp\left(\pm\frac{1}{2\pi i}\int_{-\infty}^{\infty}\frac{\mathrm{Log}L(\xi,s)}{\xi-k}\,d\xi\right), \end{gathered} \tag{2.154}$$

where functions $L^\pm(k)$ are analytic in the half-planes $\pm\Im k > 0$, respectively, and Log$k$ is the complex logarithm. Equation (2.145) can now be written in an alternative way.

$$\begin{gathered} \frac{1}{L^-(k,s)}\Psi^-(k,s) + L^+(k,s)\Psi^+(k,s) = \\ \frac{F_1}{im_1(v-v_1^f)}\frac{e^{-ikn_1}}{k-f_1^-}\frac{1}{(s+ikv)^2+\omega_1^2(k)}\frac{1}{L^-(k,s)} \\ +\frac{F_2}{im_2(v-v_2^f)}\frac{e^{-ikn_2}}{k-f_2^-}\frac{1}{(s+ikv)^2+\omega_2^2(k)}\frac{1}{L^-(k,s)}. \end{gathered} \tag{2.155}$$

Coefficients f_1^-, f_2^- are given in (2.145). At this point, as it was written in the main body of the present work, we need to multiply this equation by $s \to 0+$ and use the steady-state limits in (2.149) and (2.150). However, this operation seems to annihilate the right hand side of the equations. In this case, we need to study the right part of this equation in more details. We start with the consideration of function $L(k,s)$ for $k \to 0, s \to 0$.

2.3.2.3 Factorisation of $L(k,s)$ at $k \to 0, s \to 0+$

Function $L(k,s)$ can be written as a fraction of two functions. The numerator and denominator are expanded at $k = 0, s = 0$ and present its leading terms

in factors. For the numerator the expression is:

$$\begin{aligned}
&\frac{1}{2}\left([(s+ikv)^2+\omega_1^2(k)+2\beta_1^2][(s+ikv)^2+\omega_2^2(k)]\right.\\
&\left.+[(s+ikv)^2+\omega_2^2(k)+2\beta_2^2][(s+ikv)^2+\omega_1^2(k)]\right)\\
&=\frac{1}{2}\left([(s+ikv)^2+v_1^2k^2+2\beta_1^2][(s+ikv)^2+v_2^2k^2]\right.\\
&\left.+[(s+ikv)^2+v_2^2k^2+2\beta_2^2][(s+ikv)^2+v_1^2k^2]\right)\\
&+s^2(s^2+\beta_1^2+\beta_2^2)+O(k^2)\\
&=(v_1^2-v^2)(v_2^2-v^2)(k-z_1)(k-z_2)(k-q_1s)(k-q_2s)+O(k^2,s^2),\\
&k\to 0, s\to 0.
\end{aligned}$$

In the last factorisation an asymptotic representation of the roots with $s \to 0$ is used and the leading terms required for an analysis are kept. Collecting the corresponding terms, up to order $O(s)$, one gets the following equations for $z_{1,2}$ and $q_{1,2}$:

$$\begin{aligned}
z_1+z_2&=0,\\
(v_1^2-v^2)(v_2^2-v^2)z_1z_2&=\beta_1^2(v_2^2-v^2)+\beta_2^2(v_1^2-v^2),\\
(v_1^2-v^2)(v_2^2-v^2)(q_1+q_2)z_1z_2&=-2iv(\beta_1^2+\beta_2^2),\\
(v_1^2-v^2)(v_2^2-v^2)z_1z_2q_1q_2&=\beta_1^2+\beta_2^2.
\end{aligned}$$

From the last system of equation we derive the expression for the desirable coefficients. The factorisation of function $L(k,s)$ for this specific case is:

$$\begin{aligned}
L(k,s)&=\frac{(k-z^+)(k-z^-)(k-q^+)(k-q^-)}{(k-p_1^+)(k-p_1^-)(k-p_2^+)(k-p_2^-)},\quad k\to 0, s\to 0+,\\
p_j^\pm&=\mp is\frac{v_j\pm v}{v_j^2-v^2},\quad j=1,2,\\
z^\pm&=\mp i\sqrt{\frac{(\beta_1^2+\beta_2^2)(v_*^2-v^2)}{(v_1^2-v^2)(v_2^2-v^2)}},\quad q^\pm=\mp is\frac{v_*\pm v}{v_*^2-v^2},
\end{aligned}\tag{2.156}$$

where we also factorised denominator in $L(k,s)$ using:

$$(s+ikv)^2+\omega_j^2(k)\sim(v_j^2-v^2)(k-p_j^+)(k-p_j^-),\quad k\to 0, s\to 0.$$

The asymptotic behaviour of functions $L^{\pm}(k,s)$ is given by:

$$\begin{aligned} L^{+}(k,s) \sim R\frac{(k-z^{+})(k-q^{+})}{(k-p_1^{+})(k-p_2^{+})}, \quad L^{-}(k,s) \\ = \frac{1}{R}\frac{(k-z^{-})(k-q^{-})}{(k-p_1^{-})(k-p_2^{-})}, \quad k\to 0, \quad s\to 0+. \end{aligned} \tag{2.157}$$

Here, function R is defined in (2.176). Let us consider the following product from (2.155):

$$\begin{aligned} \frac{e^{-ikn_1}}{k-f^{-}}\frac{1}{(s+ikv)^2+\omega_1^2(k)}\frac{1}{L^{-}(k,s)} \\ \sim \frac{R}{v_1^2-v^2}\frac{1}{k-f^{-}}\frac{k-p_2^{-}}{(k-z^{-})(k-q^{-})}\frac{1}{k-p_1^{+}}, \quad s\to 0+, \quad k\to 0. \end{aligned}$$

We then decompose it into a some of fractions:

$$\begin{aligned} \frac{1}{k-f^{-}}\frac{k-p_2^{-}}{(k-z^{-})(k-q^{-})}\frac{1}{k-p_1^{+}} \\ = \frac{1}{p_1^{+}-f^{-}}\frac{1}{k-z^{-}}\left[\frac{1}{k-p_1^{+}}\frac{k-p_2^{-}}{k-q^{-}}-\frac{1}{k-f^{-}}\frac{k-p_2^{-}}{k-q^{-}}\right] \end{aligned}$$

Finally we notice that:

$$\begin{aligned} \frac{1}{k-z^{-}}\to\frac{1}{-z^{-}}, \quad s\to 0+, \quad k\to 0 \\ \frac{k-p_2^{-}}{k-q^{-}}, \frac{k-p_2^{-}}{k-q^{-}}\to 1, \quad s\to 0+, \\ \frac{1}{k-p_1^{+}}\to\frac{1}{k+i0}, \quad \frac{1}{k-f^{-}}\to\frac{1}{k-i0}, \quad s\to 0+. \end{aligned}$$

The use of all the last set of limits gives:

$$\begin{aligned} \frac{F_1}{im_1(v-v_1^f)}\frac{se^{-ikn_1}}{k-f_1^{-}}\frac{1}{(s+ikv)^2+\omega_1^2(k)}\frac{1}{L^{-}(k,s)} = \frac{C_1}{0+ik}+\frac{C_1}{0-ik}, \\ C_1 = \frac{F}{m_1(v-v_1^f)}\frac{R}{v_1^2-v^2}\frac{s}{f_1^{-}-p_1^{+}}\frac{1}{(-z^{-})} \end{aligned}$$

We treat the remaining product in (2.155) is transformed to:

$$\frac{F_2}{im_2(v-v_2^f)}\frac{se^{-ikn_2}}{k-f_2^-}\frac{1}{(s+ikv)^2+\omega_2^2(k)}\frac{1}{L^-(k,s)}=\frac{C_2}{0+ik}+\frac{C_2}{0-ik},$$

$$C_2=\frac{F_2}{m_2(v-v_2^f)}\frac{R}{v_2^2-v^2}\frac{s}{f_2^--p_2^+}\frac{1}{(-z^-)}$$

The final expressions for the constants are:

$$\begin{aligned}C_1&=\frac{F_1}{m_1}\frac{v_1-v}{v_1-v_1^f}\frac{R}{v_1^2-v^2}\sqrt{\frac{(v_1^2-v^2)(v_2^2-v^2)}{(\beta_1^2+\beta_2^2)(v_*^2-v^2)}},\\ C_2&=\frac{F_2}{m_2}\frac{v_2-v}{v_2-v_2^f}\frac{R}{v_2^2-v^2}\sqrt{\frac{(v_1^2-v^2)(v_2^2-v^2)}{(\beta_1^2+\beta_2^2)(v_*^2-v^2)}}.\end{aligned}\tag{2.158}$$

2.3.2.4 Solution of the Wiener-Hopf problem

The steady-state solution for $\Psi(k)$ follows from (2.145) after factorisation of function $L(k,s)$, multiplying by $s\to 0+$ and modifying the right-hand side of the equation. Taking into an account the notations in (2.137) we get:

$$L^+(k)\Psi^+(k)+\frac{\Psi^-(k)}{L^-(k)}=\frac{C_1+C_2}{0-ik}+\frac{C_1+C_2}{0+ik},\tag{2.159}$$

where the constants C_1, C_2 are given by (2.158). The solution of the last problem is:

$$\Psi^+(k)=\frac{C_1+C_2}{0-ik}\frac{1}{L^+(k)},\quad \Psi^-(k)=\frac{C_1+C_2}{0+ik}L^-(k).\tag{2.160}$$

The behaviour of factors $L^\pm(k)$ at infinity is written as:

$$L^\pm(k)=1\pm i\frac{Q}{k}+O\left(\frac{1}{k^2}\right),\quad k\to\infty,\tag{2.161}$$

where Q is shown in (2.176). The asymptotics of $L^\pm(k)$ are estimated to be:

$$L^\pm(k)=\sqrt{\frac{(\beta_1^2+\beta_2^2)(v_*^2-v^2)}{(v_1^2-v^2)(v_2^2-v^2)}}\frac{R^{\pm 1}}{0\mp ik}\left(1+(0\mp ik)S\right)+O(k),\quad k\to 0.\tag{2.162}$$

Coefficients R, S can be determined from (2.176). Thus, we obtain the expressions for the behaviour of Fourier transforms at infinity:

$$\Psi^{\pm}(k) = \pm\frac{(C_1+C_2)i}{k}\left(1-\frac{Qi}{k}\right)+O\left(\frac{1}{k^3}\right), \quad k\to\infty, \tag{2.163}$$

and at zero:

$$\begin{aligned}\Psi^{-}(k) &= \sqrt{\frac{(\beta_1^2+\beta_2^2)(v_*^2-v^2)}{(v_1^2-v^2)(v_2^2-v^2)}}\frac{C_1+C_2}{R}\frac{1}{(0+ik)^2}\left(1+(0+ik)S\right)\\ &\qquad +O(1), \quad k\to 0,\\ \Psi^{+}(k) &= \sqrt{\frac{(v_1^2-v^2)(v_2^2-v^2)}{(\beta_1^2+\beta_2^2)(v_*^2-v^2)}}\frac{C_1+C_2}{R}+O(k), \quad k\to 0\end{aligned} \tag{2.164}$$

The fracture condition (2.152) determines the relation on the coefficients C_1 and C_2:

$$C_1+C_2=\epsilon_c. \tag{2.165}$$

Now, we concentrate on function $\Phi(k)$.

2.3.2.5 Solution for the sum of displacements

Function $\phi(\eta,t)$ is given in (2.138) and the corresponding equation for it is (2.147). However, the last want requires some additional work to do. The obtained results for $\Psi(k,s)$ reveal the following:

$$s\Psi^{+}(k,s)=\frac{\epsilon_c}{0-ik}\frac{1}{L^{+}(k)}=\frac{\epsilon_c}{0-ik}\frac{L^{-}(k)}{L(k)}+o(s), \quad s\to 0+,$$

where the definition of factors $L^{\pm}(k)$ in (2.174) has been used. The reasoning lead to an expression for $\Psi(k,s)$ allows to simplify the part in (2.147) that involves the loads:

$$\begin{aligned}s\left[\frac{F_1}{im_1(v-v_1^f)}\frac{e^{-ikn_0}}{k-f_1^-}\frac{1}{(s+ikv)^2+\omega_1^2}-\frac{F_2}{im_2(v-v_2^f)}\frac{e^{-ikn_0}}{k-f_2^-}\frac{1}{(s+ikv)^2+\omega_2^2}\right]\\ =\left[\frac{C_1-C_2}{0-ik}+\frac{C_1-C_2}{0+ik}\right]L^{-}(k)+o(s), \quad s\to 0+\end{aligned}$$

Finally, equation (2.147) reduces to the one from which function $\Phi(k) = \lim s\Phi(k,s), s \to 0$ is possible to be found:

$$\Phi(k) = \left[\frac{C_1 - C_2}{0 + ik} + \frac{C_1 - C_2}{0 - ik} - \frac{M(k)}{L(k)}\frac{\epsilon_c}{0 - ik}\right] L^-(k) \tag{2.166}$$

We expect no explicit dependence on time which can be satisfied with an annulment of a coefficient of the last two terms in the square brackets and function $L^-(k)$ at $k \to 0$:

$$C_1 - C_2 = \epsilon_c K.$$

In the last expression we used the fact that:

$$\frac{M(k)}{L(k)} = K + O(k^2), \quad k \to 0,$$
$$K = \frac{\beta_1^2(v_2^2 - v^2) - \beta_2^2(v_1^2 - v^2)}{\beta_1^2(v_2^2 - v^2) + \beta_2^2(v_1^2 - v^2)}.$$

The expression for the computation of $\phi(\eta)$, then, is the one in (2.177). Hence, we get two equations for linking the loading parameters, crack speed and material properties:

$$C_1 + C_2 = \epsilon_c, \quad C_1 - C_2 = \epsilon_c K. \tag{2.167}$$

2.3.2.6 Special case $v_c < v < v_*$

Let us assume that $v_1 < v_2$, which makes $v_c = v_1$, according to (2.135). Moreover, we consider the crack speeds that are found within the interval:

$$v_c < v < v_*,$$

where v_* is shown in (2.135). Function $L(k,s)$ can be written in this case as:

$$L(k,s)=\frac{(k-z_1^+)(k-z_2^+)(k-q^+)(k-q^-)}{(k-\alpha_1^-)(k-\alpha_2^-)(k-p_2^+)(k-p_2^-)},\quad k\to 0,\quad s\to 0$$

$$z_{1,2}^+=-i\zeta s\pm\sqrt{\frac{(\beta_1^2+\beta_2^2)(v_*^2-v^2)}{(v^2-v_1^2)(v_2^2-v^2)}},\quad q^\pm=\mp is\frac{v_*\pm v}{v_*^2-v^2},$$

$$\alpha_{1,2}^-=is\frac{v\mp v_1}{v^2-v_1^2},\quad p_2^\pm=\mp is\frac{v_2\pm v}{v_2^2-v^2},$$

$$\zeta=v\left[\frac{1}{v_*-v^2}-\frac{1}{v_2^2-v^2}+\frac{1}{v^2-v_1^2}\right]>0.$$

From this we achieve that:

$$L^-(k,s)\sim\frac{1}{R}\frac{(k-q^-)}{(k-\alpha_1^-)(k-\alpha_2^-)(k-p_2^-)},\quad k\to 0,\quad s\to 0,$$

$$L^+(k,s)\sim R\frac{(k-z_1^+)(k-z_2^+)(k-q^+)}{(k-p_2^+)},\quad k\to 0,\quad s\to 0,$$

The dispersion relations in a limit $k\to 0$ are:

$$(s+ikv)^2+\omega_1^2(k)\sim(v_1^2-v^2)(k-\alpha_1^-)(k-\alpha_1^-),\quad k\to 0$$

$$(s+ikv)^2+\omega_2^2(k)\sim(v_2^2-v^2)(k-p_2^+)(k-p_2^-),\quad k\to 0$$

First consider the following product:

$$\frac{s}{k-f_1^-}\frac{1}{(s+ikv)^2+\omega_1^2(k)}\frac{1}{L^-(k,s)}$$

$$\sim\frac{R}{v_1^2-v^2}\frac{s}{k-f_1^-}\frac{k-p_2^-}{k-q^-},\quad k\to 0,\quad s\to 0.$$

We conclude that:

$$\frac{s}{k-f_1^-}\frac{k-p_2^-}{k-q^-}\to 0,\quad s\to 0.$$

The next product to study is:

$$\frac{s}{k-f_2^-}\frac{1}{(s+ikv)^2+\omega_2^2(k)}\frac{1}{L^-(k,s)}$$

$$\sim\frac{R}{v_1^2-v^2}\frac{s}{k-f_2^-}\frac{(k-\alpha_1^-)(k-\alpha_2^-)}{(k-p_2^+)(k-q^-)},\quad k\to 0,\quad s\to 0.$$

The product of the fractions can be factorised as:

$$\begin{aligned}
&\frac{1}{k-f_2^-}\frac{(k-\alpha_1^-)(k-\alpha_2^-)}{(k-p_2^+)(k-q^-)} \\
&= \frac{1}{f_2^- - p_2^+}\left[\frac{1}{k-f_2^-} - \frac{1}{k-p_2^+}\right]\frac{(k-\alpha_1^-)(k-\alpha_2^-)}{k-q^-} \\
&= \frac{1}{f_2^- - p_2^+}\left[\frac{\alpha_1^- - f_2^-}{q^- - f_2^-}\frac{k-\alpha_2^-}{k-f_2^-}\right. \\
&\left. + \left(\frac{q^- - \alpha_1^-}{q^- - f_2^-} - \frac{q^- - \alpha_1^-}{q^- - p_2^+}\right)\frac{k-\alpha_2^-}{k-q^-} - \frac{\alpha_1^- - p_2^+}{q^- - p_2^+}\frac{k-\alpha_2^-}{k-p_2^+}\right] \\
&= \frac{1}{f_2^- - p_2^+}\left[\frac{\alpha_1^- - f_2^-}{q^- - f_2^-}\frac{f_2^- - \alpha_2^-}{k-f_2^-}\right. \\
&\left. + \left(\frac{q^- - \alpha_1^-}{q^- - f_2^-} - \frac{q^- - \alpha_1^-}{q^- - p_2^+}\right)\frac{q^- - \alpha_2^-}{k-q^-} - \frac{\alpha_1^- - p_2^+}{q^- - p_2^+}\frac{p_2^- - \alpha_2^-}{k-p_2^+}\right].
\end{aligned}$$

Multiplication of the last expression and taking a limit $s \to 0$ results in:

$$\frac{s}{k-f_2^-}\frac{(k-\alpha_1^-)(k-\alpha_2^-)}{(k-p_2^+)(k-q^-)} \to 0, \quad s \to 0.$$

So, we conclude that in this case the final form of the equation for $\Psi(k) = s\Psi(k,s)$, $s \to 0$ is:

$$\frac{\Psi^-(k)}{L^-(k)} + L^+(k)\Psi^+(k) = 0.$$

The estimated behaviour of function $L^{\pm}(k)$ suggest that there is no physically possible solution for this case.

2.3.2.7 Special case $v_* < v < \max(v_1, v_2)$

The assumption $v_1 < v_2$ is still held for this section. But now the following range of crack speeds is taken:

$$v_* < v < v_2.$$

For this case we have the following limiting expression for $L(k,s)$:

$$L(k,s) \sim \frac{(k-z^+)(k-z^-)(k-q_1^-)(k-q_2^-)}{(k-\alpha_1^-)(k-\alpha_2^-)(k-p_2^+)(k-p_2^-)}, \quad k \to 0, \quad s \to 0$$
$$z^{\pm} = \pm i\sqrt{\frac{(\beta_1^2+\beta_2^2)(v^2-v_*^2)}{(v^2-v_1^2)(v_2^2-v^2)}}, \quad q_{1,2}^- = is\frac{v \mp v_*}{v^2-v_*^2}, \tag{2.168}$$
$$\alpha_{1,2}^- = is\frac{v \mp v_1}{v^2-v_1^2}, \quad p_2^{\pm} = \mp is\frac{v_2 \pm v}{v_2^2-v^2}.$$

For these situation function $L^-(k,s)$ in a limit is:

$$L^-(k,s) \sim \frac{1}{R}\frac{(k-z^-)(k-q_1^-)(k-q_2^-)}{(k-\alpha_1^-)(k-\alpha_2^-)(k-p_2^-)}, \quad k \to 0, \quad s \to 0$$
$$L^+(k,s) \sim R\frac{k-z^+}{k-p_2^+}, \quad k \to 0, \quad s \to 0.$$

The dispersion relations remains as previously:

$$(s+ikv)^2 + \omega_1^2(k) = (v_1^2-v^2)(k-\alpha_1^-)(k-\alpha_1^-), \quad k \to 0,$$
$$(s+ikv)^2 + \omega_2^2(k) = (v_2^2-v^2)(k-p_2^+)(k-p_2^-), \quad k \to 0.$$

Again we consider the following product:

$$\frac{s}{k-f_1^-}\frac{1}{(s+ikv)^2+\omega_1^2(k)}\frac{1}{L^-(k,s)}$$
$$\sim \frac{R}{v_1^2-v^2}\frac{s}{k-f_1^-}\frac{k-p_2^-}{(k-z^-)(k-q_1^-)(k-q_2^-)}, \quad k \to 0, \quad s \to 0.$$

The fractions can be decomposed as:

$$\frac{1}{k-f_1^-}\frac{k-p_2^-}{(k-z^-)(k-q_1^-)(k-q_2^-)}$$
$$= \frac{1}{k-z^-}\frac{1}{k-f_1^-}\left[\frac{p_2^- - q_2^-}{q_1^- - q_2^-}\frac{1}{k-q_2^-} + \frac{q_1^- - p_2^-}{q_1^- - q_2^-}\frac{1}{k-q_1^-}\right].$$

From this we estimate that:

$$\frac{s}{k-f_1^-}\frac{1}{(s+ikv)^2+\omega_1^2(k)}\frac{1}{L^-(k,s)} \to 0, \quad s \to 0. \tag{2.169}$$

The other product is:

$$\frac{s}{k-f_2^-}\frac{1}{(s+ikv)^2+\omega_2^2(k)}\frac{1}{L^-(k,s)}$$
$$\sim \frac{R}{v_2^2-v^2}\frac{s}{k-f_2^-}\frac{(k-\alpha_1^-)(k-\alpha_2^-)}{(k-z^-)(k-p_2^+)(k-q_1^-)(k-q_2^-)}, \quad k\to 0, \quad s\to 0,$$

where f_2^- is shown in (2.145). The factorisation can be done as follows:

$$\frac{1}{k-f_2^-}\frac{(k-\alpha_1^-)(k-\alpha_2^-)}{(k-z^-)(k-p_2^+)(k-q_1^-)(k-q_2^-)}$$
$$=\frac{1}{f_2^- - p_2^+}\frac{1}{k-z^-}\left[\frac{1}{k-p_2^+}-\frac{1}{k-f_2^-}\right]\frac{(k-\alpha_1^-)(k-\alpha_2^-)}{(k-q_1^-)(k-q_2^-)}$$
$$=\frac{1}{k-z^-}\frac{1}{f_2^- - p_2^+}\left[\left\{\frac{\alpha_1^- - q_1^-}{p_2^+ - q_1^-}\left(\frac{\alpha_2^- - q_2^-}{q_1^- - q_2^-}\frac{1}{k-q_2^-}+\frac{q_1^- - \alpha_2^-}{q_1^- - q_2^-}\frac{1}{k-q_1^-}\right)\right.\right.$$
$$\left.+\frac{p_2^+ - \alpha_1^-}{p_2^+ - q_1^-}\frac{\alpha_2^- - q_2^-}{p_2^+ - q_2^-}\frac{1}{k-q_2^-}\right\}\frac{1}{k-f_2^-}$$
$$\left.+\frac{p_2^+ - \alpha_1^-}{p_2^+ - q_1^-}\frac{p_2^+ - \alpha_2^-}{p_2^+ - q_2^-}\left(\frac{1}{k-f_2^-}-\frac{1}{k-p_2^+}\right)\right]$$

Finally, we conclude that:

$$\frac{F_2}{im_2(v-v_2^f)}\frac{s}{k-f_2^-}\frac{1}{(s+ikv)^2+\omega_2^2(k)}\frac{1}{L^-(k,s)}\to\frac{C}{0+ik}+\frac{C}{0-ik},$$
$$C=\frac{F_2}{m_2(v-v_2^f)}\frac{R}{v_2^2-v^2}\frac{1}{-z^-}\frac{p_2^+-\alpha_1^-}{p_2^+-q_1^-}\frac{p_2^+-\alpha_2^-}{p_2^+-q_2^-}\frac{s}{f_2^- - p_2^+}$$

The Wiener-Hopf equation for $\Psi(k)=s\Psi(k,s)$, $s\to 0$:

$$\frac{\Psi^-(k)}{L^-(k)}+L^+(k)\Psi^+(k)=\frac{C}{0+ik}+\frac{C}{0-ik},$$
$$C=\frac{F_2}{m_2}\frac{v_2-v}{v_2-v_2^f}\frac{R}{v_2^2-v^2}\sqrt{\frac{(v^2-v_1^2)(v_2^2-v)}{(\beta_1^2+\beta_2^2)(v^2-v_*^2)}}\frac{(v^2-v_*^2)(v_2^2-v_1^2)}{(v^2-v_1^2)(v_2^2-v_*^2)}, \tag{2.170}$$

where the expressions in (2.168) have been used. The solution to this problem is gained similar to the case $v<v_c$:

$$\Psi^+=\frac{C}{0-ik}\frac{1}{L^+(k)}, \quad \Psi^+=\frac{C}{0-ik}\frac{1}{L^+(k)}. \tag{2.171}$$

Utilisation of fracture condition requires:

$$C = \epsilon_c, \tag{2.172}$$

and, then, the link between loading parameters and ϵ_c are obtained. The expression for the evaluation function $\phi(\eta)$ remains the same.

2.3.2.8 Note on function evaluations

The presented results required factorisation of function $L(k)$. The estimation of asymptotics of functions $L(k)$ and $M(k)$ for the application of developed algorithms becomes easier if these functions are expressed as:

$$L(k) = \frac{L_1(k) + L_2(k)}{2}, \quad M(k) = \frac{L_1(k) - L_2(k)}{2},$$
$$L_j = \frac{(0 + ikv)^2 + \omega_j^2(k) + 2\beta_j^2}{(0 + ikv)^2 + \omega_j^2(k)}, \quad j = 1, 2.$$

The notations can be found in (2.133) and (2.144). Functions $L_{1,2}(k)$ have exactly the same form as for the problem in Chapter 2.1. Hence, the asymptotic relations for them are given in section 2.1.3 and the linear combinations of these asymptotics should be taken.

2.3.2.9 Analytical solution of the Wiener-Hopf problem

As it was pointed out above at the steady-state the displacements and their combinations have to depend only on variable η. The solution for function $\psi(\eta)$ is expressed in terms of inverse Fourier transform:

$$\begin{aligned} \psi(\eta) &= \frac{\epsilon_c}{2\pi} \int_{-\infty}^{\infty} \frac{1}{0 - ik} \frac{1}{L^+(k)}, \eta > 0, \\ \psi(\eta) &= \frac{\epsilon_c}{2\pi} \int_{-\infty}^{\infty} \frac{1}{0 + ik} L^-(k), \eta < 0. \end{aligned} \tag{2.173}$$

Functions $L^{\pm}(k)$ are related to the factorisation of function $L(k)$ from (2.150). The properties of the last allowed to use factorisation by means of a

Cauchy-type integral: The successful factorisation of function $L(k,s)$ solves the problem. We can write:

$$L^{\pm}(k) = \exp\left(\pm\frac{1}{2\pi i}\int_{-\infty}^{\infty}\frac{\mathrm{Log}L(\xi)}{\xi-k}\,d\xi\right), \quad \pm\Im k > 0. \tag{2.174}$$

Moreover, the estimation of behaviour of functions $L^{\pm}(k)$ provide the following asymptotic relations for function $\psi(\eta)$:

$$\begin{gathered}\psi(\eta) = \epsilon_c(1-Q\eta) + O(\eta^2), \quad \eta\to 0,\\ \psi(\eta) = \frac{\epsilon_c}{R}\sqrt{\frac{(\beta_1^2+\beta_2^2)(v_*^2-v^2)}{(v_1^2-v^2)(v_2^2-v^2)}}(-\eta+S) + O(1), \quad \eta\to-\infty,\\ \psi(\eta) = O(1), \quad \eta\to\infty,\end{gathered} \tag{2.175}$$

where $v_{1,2}^2$ are shown in (2.132), $\beta_{1,2}^2$ are defined in (2.133), v_* is given in (2.135). In (2.175) we also used the integral parameters that are related to the model parameters and a crack speed:

$$\begin{gathered}Q = \frac{1}{\pi}\int_0^{\infty}\log|L(k)|\,dk, \quad S = \frac{1}{\pi}\int_0^{\infty}\frac{\log|L(k)|}{k^2}\,dk,\\ R = \exp\left(\frac{1}{\pi}\int_0^{\infty}\frac{\mathrm{Arg}L(k)}{k}\,dk\right).\end{gathered} \tag{2.176}$$

Function $\phi(\eta)$ can be found separately through the inverse Fourier transform. The suitable relation for its evaluation is:

$$\phi(\eta) = \frac{\epsilon_c}{2\pi}\int_{-\infty}^{\infty}\left[\frac{K}{0+ik} + \left(K - \frac{M(k)}{L(k)}\right)\frac{1}{0-ik}\right]L^{-}(k)\,dk, \tag{2.177}$$

with constant K being:

$$K = \frac{\beta_1^2(v_2^2-v^2) - \beta_2^2(v_1^2-v^2)}{\beta_1^2(v_2^2-v^2) + \beta_2^2(v_1^2-v^2)} \tag{2.178}$$

The imposed fracture criterion in (2.152) and (2.140) allow to determine the dependence between the critical loading parameters, model parameters

and a crack speed. The relations have different form according to the value the value of v:

$$\frac{F_j}{F_0} = \frac{1}{R}\sqrt{\frac{(v_1^2 - v^2)(v_2^2 - v^2)}{(\beta_1^2 + \beta_2^2)(v_*^2 - v^2)}}\frac{v_j - v_j^f}{v_j - v}, \quad j = 1, 2, \quad v < v_c. \tag{2.179}$$

For the values grater than v_c we choose that for one of the materials the speed of sound is less than the other, specifically $v_1 < v_2$. Then, it turns out, that force F_1 does not effect the fracture process and force F_2 is a reason for a crack movement. Moreover, there is a gap in the crack velocity, i.e. with this specific type of load it can't progress for $v_c < v < v_*$. The remaining interval of possible crack speeds is:

$$\frac{F_2}{F_0} = \frac{1}{R}\sqrt{\frac{(v_1^2 - v^2)(v_2^2 - v^2)}{(\beta_1^2 + \beta_2^2)(v_*^2 - v^2)}}\frac{v_2^2 - v^2}{\mu_2 v_2^2}\frac{v_2 - v_2^f}{v_2 - v}\frac{(v - v_1^2)(v_2^2 - v_*^2)}{(v - v_*^2)(v_2^2 - v_1^2)}, \tag{2.180}$$
$$v_* < v < v_2, \quad v_1 < v_2.$$

In the last expression the integral parameter R is given by the previous formula and quantity F_0 is shown in (2.128). The last expressions turn out to be easy to verify by the numerical simulation of a dynamical system which is demonstrated below.

Functions $u(\eta)$ and $w(\eta)$ can be obtained through the linear combinations of $\psi(\eta)$ and $\phi(\eta)$. The evaluation of $\psi(\eta)$ and $\phi(\eta)$, according to equation (2.173) and (2.177), requires firstly setting certain values of the model parameters and a crack speed as well. Recall that function $\psi(\eta)$ expresses the crack opening in the broken part of the structure and the elongation of springs between the chains in the intact part of the double chain. For that reason its investigation is important. Firstly, the case $v_1 = v_2$ is observed. The plots of displacements and $\psi(\eta)$ are shown in Fig. 2.28a) and Fig. 2.28b), respectively, at crack speed $v = 0.2v_c$ and the other parameters are shown on the plots.

The feature which is worth of mentioning is that one can see the waves of different lengths emanating from a crack tip both in Fig. 2.28a). This

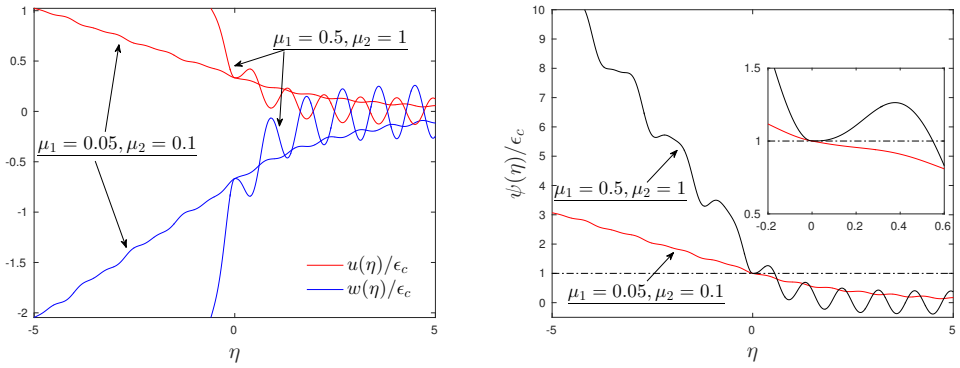

a) b)

Figure 2.28: Displacements of the chains and function $\psi(\eta)$ for different values of model parameters under condition $v_1 = v_2$ at speed $v = 0.2v_c$: a) displacements, b) function $\psi(\eta)$. The inserts show magnified plots at the vicinity of a crack tip.

peculiarity is common for fracture problems of discrete media. This is an essential trait of these problems in comparison with the dynamic fracture of continuum media.

The evaluation of the function $\psi(\eta)$ is important for checking a second part in the criterion (2.152). The violation of such criterion can be vividly observed in Fig.2.28b) for $\mu_1 = 0.5, \mu_2 = 1$. The examination of different crack speeds and sets of parameters allow to distinguish two different sets of solutions: admissible and forbidden. As previously, the selection of a certain type comes from the validity of criterion (2.152).

The other interesting observation can be made if the parameters are such that v_1 and v_2 are different. The solution predicts that there is a possible solution for the range $v_* < v < \max(v_1, v_2)$. The solution of the problem in the range $v < v_c$ for these cases is determined up to a constant, which was verified through the numerical simulations. At the constant shift of displacements was not observed for $v_* < v < \max(v_1, v_2)$. The examples of

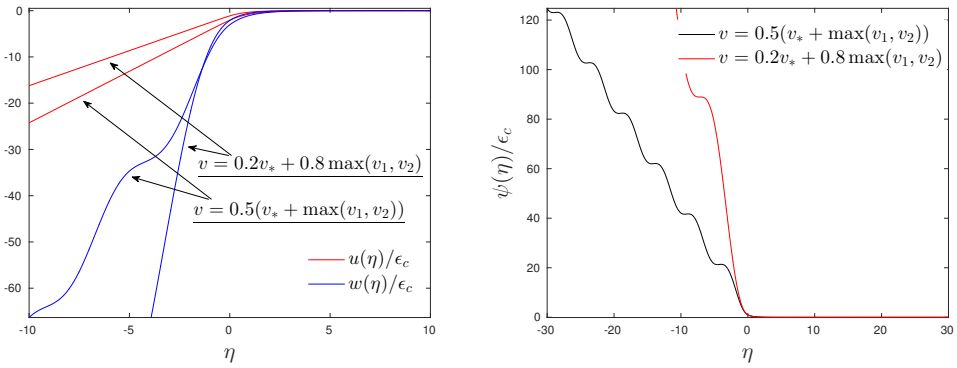

a) b)

Figure 2.29: Displacements of the chains and function $\psi(\eta)$ for $\mu_1 = 2, \mu_2 = 1$ and $v_1^2 = 0.5v_2^2$ at different crack speeds: a) displacements, b) function $\psi(\eta)$

displacement fields and function $\psi(\eta)$ for $\mu_1 = 2, \mu_2 = 1$ and $v_1^2 = 0.5v_2^2$ are given in Fig. 2.29. The interesting feature that is observed that the chain with a lower speed of sound, in the presented example v_1, experience a linear inclination in the broken part, see Fig. 2.29a). At the same time, the elastic waves propagate only along the other chain. Notice, that the only waves that appear in such cases are located behind a crack tip.

Fig. 2.29b) reveal that function $\psi(\eta)$ increases when crack speed grows. Moreover, no violation of fracture condition is observed ahead of a crack tip. The further demonstration of the results become easier when the energetic properties of the fracture process are considered.

2.3.2.10 Analysis of the energy release rate

Following the same notations used for a static problem, we would like to explore the effect of model parameters on the energy release rate and admissible regimes. The energy release ratio in this case is determined by the following relation:

$$\frac{G_0}{G} = R^2, \tag{2.181}$$

where quantity G_0 is defined in (2.129) and function R is given in (2.176). This ratio demonstrates the released energy carried out by the elastic waves seen in Fig. 2.28 and Fig. 2.29 in comparison with the fracture energy G_0. Several examples of these dependences are displayed in Fig. 2.30. For these examples we set a constraint on the parameters $v_1 = v_2$ which allows to reduces the choices of parameters. We also marked the limiting values of G_0/G for $v \to 0$ computed by (2.129). Moreover, we already demonstrate the performed analysis of admissible and forbidden regimes in this plots.

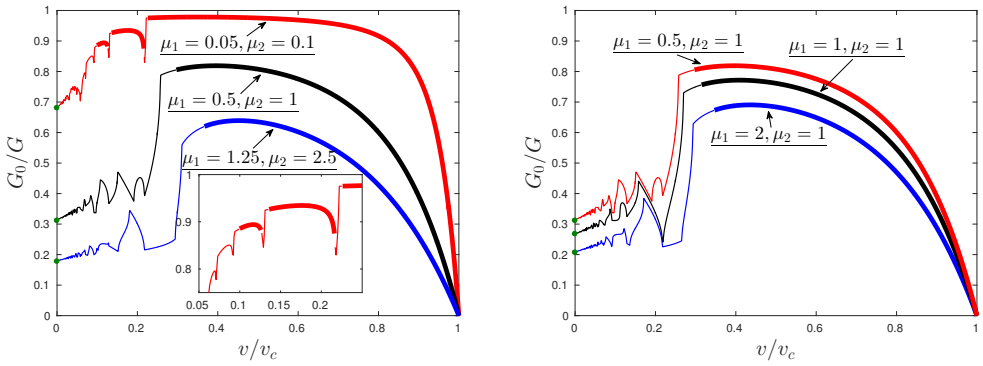

a) b)

Figure 2.30: Energy release rates ratio G_0/G for different sets of parameters under a condition $v_1 = v_2$: a) $\mu_2 = 2\mu_1$, b) $\mu_2 = 1$. Admissible regimes – thick lines, forbidden regimes – normal lines, green markers stand for the limiting values when $v \to 0$ given by (2.129).

Fig. 2.30a) refers to the situation when the stiffness of vertical springs c was varied. The interesting point is that the range of admissible regimes grow with the decrease of c. For instance, for case $\mu_1 = 0.05, \mu_2 = 0.1$ there are three distinct intervals of admissible and forbidden regimes. Such particularity is also observed for a high contrast in model parameters for a simple chain and a square-cell lattice.

The other plot, Fig. 2.30b), demonstrates the fact that even though the

macroscopic properties remain the same, such as speeds of sound $v_{1,2}$ and stiffness c of the springs between the chains, the microlevel fracture properties vary. The energy release rates take different values and, additionally, the qualitative changes of admissible regimes happen. We see the growth of the admissible regime with the increase in μ_1 while μ_2 remains the same for all presented cases. Furthermore, for a chosen value of a crack speed there are quantitative changes that are reflected in Fig. 2.28 and Fig. 2.29 for displacements, where we see the difference in the values of these function and difference in the wavelengths of the radiated waves.

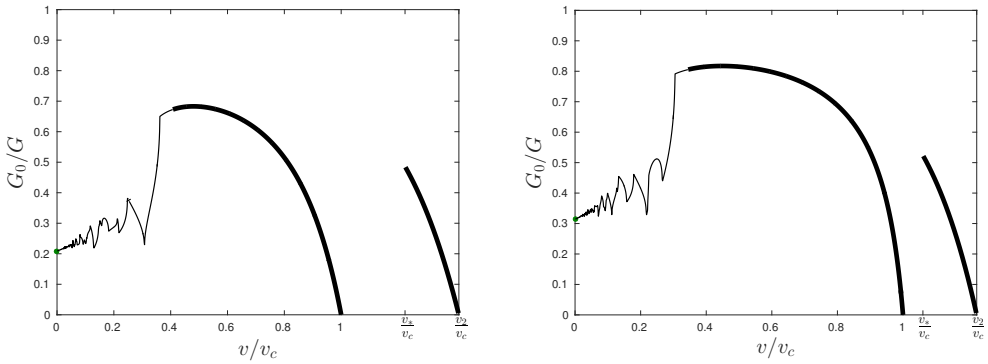

a) b)

Figure 2.31: Energy release rates ratio G_0/G for different sets of parameters: a) $\mu_1 = 2, \mu_2 = 1, v_1^2/v_2^2 = 0.5$, b) $\mu_1 = 0.5, \mu_2 = 1, v_1^2/v_2^2 = 2/3$. Admissible regimes – thick lines, forbidden regimes – normal lines, green markers stand for the limiting values when $v \to 0$ given by (2.129).

In the previous plots we studied the cases when we had a constraint in parameters $v_1 = v_2$. The different situation occurs when these parameters are different. In Fig.2.31 we display the examples when the speeds of sound are different in two chain. In Fig.2.31a) the parameters are chosen in such a way that $v_1^2 = 0.5v_2^2$ whereas in Fig.2.31b) we have $v_1^2 = 2/3v_2^2$. For both cases v_2 is the same but according to (2.132) we have different values of

v_c. We also provide the analysis of admissible regimes and limiting value at $v \to 0$ according to (2.129).

It is interesting to notice that the ratio G_0/G takes different values for the presented results. We can also observe that for the lower value of v_1 in Fig.2.31a) we achieve lower values of G_0/G in comparison with the results in Fig.2.31b). The attention on these plots is attracted by the intervals of v that correspond to the values $v > v_c$. There is a vivid restriction of the whole range of possible values of the crack speed by the values $\min(v_1, v_2), v_*$ and $\max(v_1, v_2)$ with a gap in the crack values between v_c and v_*.

Although all the demonstrated results for G_0/G reveal interesting feature of fracture in the structure under consideration we would also like to investigate the dependences of the force. One minor drawback of G_0/G plots is that they are not monotonic even for the intervals of admissible regimes. This, in turn, leads to a non-uniqueness of determination of an achieved steady-state crack speed which is supported by Chapter 2.1. Moreover, derived relations for F_1 and F_2 in (2.134) allow easier verification of delivered solution by numerical simulations. Finally, it is able to show the effects of different model parameters on the admissible regimes in terms of the applied load.

2.3.2.11 Force and a crack speed

In this section we analyse the results obtained for the relations of the forces in (2.134). We also performed the numerical simulations by solving equations (2.130) for a finite number of oscillators with free ends boundary conditions. We used 3000 masses of each sort giving total of 6000 masses. In the computations we applied the forces calculated for a certain crack speed by (2.134) and recorded the instantaneous crack speed as a function of fracture time. Afterwards for the relation of an instantaneous crack which chose a stable such dependence with small oscillations of the values which, presumably, corresponded to a steady-state from which we estimated the steady-state crack speed and, thus, checked the validity of (2.134).

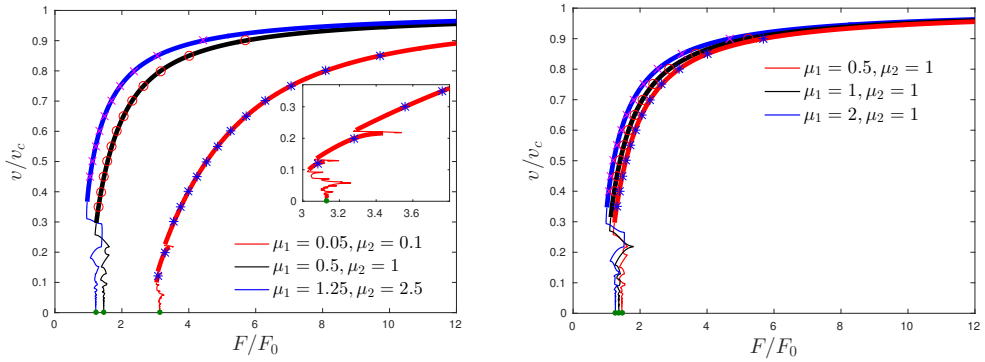

a) b)

Figure 2.32: Dependence of normalised force F/F_0, according to (2.134) and (2.182), for different sets of parameters under a condition $v_1 = v_2$ and $v_f = v_g = 0$: a) $\mu_2 = 2\mu_1$, b) $\mu_2 = 1$. Admissible regimes – thick lines, forbidden regimes – normal lines, green markers stand for the limiting values when $v \to 0$ given by (2.128). The other markers demonstrate the results of numerical simulation after solving dynamical system of equations (2.130).

All the presented results are given for the cases of a fixed force. The effect of different values of a force speeds is shown in section 2.1.5.4. Firstly, we start with the presentations of the results for cases of $v_1 = v_2$. From formula (2.134) it follows that:

$$F_1 = F_2 = F, \quad v_1 = v_2, \quad v_f = v_g = 0, \tag{2.182}$$

where F_0 is defined in (2.128). The dependences of the force ratio F/F_0 are plotted in Fig.2.32. These plots complement those for the energy release ratio in Fig.2.30. The limiting values for $v \to 0$ are computed with (2.128) and different markers show the results from the numerical simulation of (2.130) as described above.

The important specific of the plots F/F_0 is that they provide monotonic correlation between v and F within admissible regimes, besides one case $\mu_1 = 1.25, \mu_2 = 2.5$ in Fig.2.30a).

The interesting feature that is not captured by G_0/G for the cases of different v_1 and v_2 in Fig.2.31 is that the values of applied forces F_1 and F_2 should be chosen differently. This evidence is displayed in Fig.2.33.

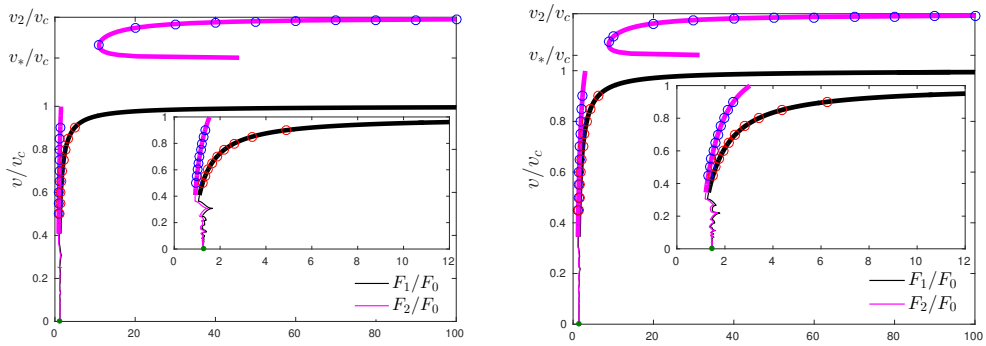

a) b)

Figure 2.33: Dependence of normalised forces F_1/F_0 and F_2/F_0, according to (2.182), for different sets of parameters and $v_1^f = v_2^f = 0$: a) $\mu_1 = 2, \mu_2 = 1, v_1^2/v_2^2 = 0.5$, b) $\mu_1 = 0.5, \mu_2 = 1, v_1^2/v_2^2 = 2/3$. Admissible regimes – thick lines, forbidden regimes – normal lines, green markers stand for the limiting values when $v \to 0$ given by (2.128). The other markers demonstrate the results of numerical simulation after solving dynamical system of equations (2.130).

After performed numerical simulations no crack speeds in a range $v_c < v < v_*$ have been observed. At the same time, for the crack speeds $v > v_*$ there was know difference in obtained values with a change of force F_1. This confirms the fact that when $v_1 < v_2$ the main role in fracture plays force F_2 making the other force irrelevant.

Nevertheless, the factorisation of function $L(k)$ is performed by Cauchy-type integrals. The poles of this function can be found by solving equations:

$$(0 + ikv)^2 + \omega_j^2(k) = 0, \quad j = 1, 2.$$

The zeros of function $L(k)$ are found after presenting it as a fraction of two functions and then the numerator is equated to zero. Apart from this, the numerical algorithms are essentially the same.

2.4 Discussion

The present chapter presented results on some chain problems. The configurations under investigations were: a chain attached to a rigid substrate, a chain with non-local interactions attached to a foundation and a double chain structure. The considered one-dimensional problems allowed to observe general effects that appear in fracture of solids and also the contributions of discrete models.

The first problem examined in section 2.1 allowed to work out the techniques which are used throughout the thesis. A full analytical solution was derived, and the relationships between the steady-state crack speed and the loading parameters (force amplitude, F, and the speed, v_f, of the force movement) were evaluated. Moreover, it was shown that accurate analysis of the analytical solution allows to separate the physically admissible and forbidden regimes of the steady-state fracture process (according to the fracture criterion). The analytical results were supported by numerical simulations of the problem. We compared the results of these theoretical and numerical approaches and found excellent correlations in the examined cases (see Fig. 2.16, Fig. 2.17 and Fig. 2.18). We showed that varying the numerical configurations and load implementations may affect the convergence rate of the solution to the steady-state regime. Although the instantaneous crack speed, $v(t_*)$, may exhibit different behaviour and depends on the limiting regime, the magnitude of the steady-state crack speed, v, numerically defined as the mean value of the instantaneous speed, gives results equal to those derived analytically within the accuracy of both computations.

A set of methods for initiation of an initiation speed, v, were identified analytically and confirmed numerically in section 2.1.5. The convergence of the transient regime to its steady-state equivalent is insensitive to the particular choice of pair (F, v_f) except when the speed v_f is very small and non-zero.

Derived in section 2.1, the relationship between the steady-state crack speed, v, and the loading parameters turns out to be more useful in the analysis than the energy release rate - speed diagram. This is because of the monotonic character of the function $v = v(F, v_f)$ for the admissible crack speeds. As a result, there is some difficulty in making a choice of load parameters that leads to the desired steady-state fracture regime.

In the same section we observed that a large difference in the elastic constants of the vertical and horizontal springs may lead to the existence of admissible regimes corresponding to a very "slow" steady-state movement that is not possible in the corresponding structure with more similar spring strengths. However, reducing the stiffnesses of the springs subjected to fracture leads to the appearance of a non-monotonic behaviour in the crack speed as a function of the applied load. This, in turn, causes uncertainty as to which regime would be expected to be the steady-state successor of the transient regime. This stiffness also makes a qualitative difference to the number of distinct intervals of admissible crack speeds. Thus, the corresponding transient problem should be considered to make more accurate predictions on crack speeds.

The modification of the problem of a simple chain, shown in section 2.2, is done by means of introduced non-local interactions which link every mass to the one next to closest neighbour. This structure showed that even though in a continuum limit the bulk properties (speed of sound, stiffness) are not sensitive to different combinations of parameters, the behaviour at the microlevel can be significantly affected. Not only the analytical solution was obtained but also the examination of admissible regimes has been performed and numerical simulations supported the results.

The results revealed the appearance of an extra smooth extremum at the energy release diagram with an increased influence of non-local interactions. This circumstance also is reflected on the relations between loading parameters and crack speed. More precisely, the monotonic character of the last

dependence within the admissible intervals is disturbed.

One of the main outcomes of section 2.2 shows that the achievable regimes can be judged from the consideration of energy release rate only. Indeed, non-local interactions created an extra minimum in a smooth part of the diagram and admissible regimes can be found on both sides from it (see Fig. 2.22 and Fig. 2.23).

From the point of view of optimisation, the presence of additional links between the oscillators may vary the amount of released energy during the fracture process. Keeping the same bulk stiffness of the structure one an increase of stiffness of non-local springs can drop the value of G_0/G.

The last problem of this chapter is concerned about the separation of two chains of oscillators with different material properties linked together by elastic springs. The mismatch in material properties allowed to detect some interesting features.

The quasi-static approach of section 2.3 revealed that the mode III fracture is caused by the application of forces with the same magnitude. The movement of crack induced the difference in force values in order to move a crack and avoid a rigid body motion. The difference in values can be created by different values of speed of sounds in the chains and speeds of force locations.

Furthermore, there is a possibility to observe cracks which are faster than speed of sound in the intact part of the structure. The mentioned speed of sound is greater than the minimum and less than the maximum of two speeds of sounds in separate chains. Crack propagation in such regimes is characterised by a high value of released energy. Moreover, fracture process in such range of crack speeds is ruled by the force applied to the chain with a higher speed of sound.

Chapter 3

Square-cell lattice problem

3.1 Anisotropic lattice

3.1.1 Mathematical formulation of the problem

The analysis of this problem is similar to the one for the one-dimensional chain. However, it has some additional peculiarities and that is why the derivation of the solution is presented. All the notations, except the specifically mentioned, are kept to be the same. The problem of crack propagation in a 2-d lattice within Mode III fracture is shown in Fig. 3.1. The linearised equations of motion with the utilised symmetry for this problem are:

$$\begin{aligned} &m = 0: \\ &M\ddot{u}_{0,n} = c_1(u_{0,n+1} + u_{0,n-1} - 2u_{1,n}) - 2c_2u_{0,n} + c_2(u_{1,n} - u_{0,n}), n \geq n_*, \\ &M\ddot{u}_{0,n} = c_1(u_{0,n+1} + u_{0,n-1} - 2u_{0,n}) + c_2(u_{1,n} - u_{0,n}), \quad n < n_*, \end{aligned} \tag{3.1}$$

$$\begin{aligned} &m \geq 1: \\ &M\ddot{u}_{m,n} = c_1(u_{m,n+1} + u_{m,n+1} - 2u_{1,n}) + c_2(u_{m+1,n} + u_{m-1,n} - 2u_{m,n}), \end{aligned} \tag{3.2}$$

where $u_{m,n} = u_{m,n}(t)$ is an out of plane displacement of an oscillator in m-th horizontal layer and n-th vertical layer of a lattice. From the assumption

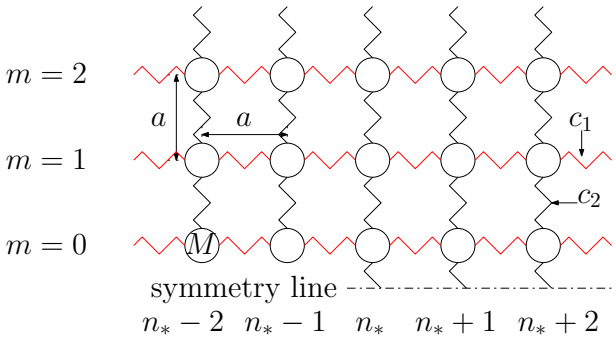

Figure 3.1: Infinite lattice of oscillators with equal masses M connected together by linear springs of stiffness c_1 in a horizontal direction and c_2 in a vertical direction. The crack position is defined by oscillator with index n_*. The vertical springs of the stiffness c_2 along the symmetry line break while the crack moves. a is an equilibrium distance between the oscillators.

of Mode III fracture the displacements of oscillators below the symmetry line have the same magnitude but an opposite sign to those to those with corresponding indices above it.

We suppose that fracture is caused due to the external energy flux coming from infinity towards a crack tip. Hence, no external force is presented in equations (3.1), (3.2). However, this fact is taken into an account later.

The fracture condition for this problem is stated as:

$$u_{0,n_*}(t_*) = u_c,$$
$$u_{0,n}(t) < u_c, \quad n > n_*(t).$$

3.1.2 Solution for steady-state crack propagation in lattice

The assumptions on the steady-state regime are the same as in Section 2.1.2.3. One of the major assumptions was that the crack, starting from some moment, starts to move with a constant speed. Thus, the change

of coordinate, with normalisation of a crack speed (2.20), is accepted:

$$\eta = n - vt, \quad v = const.$$

Coordinate η can be treated as continuous and it shifts a laboratory coordinate system to a moving frame with an origin at a crack tip. The crack speed is assumed to be limited by the value v_c (already normalised by a as in (2.20)):

$$v < v_c = \sqrt{\frac{c_1}{M}}. \tag{3.3}$$

The quantity v_c is equal, in this case, to Rayleigh speed in the square lattice. The steady-state solution is supposed to be a function of η in such a crack propagation regime:

$$u_{m,n}(t) = u_m(\eta).$$

The changes also needed to be applied to fracture conditions:

$$\begin{aligned} u_0(0) &= u_c, \\ u_m(\eta) &< u_c, \quad \eta > 0. \end{aligned} \tag{3.4}$$

The second condition guarantees that a crack tip is uniquely defined. Similarly to the analysis in Section 2.1.4, condition $(3.4)_2$ will be checked when the displacement field is evaluated. Equations of motion (3.1) and (3.2) become:

$$\begin{aligned} Mv^2\frac{d^2}{d\eta^2}u_0(\eta) &= c_1(u_0(\eta+1) + u_0(\eta-1) - 2u_0(\eta)) \\ &\quad -2c_1u_0(\eta)H(\eta) + c_2(u_1(\eta) - u_0(\eta)) \quad , m = 0, \\ Mv^2\frac{d^2}{d\eta^2}u_m(\eta) &= c_1(u_m(\eta+1) + u_m(\eta-1) - 2u_m(\eta)) \\ &\quad +c_2(u_{m+1}(\eta) + u_{m-1}(\eta) - 2u_m(\eta)) \quad , m \geq 1. \end{aligned} \tag{3.5}$$

At this point it is useful to introduce notations for the dispersion relations that are related to the present problem.

3.1.3 Dispersion relations

Dispersion relations for this problem can be written as:

$$\omega_1^2(k) = 4v_c^2 \sin^2\left(\frac{k}{2}\right) + 4\omega_0^2, \quad \omega_0^2 = \frac{c_2}{M}. \tag{3.6}$$

and:

$$\omega_2^2(k) = 4v_c^2 \sin^2\left(\frac{k}{2}\right). \tag{3.7}$$

Relations (3.6), (3.7) define the characteristics of waves that appear in the problem in mind. The plots of dispersion relations are shown in Fig. 3.2 for two values of crack speed $v = 0.2v_c$ and $v = 0.5v_c$.

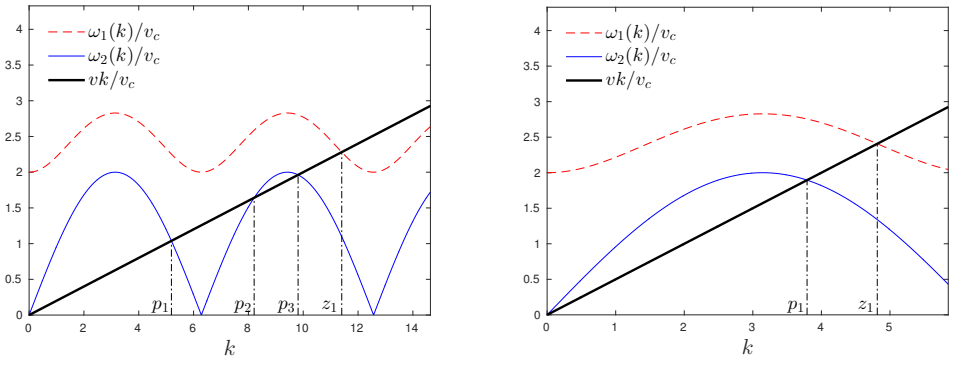

Figure 3.2: Dispersion relations for different values of crack speed and $c_2 = c_1$: a) $v = 0.2v_c$, b) $v = 0.5v_c$.

In Fig. 3.2 constants z_j and p_j are positive roots of the following equations:

$$\begin{aligned} \omega_1(z_j) - vz_j = 0, \quad j = 1...Z, \\ \omega_2(p_j) - vp_j = 0, \quad j = 1...P, \end{aligned} \tag{3.8}$$

where Z and P are the number of positive roots of the last two equations, respectively. Notice that there is also a double root $\omega_2(0) = 0$.

3.1.4 Description of problem in vertical direction

The last equation in (3.5) is:

$$\begin{aligned} Mv^2\frac{d^2}{d\eta^2}u_m(\eta) = c_1(u_m(\eta+1)+u_m(\eta-1)-2u_m(\eta)) \\ +c_2(u_m(\eta+1)+u_{m-1}(\eta)-2u_m(\eta)), \quad m \geq 1. \end{aligned} \tag{3.9}$$

The application of Fourier transform to this equation gives:

$$\left[(0+ikv)^2+\omega_2^2(k)+2\omega_0^2\right]U_m(k) = \omega_0^2(U_{m+1}(k)+U_{m-1}(k)). \tag{3.10}$$

In (3.10) the fact that a steady-state regime is already taken into an account. The reasoning that was provided within Section 2.1.2, concerning the limiting cases of a steady-state regime, is applicable here as well. The expression $(0+ikv)$ should be understood according to (2.38), i.e.:

$$(0 \pm ik) = \lim_{s\to 0+}(s \pm ik).$$

Taking advantage from the fact that the coefficients in the system of linear equations do not depend on the value of n (or, what is equivalent, that the material properties of the system do not change in the direction perpendicular to the crack line) we suppose the existence of a function $\lambda(k)$ such that:

$$U_m(k) = \lambda^m(k)U_0(k), \quad m \geq 1, \tag{3.11}$$

where the function $\lambda(k)$ should satisfy the following condition

$$|\lambda(k)| \leq 1. \tag{3.12}$$

Substituting (3.11) into (3.10) one obtains a quadratic equation to determine function $\lambda(k)$:

$$\lambda^2(k) - \frac{1}{\omega_0^2}\left((0+ikv)^2+\omega_2^2(k)+2\omega_0^2\right)\lambda(k)+1 = 0, \tag{3.13}$$

which naturally has two roots. They can be written as:

$$\lambda_1(k) = \lambda(k), \quad \lambda_2(k) = \frac{1}{\lambda(k)},$$

where a new function is introduced:

$$\lambda(k) = \frac{\sqrt{(0+ikv)^2+\omega_1^2(k)} - \sqrt{(0+ikv)^2+\omega_2^2(k)}}{\sqrt{(0+ikv)^2+\omega_1^2(k)} + \sqrt{(0+ikv)^2+\omega_2^2(k)}}. \tag{3.14}$$

The square roots in the last formula are chosen in such a way that for any $s > 0$ from the limit $(s \pm ik)$, $s \to 0+$ they represent the same branches and, hence, are continuous. If $s > 0$ then it is possible to show, as in [85], that $|\lambda(k)| \leq 1$, $k \in \mathbb{R}$ and, consequently, only the first root $\lambda_1(k)$ should be taken. Function $\lambda(k)$ possesses the following properties:

$$|\lambda(k)| = |\lambda(-k)|, \quad \mathrm{Arg}\lambda(k) = -\mathrm{Arg}\lambda(-k), \quad k \in \mathbb{R}. \tag{3.15}$$

We can also write the asymptotic behaviour of the function at infinity:

$$\lambda(k) \sim -\frac{2\omega_0^2}{v^2k^2}, \quad k \to \infty. \tag{3.16}$$

The asymptotic behaviour of $\lambda(k)$ at $k \to 0$ is derived by Taylor expansion of $\omega_{1,2}^2(k)$ and square roots presented in (3.14). The final expression becomes:

$$\lambda(k) = 1 - \sqrt{\frac{v_c^2 - v^2}{\omega_0^2}}\sqrt{0+ik}\sqrt{0-ik} + o(k), \quad k \to 0. \tag{3.17}$$

Note also that $\lambda(k)$ takes only real values within some intervals, e.g. $-p_1 < k < p_1$. To illustrate the behaviour of function $\lambda(k)$, the plots of $|\lambda(k)|$ and $\mathrm{Arg}\lambda(k)$ are shown in Fig. 3.3 for the cases $v = 0.2v_c$ and $v = 0.5v_c$ for positive values of k. In this figures it can be explicitly seen that $|\lambda(k)| = 1$ only when $(\omega_1^2(k) - k^2v^2)(\omega_2^2(k) - k^2v^2) \leq 0$ which is supported by the dispersion relations in Fig. 3.2. For the purpose of convenience the set of such point can be defined:

$$\mathcal{K} = \left\{k \in \mathbb{R} : \left(\omega_1^2(k) - k^2v^2\right)\left(\omega_2^2(k) - k^2v^2\right) \leq 0\right\}. \tag{3.18}$$

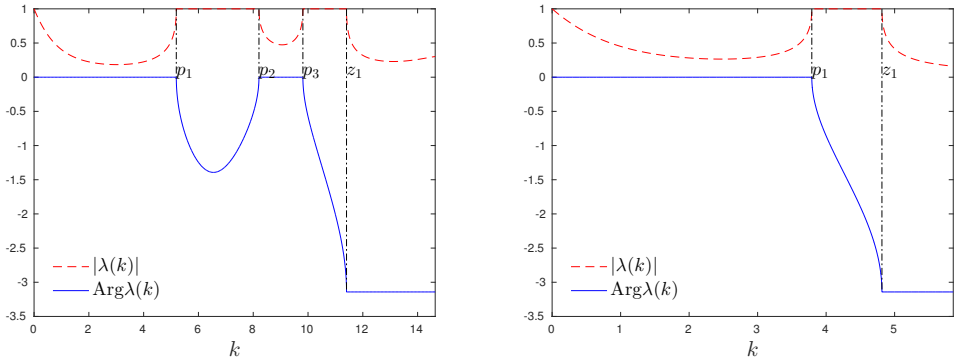

Figure 3.3: Absolute value and argument of $\lambda(k)$ for different values of crack speed and $c_2 = c_1$: a) $v = 0.2v_c$, b) $v = 0.5v_c$.

The investigation of function $\lambda(k)$ reveals that this function, for certain values of k, can be presented as:

$$\begin{gathered} \lambda(k) = e^{i\phi_\lambda(k)}, \quad \phi_\lambda(k) \in \mathbb{R}, \quad k \in \mathcal{K}, \\ \tan\frac{\phi_\lambda(k)}{2} = \sqrt{-\frac{(0+ikv)^2+\omega_2^2(k)}{(0+ikv)^2+\omega_1^2(k)}}, \quad k \in \mathcal{K}, \end{gathered} \tag{3.19}$$

where set $\mathcal{K}$ is defined in (3.18). Function $\phi_\lambda(k)$ should be chosen in such a manner that it is continuous along the entire the real axis. By straightforward substitution of roots (3.8) into expression (3.14) it is easy to check:

$$\begin{gathered} \lambda(p_j) = 1, \quad j = 1, 2, ..., P, \\ \lambda(z_j) = -1, \quad j = 1, 2, ..., Z, \\ \lambda(0) = 1. \end{gathered}$$

3.1.5 Derivation of Wiener-Hopf type equation

The application of Fourier transform to equations (3.5) reduces them to:

$$\begin{gathered}\left((0+ikv)^2+\omega_2^2(k)+2\omega_0^2\right)U^+(k)+\left((0+ikv)^2+\omega_2^2(k)\right)U^-(k)\\ =\omega_0^2\left(U_1(k)-U(k)\right),\quad m=0,\\ \left((0+ikv)^2+\omega_2^2(k)+2\omega_0^2\right)U_m(k)=\omega_0^2\left(U_{m+1}(k)-U_{m-1}(k)\right),\quad m\geq 1.\end{gathered} \tag{3.20}$$

where the notations are:

$$\begin{gathered}U(k)=U_0(k)=\int_{-\infty}^{\infty}u_0(\eta)e^{ik\eta}\,d\eta=U^+(k)+U^-(k),\\ U^{\pm}(k)=\int_{-\infty}^{\infty}u_0(\eta)H(\pm\eta)e^{ik\eta}\,d\eta,\\ U_m(k)=\int_{-\infty}^{\infty}u_m(\eta)e^{ik\eta}\,d\eta,\quad m\geq 1.\end{gathered} \tag{3.21}$$

Particular choice of the solution that is shown in Section 3.1.4 allows to satisfy the equations for $m\geq 1$. Indeed, this becomes possible with (3.11). At the same time the equation for $m=0$ can be expressed as:

$$L(k)U^+(k)+U^-(k)=0. \tag{3.22}$$

The kernel function $L(k)$ in this case is defined as:

$$L(k)=\sqrt{\frac{(0+ikv)^2+\omega_1^2(k)}{(0+ikv)^2+\omega_2^2(k)}}, \tag{3.23}$$

where the functions $\omega_{1,2}(k)$ are defined in (3.6), (3.7). Notice that structure of equation (3.22) is similar the one for the dynamic chain in (2.28). The distinction between Wiener-Hopf equations of lattice and chain problems is in the kernel function $L(k)$ (compare (3.23) and (2.37)). Hence, there will be particular differences in the solution behaviour.

In any case, function $L(k)$ in (3.23) of a lattice problem has the same properties as the kernel function of a chain problem:

$$|L(k)|=|L(-k)|,\quad \mathrm{Arg}L(k)=-\mathrm{Arg}L(-k),\quad k\in\mathbb{R} \tag{3.24}$$

The asymptotic behaviour of $L(k)$ is estimated to be:

$$L(k) = 1 - \frac{2\omega_0^2}{v^2 k^2} + O(k^{-4}), \quad k \to \infty, \tag{3.25}$$

$$L(k) \sim \frac{2\omega_0}{\sqrt{v_c^2 - v^2}} \frac{1}{\sqrt{(0+ik)(0-ik)}}, \quad k \to 0, \tag{3.26}$$

The notations of v_c^2 and ω_0^2 are given in (3.3) and (3.6), respectively.

3.1.6 Solution of the Wiener-Hopf equation

Properties of function $L(k)$ in (3.24) and its asymptotic behaviour (3.25), (3.26) makes it possible to use factorisation by means of Cauchy-type integral (2.32). In other words, $L(k)$ is expressed as:

$$L(k) = L^+(k)L^-(k), \quad L^\pm(k) = \exp\left(\pm\frac{1}{2\pi i}\int\limits_{-\infty}^{\infty} \frac{\mathrm{Log}L(\xi)}{\xi - k}\, d\xi\right). \tag{3.27}$$

The factors $L^\pm(k)$ are analytic in the half-planes $\pm\Im k > 0$ and satisfy the following asymptotic relations:

$$L^\pm(k) = 1 \pm i\frac{Q}{k} + O\left(\frac{1}{k^2}\right), \quad k \to \infty, \quad Q = \frac{1}{\pi}\int\limits_0^\infty \log|L(k)|\, dk. \tag{3.28}$$

One can estimate asymptotic behaviour of the factors at zero with the use of (3.26), (3.27) and the Sokhotski-Plemelj theorem::

$$\begin{gathered} L^\pm(k) = R^{\pm 1}\left(\frac{4\omega_0^2}{v_c^2 - v^2}\right)^{1/4} \frac{1}{\sqrt{0 \mp ik}}\,(1 + (0 \mp ik)S) + o(1), \quad k \to 0, \\ R = \exp\left(\frac{1}{\pi}\int\limits_0^\infty \frac{\mathrm{Arg}L(k)}{k}\, dk\right), \quad S = \frac{1}{\pi}\int\limits_0^\infty \frac{\log|L(k)|}{k^2}\, dk. \end{gathered} \tag{3.29}$$

Such asymptotic behaviour follows from the fact that $v < v_c$ and the particular form of the kernel function $L(k)$ in (3.23). Notice that there is a

square root singularity of functions $L^{\pm}(k)$. The factors of a chain problem had k^{-1} singularity which is highlighted in (2.59). There is also a difference in the computation of constant R. Plots of argument of $L(k)$ are presented in Fig. 3.4 for $v = 0.2v_c$ and $v = 0.5v_c$. The calculations of R are displayed on those plots as well. In these figures we observe that function $\mathrm{Arg}L(k)$ is a stepwise. It experiences jumps of magnitude $\pi/2$ at poles and zeros of function $L(k)$, which is in the contrast to the argument of kernel function of a chain problem. In the latter case function experienced jumps of magnitude π (see Fig. 2.7).

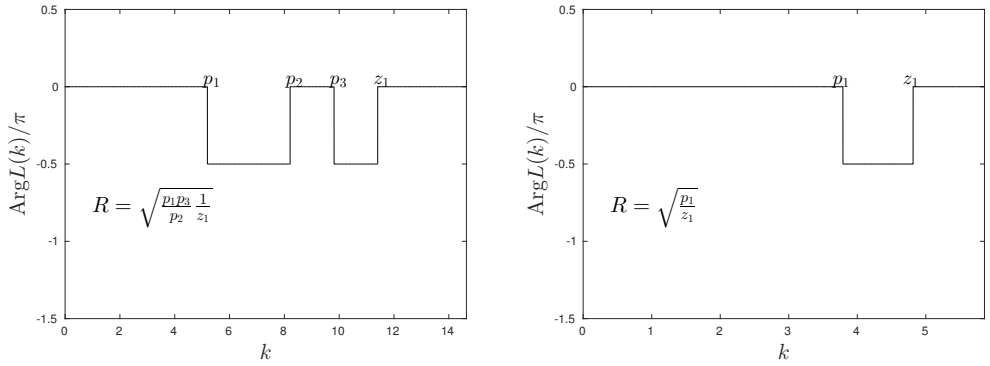

a) b)

Figure 3.4: Argument of $L(k)$ for different values of crack speed and $\mu = 1$: a) $v = 0.2v_c$, b) $v = 0.5v_c$. The way to calculate function R in (3.29) is shown for the presented cases.

Taking into an account the asymptotic relations (3.28) and (3.29) the right hand-side of equation (3.22) can be modified [85]:

$$L^+(k)U^+(k) + \frac{1}{L^-(k)}U^-(k) = \frac{C}{0 - ik} + \frac{C}{0 + ik},$$

where $C = const$. The solution of the problem should experience a proper asymptotic behaviour. To be more precise, we expect the solution to match the square-root behaviour of the displacement at the crack tip that appears

in the analysis of linear elastic fracture mechanics for mode III fracture [85]. It will be shown explicitly below.

Thus, accordingly with [85], we obtain:

$$U^+(k) = \frac{C}{0-ik}\frac{1}{L^+(k)}, \quad U^-(k) = \frac{C}{0+ik}L^-(k) \tag{3.30}$$

Utilising the same reasoning as in Section 2.1.3.5 the expression for displacement $u_0(\eta)$ is:

$$u_0(\eta) = \frac{1}{2\pi}\int_{-\infty}^{\infty} U^{\pm}(k)e^{-ik\eta}\,dk, \quad \pm\eta > 0. \tag{3.31}$$

From (3.28), (3.29) and (3.30) it follows that:

$$\begin{gathered} U^{\pm}(k) = \pm\frac{Ci}{k}\left(1-\frac{Q}{k}\right) + O\left(\frac{1}{k^3}\right), \quad k \to \infty, \\ U^+(k) = \frac{C}{R}\left(\frac{v_c^2-v^2}{4\omega_0^2}\right)^{1/4}\frac{1}{\sqrt{0-ik}} + o(1), \quad k \to +0, \\ U^-(k) = \frac{C}{R}\left(\frac{4\omega_0^2}{v_c^2-v^2}\right)^{1/4}\left(\frac{1}{(0+ik)^{3/2}} + \frac{S}{\sqrt{0+ik}}\right) + o(1), \quad k \to -0. \end{gathered} \tag{3.32}$$

First relations in (3.32) give the asymptotic behaviour of solution $u(\eta)$ at zero:

$$u_0(\eta) = C(1-Q\eta) + O(\eta^2), \quad \eta \to 0, \tag{3.33}$$

whereas from the last 2 expressions in (3.32) by means of contour integration we conclude:

$$\begin{gathered} u_0(\eta) = \frac{C}{R}\left(\frac{v_c^2-v^2}{4\omega_0^2}\right)^{1/4}\frac{1}{\sqrt{\pi\eta}} + o(1), \quad \eta \to \infty, \\ u_0(\eta) = \frac{C}{R}\left(\frac{4\omega_0^2}{v_c^2-v^2}\right)^{1/4}\left(2\sqrt{\frac{-\eta}{\pi}} + \frac{S}{\sqrt{-\pi\eta}}\right) + o(1), \quad \eta \to -\infty. \end{gathered} \tag{3.34}$$

The specifics of a lattice problem reveal different behaviour of a solution far from the crack tip. For a chain problem, for comparison, there was a

linear growth at $\eta \to -\infty$ and possible oscillations ahead of a crack tip which is given by (2.63). Meanwhile, the behaviour at the crack tip remains linear. Constant C in (3.31) is found from the fracture criterion (3.4):

$$C = u_c. \tag{3.35}$$

According to (3.11), the displacements of layers are constructed as follows:

$$u_m(\eta) = \frac{1}{2\pi} \int_{-\infty}^{\infty} \lambda^m(k)[U^+(k) + U^-(k)]e^{-ik\eta}\, dk, \quad m \geq 1. \tag{3.36}$$

3.1.7 Factorisation of $L(k)$ and asymptotic analysis

The function $L(k)$ in (3.23) can be expressed as:

$$\begin{gathered} L(k) = \sqrt{L_0(k)l(k)}, \quad l(k) = l^+(k)l^-(k), \\ L_0(k)l(k) = \frac{(0+ikv)^2 + \omega_1^2(k)}{(0+ikv)^2 + \omega_2^2(k)}, \end{gathered} \tag{3.37}$$

where dispersion relations $\omega_{1,2}(k)$ are defined in (3.6) and (3.7), respectively. The expression for product $L_0(k)l(k)$ has the same form as the one that was used for a factorisation of function $L(k)$ in a chain problem. Thus, all the results obtained in Section 2.1.3.5 can be adopted. Functions $l^{\pm}(k)$, hence, have the form in (2.68) and function $L_0(k) = L_0^+(k)L_0^-(k)$ is shown in (2.70). The factorisation of function $L(k)$ for a lattice problem turns into:

$$L(k) = L^+(k)L^-(k), \quad L^{\pm}(k) = \sqrt{L_0^{\pm}(k)l^{\pm}(k)}.$$

In this section the asymptotic expressions for $U^{\pm}(k)$ from (3.30) are developed. Firstly, the behaviour of functions $l^{\pm}(k)$ at infinity is derived in (2.73). For the current analysis it can be presented as:

$$l^{\pm} = 1 \pm \frac{i(p_0 + dp_0)}{k} + O\left(\frac{1}{k^2}\right), \quad k \to \infty. \tag{3.38}$$

The notations for d and p_0 can be found in (2.68) and (2.69), respectively. Taking into an account the estimates of the behaviour of functions $L_0^{\pm}(k)$ in (2.77), the expression the is used here is:

$$L_0^{\pm}(k) = 1 \pm i\frac{Q_0}{k}, \quad k \to \infty, \quad Q_0 = \frac{1}{\pi}\int\limits_0^{\infty} \log|L_0(k)|\, dk. \tag{3.39}$$

Expressions (3.30),(3.38) and (3.39) reveal:

$$U^{\pm} = \pm\frac{u_c i}{k}\left[1 - \frac{i}{2}\frac{p_0 + 2dp_0 + Q_0}{k}\right] + O\left(\frac{1}{k^3}\right), \quad k \to \infty. \tag{3.40}$$

The necessity in getting (3.40) is explained by the numerical algorithms that are used for evaluating the inverse Fourier transform. For that method the behaviour of functions at infinity is required (see Section A.2).

Now we study the behaviour of functions at $k = 0$. According to (2.80), the behaviour of functions $l^{\pm}(k)$ is:

$$\begin{aligned} l^{+}(k) &= \frac{-i\alpha_1^{+}}{0 - ik}, \quad k \to 0, \\ l^{-}(k) &= \frac{i\alpha_1^{-}}{0 + ik} + \alpha_2^{-}, \quad k \to 0, \end{aligned} \tag{3.41}$$

where coefficients $\alpha_1^{\pm}, \alpha_2^{-}$ are shown in (2.80). The asymptotic expressions for $L_0^{\pm}(k)$ comes from (2.85):

$$L_0^{\pm} = 1 + S_0(0 \mp ik) + o(k), \quad k \to 0, \quad S_0 = \frac{1}{\pi}\int_0^{\infty} \frac{\log|L_0(k)|}{k^2}\, dk. \tag{3.42}$$

In (3.41) and (3.42) notations $(0 \pm ik)$ have been used which becomes useful for the treating of square roots. With the last formulae it is possible to write down the expressions for behaviour of functions $U^{\pm}(k)$ for a lattice

problem:

$$
\begin{aligned}
U^+(k) &= \frac{f^+_{1/2}}{\sqrt{0-ik}} + o(1), k \to 0, \\
U^-(k) &= \frac{f^-_{3/2}}{(0+ik)^{3/2}} + \frac{f^-_{1/2}}{\sqrt{0+ik}} + o(1), k \to 0, \\
f^+_{1/2} &= \frac{u_c}{\sqrt{-i\alpha^+_1}}, \quad f^-_{3/2} = u_c\sqrt{i\alpha^-_1}, \quad f^-_{1/2} = u_c\frac{\alpha^-_2 + i\alpha^-_1 S_0}{2\sqrt{i\alpha^-_1}}.
\end{aligned}
\tag{3.43}
$$

Finally, the solution for $U^{\pm}(k)$ in (3.30) provides the following asymptotic behaviour at their non-zero singular points:

$$
\begin{aligned}
U^+(k) &\sim \frac{\sqrt{W^+_j}}{\sqrt{0-i(k-z_{2j})}}, \quad k \to z_{2j}, \quad j = 1, 2, ..Z', \\
U^-(k) &\sim \frac{\sqrt{W^-_j}}{\sqrt{0+i(k-p_{2j-1})}}, \quad k \to p_{2j}, \quad j = 1, 2, ..P',
\end{aligned}
\tag{3.44}
$$

where z_{2j}, p_{2j-1}, Z, P are defined in (3.8), $\lceil x \rceil$ is a ceiling of number x. Coefficients $W^{\pm}_j$ are defined in (2.87) and (2.88). The properties of functions $L^{\pm}(k)$ in (3.24) lead to:

$$
\begin{aligned}
U^+(k) &\sim \frac{\sqrt{\overline{W^+_j}}}{\sqrt{0-i(k+z_{2j})}}, \quad k \to -z_{2j}, \quad j = 1, 2, ..Z', \\
U^-(k) &\sim \frac{\sqrt{\overline{W^-_j}}}{\sqrt{0+i(k+p_{2j-1})}}, \quad k \to -p_{2j}, \quad j = 1, 2, ..P'.
\end{aligned}
$$

In the presentation of final results it is convenient to use notations for $W^{\pm}(k)$ in (2.89):

$$
\begin{aligned}
\rho^+_j &= \left|W^+_j\right|, \beta^+_j = \mathrm{Arg}\left(W^+_j\right), \quad j = 1, 2, ..., Z', \\
\rho^-_j &= \left|W^-_j\right|, \beta^-_j = \mathrm{Arg}\left(W^-_j\right), \quad j = 1, 2, ..P'.
\end{aligned}
\tag{3.45}
$$

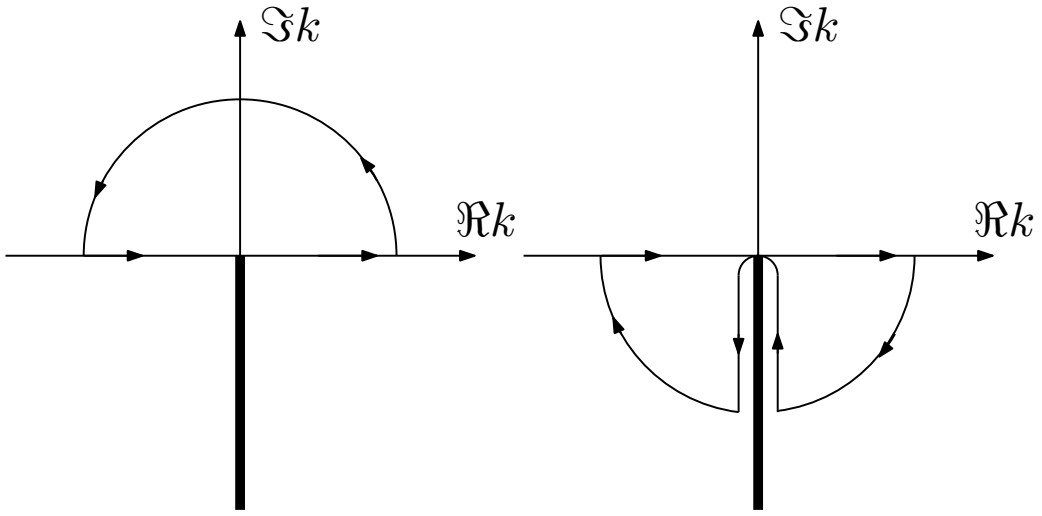

Figure 3.5: a) Contour of integration for $\eta < 0$, b) Contour of integration for $\eta > 0$

3.1.8 Evaluation of related integrals

We have to evaluate the integrals of type:

$$\int_{-\infty}^{\infty} \frac{e^{-ik\eta}}{\sqrt{0-ik}}\, dk, \tag{3.46}$$

which can be done by means of the contour integrations. By introducing the new variable $z > 0$, the square root in (3.46) is taken as follows:

$$\sqrt{0-ik} = \begin{cases} i\sqrt{z}, & \Im k < 0, \quad \Re k \to 0-, \\ -i\sqrt{z}, & \Im k < 0, \quad \Re k \to 0+. \end{cases} \tag{3.47}$$

There are two different scenarios for the evaluation of integral (3.46). If $\eta < 0$ then the contour in Fig. 3.5a) should be picked. There are no singularities of integrand inside that contour, hence, the integral of function inside (3.46) along that contour is zero. Next, due the fact that function $e^{-ik\eta}$ is decaying for $\Im k > 0$, $\eta > 0$ and with the help of Jordan's lemma from

complex analysis we conclude that the integral along a semicircle vanishes when its radius tends to infinity. To sum up:

$$\int_{-\infty}^{\infty} \frac{e^{-ik\eta}}{\sqrt{0-ik}}\,dk = 0, \quad \eta < 0.$$

In the case $\eta > 0$ contour shown in Fig. 3.5b) should be considered. Again, there are no singularities of function inside that contour. Consequently, from Cauchy residue theorem the integral along the contour annihilates. Moreover, the integration along the quarters of a circle gives zero when the radius tends to infinity, with a help of Jordan's lemma. Finally, with the utilisation of the chosen root definition we get:

$$\int_{-\infty}^{\infty} \frac{e^{-ik\eta}}{\sqrt{0-ik}}\,dk = 2\int_{0}^{\infty} \frac{e^{-z\eta}}{\sqrt{z}}\,dz.$$

The successful integration of the last integral gives the final result:

$$\int_{-\infty}^{\infty} \frac{e^{-ik\eta}}{\sqrt{0-ik}}\,dk = 2\sqrt{\frac{\pi}{\eta}}H(\eta). \tag{3.48}$$

The different types of integral that appear in a lattice problem have a term $\sqrt{0-ik}$. By means of change of variables and similar considerations of contour integrals we obtain:

$$\int_{-\infty}^{\infty} \frac{e^{-ik\eta}}{\sqrt{0+ik}}\,dk = 2\sqrt{-\frac{\pi}{\eta}}H(-\eta). \tag{3.49}$$

From the last expression and with the integration by parts the following is valid:

$$\int_{-\infty}^{\infty} \frac{e^{-ik\eta}}{(0+ik)^{3/2}}\,dk = -4\eta\sqrt{-\frac{\pi}{\eta}}H(-\eta). \tag{3.50}$$

Finally, contour integration in case $\eta > 0$ gives the exact value for the integral:

$$\int_{-\infty}^{\infty} \frac{\sqrt{0-ik}}{(0+ik)}e^{-ik\eta}\,dk = -2\sqrt{\frac{\pi}{\eta}}H(\eta). \tag{3.51}$$

3.1.9 Solution representation for $m = 0$

The final result for $u_0(k)$ is expressed through inverse Fourier transform as shown in (3.31). Let us subtract the singularities from functions $U^{\pm}(k)$ and introduce notations:

$$\hat{U}^{+}(k) = U^{+}(k) - \frac{f^{+}_{1/2}}{\sqrt{0 - ik}} - \sum_{j=1}^{Z'} \left[\frac{\sqrt{\rho^{+}_{j}} e^{i\beta^{+}_{j}/2}}{\sqrt{0 - i(k - z_{2j})}} + \frac{\sqrt{\rho^{+}_{j}} e^{-i\beta^{+}_{j}/2}}{\sqrt{0 - i(k + z_{2j})}} \right],$$

$$\hat{U}^{-}(k) = U^{-}(k) - \frac{f^{-}_{3/2}}{(0 + ik)^{3/2}} - \frac{f^{-}_{1/2}}{\sqrt{0 - ik}} - \sum_{j=1}^{P'} \left[\frac{\sqrt{\rho^{-}_{j}} e^{i\beta^{-}_{j}/2}}{\sqrt{0 + i(k - p_{2j-1})}} + \frac{\sqrt{\rho^{-}_{j}} e^{-i\beta^{-}_{j}/2}}{\sqrt{0 + i(k + p_{2j-1})}} \right],$$

where $f^{\pm}_{1/2}, f^{-}_{3/2}$ can be found in (3.43) and notations (3.45) are used. The results of contour integration now can be applied that are given in (3.48), (3.49) and (3.50). Properties of functions $L^{\pm}(k)$ in (3.24), and the same of $\hat{U}^{\pm}(k)$, possible to write the expression for $u_0(\eta)$ in (3.31) as:

$$\begin{aligned} u_0(\eta) &= \frac{1}{\pi} \Re \left(\int_{-\infty}^{\infty} \hat{U}^{+}(k) e^{-ik\eta}\, dk \right) + \frac{f^{+}_{1/2}}{\sqrt{\pi\eta}} \\ &\quad + \sum_{j=1}^{Z'} \frac{2\sqrt{\rho^{+}_{j}} \cos\left(z_{2j}\eta - \frac{\beta^{+}_{j}}{2} \right)}{\sqrt{\pi\eta}}, \quad \eta > 0, \\ u_0(\eta) &= \frac{1}{\pi} \Re \left(\int_{-\infty}^{\infty} \hat{U}^{-}(k) e^{-ik\eta}\, dk \right) + 2 f^{-}_{3/2} \sqrt{-\frac{\eta}{\pi}} + \frac{f^{-}_{1/2}}{\sqrt{-\pi\eta}} \\ &\quad + \sum_{j=1}^{P'} \frac{2\sqrt{\rho^{-}_{j}} \cos\left(p_{2j-1}\eta - \frac{\beta^{-}_{j}}{2} \right)}{\sqrt{-\pi\eta}}, \quad \eta < 0. \end{aligned} \tag{3.52}$$

In this form the integration does not cause computational difficulties any

longer because the functions $\hat{U}^{\pm}(k)$ do not contain singularities along the integration path. It was used for presenting the final results.

3.1.10 Solution representation for $m \geq 1$

For the integration in the expressions of $u_m(\eta)$, $m \geq 1$ in (3.36) the information about the behaviour of $\lambda^m(k)U^{\pm}(k)$ should be extracted. The asymptotic behaviour of $\lambda(k)$ at infinity in (3.16) and relations (3.40) provide:

$$\lambda^m(k)U^{\pm}(k) = \pm\left(-\frac{2\omega_0^2}{v^2}\right)^m \frac{i}{k^{2m+1}}\left(1 - \frac{i}{2}\frac{p_0 + 2dp_0 + Q_0}{k}\right) + O\left(\frac{1}{k^{2m+3}}\right), \quad k \to \infty.$$

The asymptotic behaviour of λ can be found in (3.17). Its combination with (3.43) gives:

$$\lambda^m(k)U^{+}(k) = \frac{f_{1/2}^{+}}{\sqrt{0 - ik}} + o(1), \quad k \to 0,$$
$$\lambda^m(k)U^{-}(k) = \frac{f_{1/2}^{-}}{\sqrt{0 + ik}} + \frac{f_{3/2}^{-}}{(0 + ik)^{3/2}} - mf_{3/2}^{-}\sqrt{\frac{v_c^2 - v^2}{\omega_0^2}}\frac{\sqrt{0 - ik}}{0 + ik}.$$

The properties of function $\lambda(k)$ in (3.19) are also worth of recalling:

$$\lambda(p_j) = 1, \quad j = 1, 2, ..., P,$$
$$\lambda(z_j) = e^{-i\pi}, \quad j = 1, 2, ..., Z.$$

Now, the singularities of functions $\lambda^m(k)U^{\pm}(k)$ can be subtracted. The

regular functions are introduced:

$$\hat{U}_m^{(1)}(k) = \lambda^m(k)U^+(k) - \frac{f_{1/2}^+}{\sqrt{0-ik}} - \sum_{j=1}^{Z'}\left[\frac{\sqrt{\rho_j^+}e^{i(\beta_j^+/2-m\pi)}}{\sqrt{0-i(k-z_{2j})}} + \frac{\sqrt{\rho_j^+}e^{-i(\beta_j^+/2+m\pi)}}{\sqrt{0-i(k+z_{2j})}}\right],$$
$$\hat{U}_m^{(2)}(k) = \lambda^m(k)U^-(k) + mf_{3/2}^-\sqrt{\frac{v_c^2-v^2}{\omega_0^2}}\frac{\sqrt{0-ik}}{0+ik} - \frac{f_{3/2}^-}{(0+ik)^{3/2}} - \frac{f_{1/2}^-}{\sqrt{0+ik}} - \sum_{j=1}^{P'}\left[\frac{\sqrt{\rho_j^-}e^{i\beta_j^-/2}}{\sqrt{0+i(k-p_{2j-1})}} + \frac{\sqrt{\rho_j^-}e^{-i\beta_j^-/2}}{\sqrt{0+i(k+p_{2j-1})}}\right]. \tag{3.53}$$

Using the expressions for integrals in (3.48),(3.49),(3.50) and (3.51) we get:

$$u_m(\eta) = \frac{1}{\pi}\Re\left(\int_{-\infty}^{\infty}\left[\hat{U}_m^{(1)}(k) + \hat{U}_m^{(2)}(k)\right]e^{-ik\eta}\right)dk + \left[\frac{f_{1/2}^+}{\sqrt{\pi\eta}} + m\sqrt{\frac{v_c^2-v^2}{\omega_0^2}}\frac{f_{3/2}^-}{\sqrt{\pi\eta}} + \sum_{j=1}^{Z'}\frac{2\sqrt{\rho_j^+}\cos\left(z_{2j}\eta - \left(\frac{\beta_j^+}{2} - m\pi\right)\right)}{\sqrt{\pi\eta}}\right]H(\eta) + \left[2f_{3/2}^-\sqrt{-\frac{\eta}{\pi}} + \frac{f_{1/2}^-}{\sqrt{-\pi\eta}} + \sum_{j=1}^{P'}\frac{2\sqrt{\rho_j^-}\cos\left(p_{2j-1}\eta - \frac{\beta_j^-}{2}\right)}{\sqrt{-\pi\eta}}\right]H(-\eta). \tag{3.54}$$

Here, $f_{1/2}^{\pm}, f_{3/2}^-$ are given in (3.43), $\rho_j^{\pm}, \beta_j^{\pm}$ are shown in (3.45). Expression (3.54) was used for the evaluation of displacements of the layers $m \geq 1$

3.1.11 Asymptotic behaviour of the solution at infinity

In order to obtain the required asymptotic behaviour when $m \to \infty$ we need to take into an account the behaviour of functions $\lambda(k)$ and $U_0^-(k)$ at zero from (3.17) and (3.32), respectively. Indeed, when $m \to \infty$ the integration in the expressions for $u_m(\eta)$ (see (3.36)) should be performed only within the intervals where $|\lambda(k)| = 1$. However, the leading term of the asymptotic

behaviour of $u_m(\eta)$ when $m \to \infty$ is provided by the singularity, encompassed in $U_0^-(k)$ when $k \to 0$. To show this, let us subtract the leading terms of $U_0^-(k)$ and $\lambda(k)$ when $k \to \infty$ from the expressions for $u_m(\eta)$ and perform the analytical integration.

Firstly, we consider case $\eta > 0$ and the integral to estimate is:

$$\int_{-\infty}^{\infty} (1 - A\sqrt{0+ik}\sqrt{0-ik})^m \frac{a}{(0+ik)^{3/2}} e^{-ik\eta}\, d\eta, \tag{3.55}$$

where

$$U^-(k) = \frac{a}{(0+ik)^{3/2}}, \quad \lambda(k) = 1 - A\sqrt{0+ik}\sqrt{0-ik}, \quad k \to 0.$$

Constants $a, A > 0$ are defined for the sake of reducing long expressions and will be substituted for the final expressions (see (3.17) and (3.32)). For this, we use the contour shown in Fig.3.5b). Applying the similar reasoning as in section 3.1.8 we get:

$$\begin{aligned}
&\int_{-\infty}^{\infty} (1 - A\sqrt{0+ik}\sqrt{0-ik})^m \frac{a}{(0+ik)^{3/2}} e^{-ik\eta} \\
&= -\frac{1}{i}\int_{\infty}^{0} (1+iAz)^m \frac{a}{z\sqrt{z}} e^{-z\eta}\, dz - \frac{1}{i}\int_{0}^{\infty} (1-iAz)^m \frac{a}{z\sqrt{z}} e^{-z\eta}\, dz \\
&= \int_0^{\infty} \frac{(1+iAz)^m - (1-iAz)^m}{iz\sqrt{z}} a e^{-z\eta}\, dz \\
&= \int_0^{1/m} \frac{(1+iAz)^m - (1-iAz)^m}{iz\sqrt{z}} a e^{-z\eta}\, dz \\
&+ \int_{1/m}^{\infty} \frac{(1+iAz)^m - (1-iAz)^m}{iz\sqrt{z}} a e^{-z\eta}\, dz.
\end{aligned}$$

Next, we are interested in the solutions along the ray:

$$\eta = \alpha m.$$

Hence, in the last equation of the derivation we apply the change of variable $t = mz$. We then notice that:

$$\left(1 + iA\frac{t}{m}\right)^m \to e^{iAt}, \quad \left(1 - iA\frac{t}{m}\right)^m \to e^{-iAt}, \quad m \to \infty.$$

With this in mind we continue the derivation:

$$\begin{aligned}
&\int_0^{1/m} \frac{(1+iAz)^m-(1-iAz)^m}{iz\sqrt{z}} a e^{-z\eta}\,dz \\
&\quad + \int_{1/m}^{\infty} \frac{(1+iAz)^m-(1-iAz)^m}{iz\sqrt{z}} a e^{-z\eta}\,dz \\
&= a\sqrt{m}\int_0^{\infty} \frac{\left(1+iA\frac{t}{m}\right)^m-\left(1-iA\frac{t}{m}\right)^m}{t\sqrt{t}} e^{-\alpha t}\,dt \\
&= 2a\sqrt{m}\int_0^{\infty} \frac{\sin At}{t\sqrt{t}} e^{-\alpha t}\,dt = 2a\sqrt{m}\sqrt{A}\int_0^{\infty} \frac{\sin x}{x\sqrt{x}} e^{-(\alpha/A)x} dx \\
&= 2aA\sqrt{m}\frac{\sqrt{2\pi}}{\sqrt{\alpha+\sqrt{\alpha^2+A^2}}}.
\end{aligned}$$

Finally, when $\eta > 0$, we achieve:

$$\begin{aligned}
u_m(\alpha m) \sim \sqrt{\frac{2}{\pi}}\sqrt{\frac{v_c^2-v^2}{\omega_0^2}}\left(\frac{4\omega_0^2}{v_c^2-v^2}\right)^{1/4}\frac{u_c}{R}\times \\
\times\frac{\sqrt{m}}{\sqrt{\alpha+\sqrt{\alpha^2+\frac{v_c^2-v^2}{\omega_0^2}}}}, \quad \alpha>0, \quad m\to\infty,
\end{aligned} \tag{3.56}$$

where the utilised notations are introduced earlier in this section. Let us now turn to the situation when $\eta < 0$. The integral in (3.55) can be written as:

$$\begin{aligned}
&\int_{-\infty}^{\infty} (1-A\sqrt{0+ik}\sqrt{0-ik})^m \frac{a}{(0+ik)^{3/2}} e^{-ik\eta}\,d\eta \\
&= \int_{-\infty}^{\infty} \left[(1-A\sqrt{0+ik}\sqrt{0-ik})^m - 1\right] \frac{a}{(0+ik)^{3/2}} e^{-ik\eta}\,d\eta \\
&\quad + \int_{-\infty}^{\infty} \frac{a}{(0+ik)^{3/2}} e^{-ik\eta}\,d\eta.
\end{aligned} \tag{3.57}$$

The evaluation of the second integral gives a straightforward result by means of the contour integration:

$$\int_{-\infty}^{\infty} \frac{a}{(0+ik)^{3/2}} e^{-ik\eta}\,d\eta = 4a\sqrt{-\pi\eta}, \quad \eta<0. \tag{3.58}$$

Notice, that in this case we need to consider a contour in the half-plane $\Im k > 0$, where $\sqrt{0+ik}$ possesses a cut:

$$\sqrt{0+ik} = \begin{cases} i\sqrt{z}, \Re k \to 0+, \\ -i\sqrt{z}, \Re k \to 0-, \end{cases}$$

where $k = iz$, $z > 0$, whereas $\sqrt{0-ik} = \sqrt{z}$. The Cauchy residue theorem and Jordan's lemma lead to:

$$\begin{aligned} &\int_{-\infty}^{\infty} \left[(1 - A\sqrt{0+ik}\sqrt{0-ik})^m - 1\right] \frac{a}{(0+ik)^{3/2}} e^{-ik\eta} \\ &= \int_{\infty}^{0} \left[(1+iAz)^m - 1\right] \frac{a}{z\sqrt{z}} e^{z\eta}\, dz - \int_{0}^{\infty} \left[(1-iAz)^m - 1\right] \frac{a}{z\sqrt{z}} e^{z\eta}\, dz \\ &= \int_{0}^{\infty} \frac{2 - (1+iAz)^m - (1-iAz)^m}{z\sqrt{z}} a e^{z\eta}\, dz \\ &= \int_{0}^{1/m} \frac{2 - (1+iAz)^m - (1-iAz)^m}{iz\sqrt{z}} a e^{z\eta}\, dz \\ &+ \int_{1/m}^{\infty} \frac{2 - (1+iAz)^m - (1-iAz)^m}{iz\sqrt{z}} a e^{z\eta}\, dz. \end{aligned}$$

Again, we make a change of variable $t = mz$ and assume that:

$$\eta = -\alpha m.$$

Taking the limit $m \to \infty$ we get the following expression:

$$\begin{aligned} &\int_{0}^{1/m} \frac{2 - (1+iAz)^m - (1-iAz)^m}{iz\sqrt{z}} a e^{z\eta}\, dz \\ &+ \int_{1/m}^{\infty} \frac{2 - (1+iAz)^m - (1-iAz)^m}{iz\sqrt{z}} a e^{z\eta}\, dz \\ &= a\sqrt{m} \int_{0}^{\infty} \frac{1 - \cos At}{t\sqrt{t}} e^{-\alpha t}\, dt = 2a\sqrt{m}\sqrt{A} \int_{0}^{\infty} \frac{1 - \cos x}{x\sqrt{x}} e^{-(\alpha/A)x}\, dx \\ &= 4a\sqrt{\pi m} \left(-\sqrt{\alpha} + (\alpha^2 + A^2)^{1/4} \cos\left(\frac{\operatorname{arccot} \frac{\alpha}{A}}{2} \right) \right), \end{aligned} \tag{3.59}$$

where $\operatorname{arccot} x$ is the inverse cotangent function. Sum of the last result with (3.58) provides the final for of asymptotic behaviour:

$$u_m(-\alpha\eta) \sim \frac{2u_c}{\sqrt{\pi}}\frac{1}{R}\left(\frac{4\omega_0^2}{v_c^2-v^2}\right)^{1/4}\left(\alpha^2+\frac{v_c^2-v^2}{\omega_0^2}\right)^{1/4}\times$$
$$\times\cos\left(\frac{\operatorname{arccot}\left(-\alpha\sqrt{\frac{\omega_0^2}{v_c^2-v^2}}\right)}{2}\right)\sqrt{m}, \quad m\to\infty, \alpha>0.$$

One can simplify the trigonometric term in the last expression using the following expressions:

$$\operatorname{arccot}\left(\frac{1}{x}\right)=\arctan(x), \quad \arctan(x)=2\arctan\left(\frac{x}{1+\sqrt{x^2+1}}\right),$$
$$\cos(\arctan(x))=\frac{1}{\sqrt{1+x^2}},$$

to obtain:

$$u_m(-\alpha\eta) \sim \sqrt{\frac{2}{\pi}}\sqrt{\frac{v_c^2-v^2}{\omega_0^2}}\left(\frac{4\omega_0^2}{v_c^2-v^2}\right)^{1/4}\frac{u_c}{R}\times$$
$$\times\frac{\sqrt{m}}{\sqrt{-\alpha+\sqrt{\alpha^2+\frac{v_c^2-v^2}{\omega_0^2}}}}, \quad \alpha>0, \quad m\to\infty$$

Notice, that the last expression is of the same form as in the previously considered case $\eta<0$. Thus, we can present the final formula of the asymptotic expression:

$$u_m(\alpha m) \sim \frac{2u_c}{R}\left(\frac{4\omega_0^2}{v_c^2-v^2}\right)^{1/4}\sqrt{\frac{m}{2\pi}}\times$$
$$\times\left(\frac{v_c^2-v^2}{\omega_0^2}\frac{1}{\alpha+\sqrt{\alpha^2+\frac{v_c^2-v^2}{\omega_0^2}}}\right)^{1/2}, \quad m\to\infty. \tag{3.60}$$

One can see that introducing the radius vector $\rho=\sqrt{m^2+\eta^2}=m\sqrt{1+\alpha^2}$ and the angle θ, such that $\cot\theta=\alpha$ (and, thus, $m=\rho\sin\theta$, $\eta=\rho\cos\theta$), the representation (3.60) can be conveniently rewritten in the

following manner:

$$u_m(\eta) \sim \frac{2u_c}{R}\left(\frac{4\omega_0^2}{v_c^2-v^2}\right)^{1/4}\sqrt{\frac{\rho}{2\pi}}\ \Phi(\theta,v), \quad \rho\to\infty, \tag{3.61}$$

$$\Phi(\theta,v) = \left(\sqrt{\cos^2\theta + \frac{v_c^2-v^2}{\omega_0^2}\sin^2\theta} - \cos\theta\right)^{1/2}, \quad 0\le\theta<\pi, \tag{3.62}$$

Using the relationship in (3.64), asymptotics (3.61) can be presented as:

$$u_m(\eta) \sim 2\sqrt{\frac{aG}{c_1}}\left(\frac{\omega_0^2}{v_c^2-v^2}\right)^{1/4}\sqrt{\frac{\rho}{2\pi}}\ \Phi(\theta,v), \quad \rho\to\infty. \tag{3.63}$$

It is worth of mentioning that continuum formulation similar problem with moving crack $v>0$ under mode III in the case of homogeneous material leads to the following asymptotic behaviour of the displacement field at the crack tip (see e.g. [10, p.356-360]):

$$u(r,\theta) \sim 2\sqrt{\frac{\mathcal{G}}{\hat{\mu}}}\left(1-\frac{v^2}{v_c^2}\right)^{-1/4}\sqrt{\frac{r}{2\pi}}\left(\sqrt{1-\frac{v^2}{v_c^2}\sin^2\theta}-\cos\theta\right), \quad r\to 0,$$

where $\hat{\mu}$ – shear modulus, $\mathcal{G}$ – macroscopic energy release rate and v_c is a shear wave speed in this case. Thus, the considered microscopic solution matches the behaviour of the macroscopic case.

3.1.12 Solution presentation and its analysis

In the works of Slepyan [86, 85] the energetic relations were derived. It was shown that the ratio between the local energy release rate and global energy release rate is:

$$\frac{G_0}{G} = R^2, \quad G_0 = \frac{2c_2u_c^2}{a}, \tag{3.64}$$

where parameter R is defined in (3.29). The quantity G_0/a is equal to the energy released due to the breakage of one link between the oscillators whereas G demonstrate the bulk change of energy. Apart from these quantities we

also introduce the energy that would have been released if the horizontal links would break at potential breakage position $\eta = \eta_*$:

$$G_1 = \frac{1}{2}\frac{c_1(u_0(\eta_* + 1) - u(\eta_*))^2}{a}. \tag{3.65}$$

As previously, the parameter that characterise contrast in elastic properties is:

$$\mu = \frac{c_2}{c_1}. \tag{3.66}$$

For the demonstration of the results we choose values $\mu = 0.1, 0.5, 1, 2$. The computations of the displacement fields require the prescribed values of v. The examples of displacement field $u_0(\eta)$ for different values of μ are shown in Fig. 3.6.

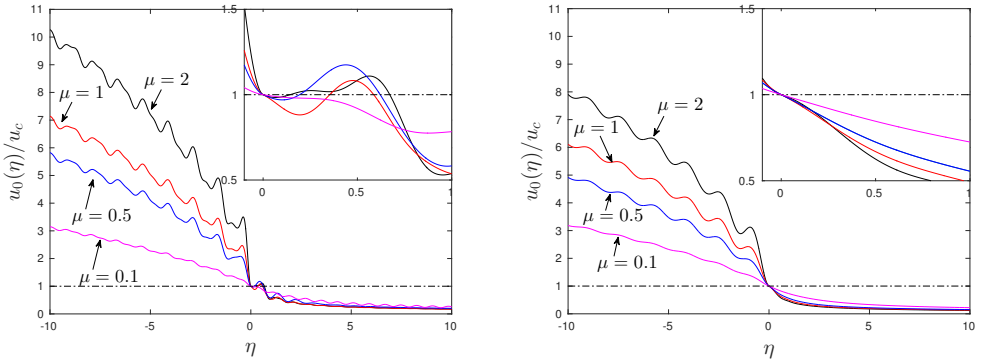

a) b)

Figure 3.6: Displacement field $u_0(\eta)$ for different values of crack speed and μ: a) $v = 0.2v_c$, b) $v = 0.5v_c$. The inserts show a zoom of the displacement profile in the neighbourhood of the crack tip. The dash-dot line shows the level of displacement $u(\eta) = u_c$.

After evaluation of displacement fields we can validate the second part of fracture criterion in (3.4). In Fig.3.6a) we observe the violation of this criterion in the cases $\mu = 0.5, 1, 2$ which makes these solutions unphysical for

$v = 0.2v_c$. At the same time the criterion (3.4) is hold for every chosen value of μ at $v = 0.5$ in fig. 3.6b).

Repeating the same terminology for classes of solution in Section 2.1.4 we distinguish types of regimes: admissible and forbidden. Again, for admissible ones criterion (3.4) holds while for another case it is violated. Besides that we would also check the integrity of horizontal springs of stiffness c_1 within the admissible regimes. We perform such analysis by means the condition:

$$\frac{G_0}{G_1} = \mu \tag{3.67}$$

By this, we assume that the ratio released energy when spring snaps is proportional to the spring constant which follows from the estimates of the theoretical strength in crystals. Posing either of these conditions allows to cut off the high values of the energy release rate as well as the high values of crack speed.

We perform the proceeding investigation of the obtained solution by means of definitions of admissible and forbidden regimes as well as conditions (3.67). Similar analysis was carried out for a triangular cell lattice [24, 64, 51]. The complete analysis is shown in Fig. 3.7 where the dependence of ratio G_0/G on crack speed is presented according to (3.64). In this figure admissible regimes are marked with thick lines, forbidden regimes – normal lines. Finally, the dash-line define the domains where condition (3.67) is met.

As said in [85], the ratio G_0/G demonstrates the fact that during the crack propagation not only the fracture energy (associated to term G) is released but also the elastic energy contained by the mechanical waves radiated by the crack tip. This fact is also observed in the dynamic fracture tests of materials [73]. That is to say, the lesser ratio G_0/G is the more energy is carried by the fracture waves. Notice in Fig. 3.7 that with increase of parameter μ, characterising the lattice anisotropy, for a chosen value v, ratio G_0/G decreases. This is reflected in the behaviour of $u_0(\eta)$ in Fig. 3.6 by the

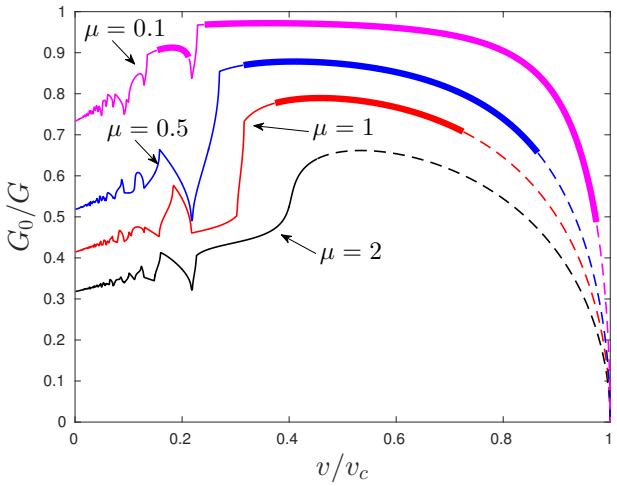

Figure 3.7: Dependence of energy release rate ratio G_0/G on crack speed. Admissible regimes – thick lines, forbidden regimes – normal lines, dash-lines – domains where the breakage of horizontal springs condition (3.67) is met.

increase of amplitude of the waves with increase of μ.

Here, again the non-monotonicity in G_0/G is observed as well as in a chain problem (see Fig. 2.92a)). This leads to uncertainty in definition of an external load that causes fracture. Indeed, choosing a certain value of G_0/G there can happen multiple intersections with the curves in Fig. 3.7 which induce a non-unique value of v. However, for this analysis we would like to stress the difference in admissible regimes caused by difference in material properties.

The solution analysis reveals a qualitative effect of introduced material anisotropy. Particularly, with a significant contrast in the properties some separate intervals of admissible and forbidden regimes appear within a condition (3.67). This is vividly noticed for $\mu = 0.1$ in fig. 3.7a). This gives an opportunity of a crack propagation at low speeds which is not a case for isotropic lattice. In terms of (3.67) the increase of parameter μ leads to the shrinkage of admissible domains and the possibility of failure of horizontal

springs grows. This circumstance is related to the increase of released elastic energy with an increase of μ. It finally bring a complete suppression of admissible regimes for $\mu = 2$.

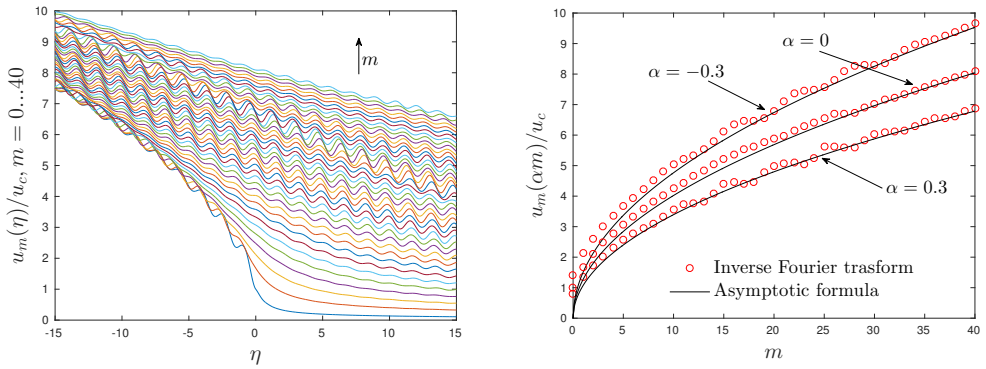

a) b)

Figure 3.8: Displacements $u_m(\eta), m = 0..40$ for $\mu = 1, v = 0.5v_c$: a) general picture, b) along the ray $\eta = \alpha m$ for different values of α. Markers stand for the points evaluated by the integration in (3.36), the solid line is given by (3.60).

Finally, we present a plot of displacements $u_m(\eta), m = 0..40$ for the case of isotropic lattice, $\mu = 1$, and $v = 0.5v_c$ in Fig. 3.8a). The change in vertical directions of $u_m(\eta)$ at point $\eta = 0$ and the same parameters μ, v is shown in Fig. 3.8b). From these figures we conclude that the amplitude of the waves in each layer m is different (see, Fig. 3.8a)) and there is a tendency in slow growth of displacements in vertical direction which can be clearly seen in Fig. 3.8b) and also supported by asymptotic expressions in (3.60) and (3.61). We also notice that the most dangerous elongations are found to be between layers $m = 0$ and $m = 1$ in the neighbourhood of a crack tip besides those layers adjacent to the symmetry line of a lattice. Nevertheless, these elongations do not exceed the threshold and remain to be less meaningful, in terms of fracture, than the elongations in horizontal direction. Additionally,

we pay an attention to the fact that the displacement field in Fig. 3.8a), essentially, is a sum of two components: the waves radiated from a crack tip which amplitude is decaying with the distance from a crack tip and monotonic deformation which increases closer to infinity.

3.2 Dissimilar lattice

3.2.1 Mathematical formulation of the problem

We proceed to the consideration of crack propagation in dissimilar square-cell lattice shown in Fig. 3.9. Material parameters of a top lattice are defined by index 1 while parameters of a bottom one are characterised by index 2. Masses of oscillators are $M_{1,2}$, horizontal and vertical springs inside lattices are prescribed as $c_{1,2}$ and $d_{1,2}$, respectively. A crack is supposed to propagate along an interface between lattices and occupies a half-line $n < n_*$, where index $n_* = n_*(t)$ marks a crack tip. The lattices are linked between each other along by linear springs c. An equilibrium distance between oscillators in horizontal and vertical direction is a.

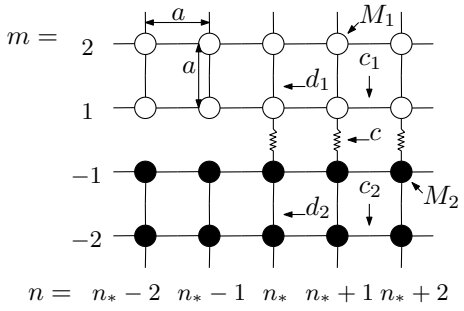

Figure 3.9: Dissimilar lattice compounded from two different materials attached together by linear springs of stiffness c. Masses of oscillators $M_{1,2}$ are connected between each other inside a corresponding lattice with springs of stiffness $c_{1,2}$ in horizontal direction and $d_{1,2}$ in vertical. Indices 1 and 2 refer to top and bottom lattices, respectively. Column n_* along the interface between the lattices marks a location of a crack tip. An equilibrium distance between oscillators in horizontal and vertical direction is a.

We study mode III fracture and assume that crack propagates along the interface following a straight path. The governing equations for this problem

are:

$$
\begin{aligned}
&\underline{m > 1}: \\
&M_1\ddot{u}_{m,n} = c_1(u_{m,n+1} + u_{m,n-1} - 2u_{m,n}) \\
&\qquad\qquad + d_1(u_{m+1,n} + u_{m-1,n} - 2u_{m,n}), \\
&\\
&\underline{m = 1}: \\
&M_1\ddot{u}_{1,n} = c_1(u_{1,n+1} + u_{1,n-1} - 2u_{1,n}) - c(u_{1,n} - w_{1,n}) \\
&\qquad\qquad + d_1(u_{2,n} - u_{1,n}),\ n \geq n_*, \\
&M_1\ddot{u}_{1,n} = c_1(u_{1,n+1} + u_{1,n-1} - 2u_{1,n}) + d_1(u_{2,n} - u_{1,n}), \quad n < n_*, \\
&\underline{m = -1}: \\
&M_2\ddot{w}_{1,n} = c_2(w_{1,n+1} + w_{1,n-1} - 2w_{1,n}) + c(u_{1,n} - w_{1,n}) \\
&\qquad\qquad + d_2(w_{2,n} - w_{1,n}),\ n \geq n_*, \\
&M_2\ddot{w}_{1,n} = c_2(w_{1,n+1} + w_{1,n-1} - 2w_{1,n}) + d_2(w_{2,n} - w_{1,n}), \quad n < n_*, \\
&\\
&\underline{m < -1}: \\
&M_2\ddot{w}_{-m,n} = c_2(w_{-m,n+1} + w_{-m,n-1} - 2w_{-m,n}) \\
&\qquad\qquad + d_2(w_{-m+1,n} + w_{-m-1,n} - 2w_{-m,n}),
\end{aligned}
\tag{3.68}
$$

where $u_{m,n} = u_{m,n}(t)$ is an out-of-plane displacement of an oscillator in m-th horizontal layer and n-th vertical layer of a top lattice lattice, and, similarly, $w_{m,n} = u_{m,n}(t)$ is an in-plane of a bottom lattice. Similarly to a previous problem in section 3.1, a crack movement is supposed to be caused by an energy flux coming from infinity towards a crack tip. This condition is not explicitly presented in the equations but will be taken into an account in the further analysis.

The fracture condition for this problem is stated as:

$$
|u_{1,n_*}(t_*) - w_{1,n_*}(t_*)| = \epsilon_c, \tag{3.69}
$$

where ϵ_c is a critical elongation of a spring which is considered as a material

property. We set an additional requirement to be satisfied:

$$|u_{1,n}(t) - w_{1,n}(t)| < \epsilon_c, \quad n > n_*, \quad \forall t. \tag{3.70}$$

In the last expressions t_* is fracture time and (3.70) provides the uniqueness of a crack tip along its path. Indeed, when it is violated one can detect a failure of a spring somewhere ahead of the main crack, $n > n_*$. In such cases a special analysis should be performed whereas in this study we concentrate at steady-state regimes.

It is convenient to introduce the following notations for the combinations of model parameters:

$$v_j = \sqrt{\frac{c_j}{M_j}}, \quad \beta_j = \sqrt{\frac{d_j}{M_j}}, \quad \mu_j = \frac{c}{d_j}, \quad j = 1, 2. \tag{3.71}$$

where quantities $v_{1,2}$ define the Rayleigh wave speeds,normalised by a, for top and bottom lattices, respectively. Parameters $\mu_{1,2}$ show contrast in elastic properties between an interface and lattices in vertical direction.

3.2.2 Steady-state crack propagation

A steady-state crack propagation implies a crack speed to have constant value v, which we keep normalised by a. A crack speed is limited by a critical value:

$$v < v_c, \quad v = \min(v_1, v_2), \tag{3.72}$$

where notations from (3.71) are involved. We switch to a moving reference frame with an origin at a crack tip:

$$\eta = n - vt, \quad v = const. \tag{3.73}$$

In (3.73) we assume that the coordinate η can be treated as continuous. In the contrary to the complementary one-dimensional problem of the double chain in section 2.3, the crack speed here is limited by the lowest speeds

of sounds. We also assume that steady-state displacements depend only on function η:

$$u_{m,n}(t) = u_m(\eta), \quad w_{m,n}(t) = w_m(\eta).$$

Hence, we eliminate the explicit dependence on time t. Fracture conditions in (3.69) and (3.70) are modified as:

$$|u_1(0) - w_1(0)| = \epsilon_c, \tag{3.74}$$

$$|u_1(\eta) - w_1(\eta)| < \epsilon_c, \quad \eta > 0. \tag{3.75}$$

Introduction of variable η causes changes in equations of motion (3.68), which become:

$$\begin{aligned} M_1 v^2 \frac{d^2}{d\eta^2} u_m(\eta) &= c_1(u_m(\eta+1) + u_m(\eta-1) - 2u_m(\eta)) \\ &+ d_1(u_{m+1}(\eta) + u_{m-1}(\eta) - 2u_m(\eta)), \\ M_1 v^2 \frac{d^2}{d\eta^2} u_1(\eta) &= c_1(u_1(\eta+1) + u_1(\eta-1) - 2u_1(\eta)) \\ &- c(u_1(\eta) - w_1(\eta))H(\eta) + d_1(u_2(\eta) - u_1(\eta)). \end{aligned} \tag{3.76}$$

for $m \geq 1$, and

$$\begin{aligned} M_2 v^2 \frac{d^2}{d\eta^2} w_{-m}(\eta) &= c_2(w_{-m}(\eta+1) + w_{-m}(\eta-1) - 2w_{-m}(\eta)) \\ &+ d_1(w_{-m+1}(\eta) + w_{-m-1}(\eta) - 2w_{-m}(\eta)), \\ M_2 v^2 \frac{d^2}{d\eta^2} w_1(\eta) &= c_2(w_1(\eta+1) + w_1(\eta-1) - 2w_1(\eta)) \\ &+ c(u_1(\eta) - w_1(\eta))H(\eta) + d_2(w_2(\eta) - w_1(\eta)). \end{aligned} \tag{3.77}$$

for $m \leq -1$. For the further analysis the following notations are useful:

$$\omega_j^2(k) = 4v_j^2 \sin^2\left(\frac{k}{2}\right), \quad j = 1, 2. \tag{3.78}$$

The last functions are related to wave characteristics and are involved in the definition of kernel functions that appear in the problem.

3.2.3 Description of problem in vertical direction

Let us consider the first equations in (3.76) and (3.77). The application of Fourier transform to this equation gives:

$$\begin{gathered}\left[(0+ikv)^2+\omega_1^2(k)+2\beta_1^2\right]U_m(k)=\beta_1^2(U_{m+1}(k)+U_{m-1}(k)),\quad m>1,\\ \left[(0+ikv)^2+\omega_2^2(k)+2\beta_2^2\right]W_{-m}(k)=\beta_2^2(W_{-m+1}(k)+W_{-m-1}(k)),\quad m<-1.\end{gathered} \tag{3.79}$$

Fourier transforms of displacements are given by:

$$U_m=\int_{-\infty}^{\infty}u_m e^{ik\eta}\,d\eta,\quad W_m=\int_{-\infty}^{\infty}w_m e^{ik\eta}\,d\eta. \tag{3.80}$$

and the notation $(0\pm k)$, that appears throughout the analysis, should be taken as follows:

$$(0\pm ik)=\lim_{s\to 0+}(s\pm ik). \tag{3.81}$$

Taking advantage from the fact that the coefficients in the system of linear equations do not depend on the value of n (or what is equivalent that the material properties of the system do not change in the direction perpendicular to the crack line we assume existence of functions $\lambda_{1,2}(k)$ such that:

$$\begin{aligned}U_m(k)&=\lambda_1^{m-1}(k)U_1(k),\quad m>1,\\ W_{-m}(k)&=\lambda_2^{-m-1}(k)W_1(k),\quad m<-1,\end{aligned} \tag{3.82}$$

where the functions $\lambda_{1,2}(k)$ should satisfy the following condition

$$|\lambda_j(k)|\le 1,\quad j=1,2. \tag{3.83}$$

Substituting (3.82) into (3.79), one obtains a quadratic equation to determine function $\lambda_{1,2}(k)$:

$$\lambda_j^2(k)-\frac{1}{\beta_j^2}\left((0+ikv)^2+\omega_j^2(k)+2\beta_j^2\right)\lambda_j(k)+1=0,\quad j=1,2. \tag{3.84}$$

The last equation delivers two solutions among which we choose the one that satisfy the requirement on $\lambda_{1,2}(k)$. Functions $\lambda_1(k)$ and $\lambda_2(k)$ are written as:

$$\lambda_j(k)=\frac{\sqrt{(0+ikv)^2+\omega_j^2(k)+4\beta_j^2}-\sqrt{(0+ikv)^2+\omega_j^2(k)}}{\sqrt{(0+ikv)^2+\omega_j^2(k)+4\beta_j^2}+\sqrt{(0+ikv)^2+\omega_j^2(k)}},\ j=1,2. \tag{3.85}$$

One can derive an asymptotic behaviour of functions $\lambda_{1,2}(k)$ at infinity:

$$\lambda_j(k) \sim -\frac{2\beta_j^2}{v^2k^2}, \quad k \to \infty, \quad j = 1, 2, \tag{3.86}$$

and at zero:

$$\lambda_j(k) = 1 - \frac{\sqrt{v_j^2 - v^2}}{\beta_j}\sqrt{(0 - ik)(0 + ik)} + o(k), \quad k \to 0, \quad j = 1, 2. \tag{3.87}$$

At this moment, the equations for derivation of the displacements $u_1(\eta)$ and $w_1(\eta)$ can be carried out.

3.2.4 Reduction of the problem to the Wiener-Hopf type equation

We turn to the examinations of the second equations in (3.76) and (3.77), which describe the displacements of oscillators along the interface. For their analysis it is useful to introduce linear combinations of displacements:

$$\psi(\eta) = u_1(\eta) - w_1(\eta), \quad \phi(\eta) = u_1(\eta) + w_1(\eta). \tag{3.88}$$

Function $\psi(k)$ represents a crack opening for $\eta < 0$ and a spring elongation for $\eta > 0$. Conditions (3.74) and (3.75) can be reformulated in terms of function $\psi(\eta)$:

$$|\psi(0)| = \epsilon_c, \quad |\psi(\eta)| < \epsilon_c, \, \eta > 0. \tag{3.89}$$

The introduction of function $\phi(k)$ provides the presentation of the equations in a compact form. Fourier transforms of newly set up functions are:

$$\begin{gathered} \Psi(k) = \int_{-\infty}^{\infty} \psi(\eta) e^{ik\eta} \, d\eta, \quad \Phi(k) = \int_{-\infty}^{\infty} \phi(\eta) e^{ik\eta} \, d\eta, \\ \Psi(k) = \Psi^+(k) + \Psi^-(k), \quad \Psi^{\pm}(k) = \int_{-\infty}^{\infty} \psi(\eta) H(\pm\eta) e^{ik\eta} \, d\eta. \end{gathered} \tag{3.90}$$

The use of Fourier transform for equations (3.76) and (3.77) for $m = 1$ and $m = -1$, respectively, reduces the problem to equations:

$$\begin{aligned}\left[(0+ikv)^2+\omega_1^2(k)\right]U_1(k) &= -\frac{c}{M_1}\Psi^+(k)+\beta_1^2(\lambda_1(k)-1)U_1,\\ \left[(0+ikv)^2+\omega_2^2(k)\right]W_1(k) &= \frac{c}{M_2}\Psi^+(k)+\beta_2^2(\lambda_2(k)-1)W_1.\end{aligned} \tag{3.91}$$

where we utilised the definitions of $\lambda_{1,2}(k)$ given earlier. Notice that (3.84) allow to modify the last equations to:

$$U_1 = -\mu_1\frac{\lambda_1}{1-\lambda_1}\Psi^+(k), \quad W_1 = \mu_2\frac{\lambda_2}{1-\lambda_2}\Psi^+(k). \tag{3.92}$$

Finally, we arrive to the equations:

$$\begin{aligned}\Psi^-(k)+L(k)\Psi^+(k) &= 0,\\ \Phi(k) &= -M(k)\Psi^+(k),\end{aligned} \tag{3.93}$$

where

$$\begin{aligned}L(k) &= \frac{L_1(k)+L_2(k)}{2}, \quad M(k) = \frac{L_1(k)-L_2(k)}{2},\\ L_j(k) &= \mu_j\sqrt{\frac{(0+ikv)^2+\omega_j^2+4\beta_j^2}{(0+ikv)^2+\omega_j^2}}+(1-\mu_j), \quad j=1,2.\end{aligned} \tag{3.94}$$

One can see that the first equation (3.93) is a Wiener-Hopf problem for which the factorisation of function $L(k)$ is required as well as the estimation of asymptotic behaviour is needed. At the same time, solution to the second equation of (3.93) will be readily solved if $\Psi^+(k)$ is found.

3.2.5 Asymptotic behaviour of functions

Firstly, one can write down the behaviour of functions $L_{1,2}(k)$ from at (3.94):

$$\begin{aligned}L_j(k) &= 1-\frac{2\beta_j^2}{v^2k^2}+O\left(\frac{1}{k^4}\right), \quad k\to\infty,\\ L_j(k) &= \frac{2\mu_j\beta_j}{\sqrt{v_j^2-v^2}}\frac{1}{\sqrt{(0+ik)(0-ik)}}+(1-\mu_j)+O(k^2), \quad k\to 0.\end{aligned}$$

From the last expression one can easily get asymptotics of $L(k)$ and $M(k)$ at infinity:

$$\begin{aligned} L(k) &= 1 - \frac{\beta_1^2 + \beta_2^2}{v^2 k^2} + O\left(\frac{1}{k^4}\right), \quad k \to \infty, \\ M(k) &= -\frac{\beta_1^2 - \beta_2^2}{v^2 k^2} + O\left(\frac{1}{k^4}\right), \quad k \to \infty. \end{aligned} \tag{3.95}$$

The behaviour of these functions at zero is given by:

$$\begin{aligned} L(k) &= \frac{\Theta^2}{\sqrt{(0+ik)(0-ik)}} + \frac{2 - \mu_1 - \mu_2}{2} + O(k^2), \quad k \to 0, \\ M(k) &= \left(\frac{\mu_1 \beta_1}{\sqrt{v_1^2 - v^2}} - \frac{\mu_2 \beta_2}{\sqrt{v_2^2 - v^2}} \right) \frac{1}{\sqrt{(0+ik)(0-ik)}} \\ &\quad - \frac{\mu_1 - \mu_2}{2} + O(k^2), \quad k \to 0, \end{aligned} \tag{3.96}$$

where

$$\Theta^2 = \left(\frac{\mu_1 \beta_1}{\sqrt{v_1^2 - v^2}} + \frac{\mu_2 \beta_2}{\sqrt{v_2^2 - v^2}} \right) \tag{3.97}$$

Function $L(k)$ possesses the following properties:

$$|L(k)| = |L(-k)|, \quad \mathrm{Arg} L(k) = -\mathrm{Arg} L(-k),$$

and also the index (winding number) of this function is zero. Hence, we can factorise the kernel function $L(k) = L^+(k) L^-(k)$ with use of the Cauchy-type integral as:

$$L^{\pm}(k) = \exp\left(\pm \frac{1}{2\pi i} \int\limits_{-\infty}^{\infty} \frac{\mathrm{Log} L(\xi)}{\xi - k} \, d\xi \right), \quad \pm \Im k > 0 \tag{3.98}$$

The factors $L^{\pm}(k)$ are analytic in the half-planes $\pm \Im k > 0$ and satisfy the following asymptotic relations:

$$L^{\pm}(k) - 1 \sim \pm i \frac{Q}{k}, \quad k \to \infty, \quad Q = \frac{1}{\pi} \int\limits_0^{\infty} \log|L(\xi)| \, d\xi. \tag{3.99}$$

One can also find an asymptotic behaviour of the factors in the neighbourhood of a zero point with the use of (3.95) and the Sokhotski-Plemelj theorem:

$$L^{\pm}(k) \sim R^{\pm 1} \frac{\Theta}{\sqrt{0 \mp ik}}, \quad k \to 0, \quad R = \exp\left(\frac{1}{\pi} \int_0^{\infty} \frac{\mathrm{Arg} L(\xi)}{\xi} \, d\xi \right). \quad (3.100)$$

Looking at the definitions of functions involved in the problem, given in (3.78),(3.85) and (3.94), one can notice that it is sufficient to vary ratios $\beta_1^2/v_1^2, \beta_2^2/v_2^2, v_1^2/v_2^2$ and μ_1, μ_2 from (3.71) for different results. In other words, the mentioned ratios represent a set of settings that defines the distinction between various solutions. In the further presentation of computations we operate with mentioned ratios.

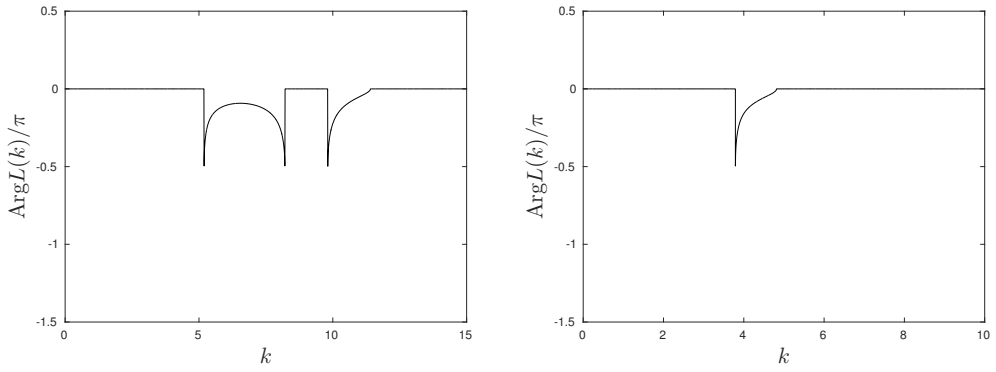

a) b)

Figure 3.10: Argument of $L(k)$ for different values of crack speed and $\beta_1^2/v_1^2 = \beta_2^2/v_2^2 = v_1^2/v_2^2 = 1$ and $\mu_1 = \mu_2 = 0.2$: a) $v = 0.2v_c$, b) $v = 0.5v_c$.

Function $\mathrm{Arg}L(k)$ is presented for the chosen set of parameters given in the caption is shown in Fig. 3.10 for $v = 0.2v_c$ and $v = 0.5v_c$. As one can observe, the behaviour of this function differs from previously considered cases. Thus, the direct integration is required for evaluation of R. It was performed by a simple trapezoidal rule.

3.2.6 Solution of the problem

The final part of solution derivation start with obtaining of solution for function $\psi(\eta)$. Determined asymptotics for functions $L^{\pm}(k)$, given in (3.99) and (3.100), lead to the following equation arising from (3.93):

$$L^{+}(k)\Psi^{+}(k) + \frac{1}{L^{-}(k)}\Psi^{-}(k) = \frac{C}{0-ik} + \frac{C}{0+ik},$$

where $C = const$. The right-hand side of the last equation take into an account the fact that the fact the the fracture is ran by an energy flux from infinity [85]. Thus, the appeared functions make possible to observe desirable behaviour of resulting functions. The solution of the last equation is:

$$\Psi^{+}(k) = \frac{C}{0-ik}\frac{1}{L^{+}(k)}, \quad \Psi^{-}(k) = \frac{C}{0+ik}L^{-}(k) \tag{3.101}$$

From (3.99), (3.100) and (3.101) it follows that:

$$\begin{gathered}
\Psi^{\pm}(k) = C\left(\pm\frac{i}{k} \pm \frac{Q}{k^2}\right) + O\left(\frac{1}{k^3}\right), \quad k \to \infty, \\
\Psi^{+}(k) \sim \frac{C}{R\Theta}\frac{1}{\sqrt{0-ik}}, \quad k \to 0, \\
\Psi^{-}(k) \sim \frac{C\Theta}{R}\frac{1}{(0+ik)^{3/2}}, \quad k \to 0.
\end{gathered} \tag{3.102}$$

First relations in (3.102) give the asymptotic behaviour of solution $\psi(\eta)$ at zero:

$$\psi(\eta) = C(1 - Q\eta) + O(\eta^2), \quad \eta \to 0, \tag{3.103}$$

whereas from the last 2 expressions in (3.102) by means of contour integration we conclude:

$$\begin{gathered}
\psi(\eta) \sim \frac{C}{R\Theta}\frac{1}{\sqrt{\pi\eta}}, \quad \eta \to \infty, \\
\psi(\eta) \sim 2\frac{C\Theta}{R}\sqrt{\frac{-\eta}{\pi}}, \quad \eta \to -\infty
\end{gathered} \tag{3.104}$$

Constant C is found from the fracture criterion (3.89):

$$C = \epsilon_c \tag{3.105}$$

The remaining function to find is $\Phi(k)$, which can be obtained from (3.93). However, the behaviour of the solution should be kept in mind. The final expression for function $\Phi(k)$, that properly captures the aspects of the solution, is:

$$\Phi(k) = \epsilon_c \left[\frac{K}{0+ik} + \left(K - \frac{M(k)}{L(k)} \right) \frac{1}{0-ik} \right] L^-(k)$$

where:

$$\begin{gathered} \frac{M(k)}{L(k)} \sim K, \quad k \to 0, \\ K = \left(\frac{\mu_1\beta_1}{\sqrt{v_1^2 - v^2}} - \frac{\mu_2\beta_2}{\sqrt{v_2^2 - v^2}} \right) \left(\frac{\mu_1\beta_1}{\sqrt{v_1^2 - v^2}} + \frac{\mu_2\beta_2}{\sqrt{v_2^2 - v^2}} \right)^{-1} \end{gathered} \tag{3.106}$$

Alternatively, function $\Phi(k)$ can be presented as:

$$\Phi(k) = K\Psi^-(k) + \epsilon_c \left(K - \frac{M(k)}{L(k)} \right) \frac{L^-(k)}{0-ik}. \tag{3.107}$$

The last expression is better for the evaluation of integral transforms. Notice that:

$$\begin{gathered} \left(K - \frac{M(k)}{L(k)} \right) \frac{L^-(k)}{0-ik} = \frac{K}{k} \left(i + \frac{Q}{k} \right) + O\left(\frac{1}{k^3} \right), \quad k \to \infty, \\ \left(K - \frac{M(k)}{L(k)} \right) \frac{L^-(k)}{0-ik} \sim \left(\frac{\mu_1 - \mu_2}{2} + \frac{2 - \mu_1 - \mu_2}{2} K \right) \\ \times \left(\frac{\mu_1\beta_1}{\sqrt{v_1^2 - v^2}} + \frac{\mu_2\beta_2}{\sqrt{v_2^2 - v^2}} \right)^{-1} \frac{1}{R} \frac{1}{\sqrt{0-ik}}, \quad k \to 0 \end{gathered}$$

The displacements are expressed in terms of inverse Fourier transform:

$$\begin{aligned} u_m(\eta) &= \frac{1}{2\pi} \int_{-\infty}^{\infty} \lambda_1^{m-1}(k) \frac{\Psi(k) + \Phi(k)}{2} e^{-ik\eta}\, dk, \quad m \geq 1, \\ w_m(\eta) &= \frac{1}{2\pi} \int_{-\infty}^{\infty} \lambda_2^{-m-1}(k) \frac{\Psi(k) - \Phi(k)}{2} e^{-ik\eta}\, dk, \quad m \leq -1 \end{aligned} \tag{3.108}$$

The behaviour of function $L(k)$ doesn't allow to perform the factorisation procedures as it was done in the previous cases. Instead, expression (3.81)

is utilised in the further computations of displacement fields. We choose $s = 10^{-2}$ for this reason whereas quantity R is evaluated for $s = 10^{-13}$.

The asymptotic analysis of functions $\lambda_{1,2}(k)$ in (3.87) and functions $\Psi^-(k)$ and $\Phi^-(k)$ (see (3.102) and (3.107)) at zero point allows to estimate the behaviour of functions $u_m(\eta)$ and $w_m(\eta)$ when $|m| \to \infty$. This analysis can be performed in the same way as in section 3.1.11. The results along the ray $\eta = \alpha m$ can be written as:

$$\begin{aligned} u_m(\alpha m) &\sim \epsilon_c \frac{\Theta(K+1)}{R}\sqrt{\frac{m}{2\pi}}\left(\sqrt{\alpha^2 + \frac{v_1^2 - v^2}{\beta_1^2}} - \alpha\right)^{1/2}, \quad m \to \infty, \\ w_m(\alpha m) &\sim \epsilon_c \frac{\Theta(K-1)}{R}\sqrt{\frac{-m}{2\pi}}\left(\sqrt{\alpha^2 + \frac{v_2^2 - v^2}{\beta_2^2}} + \alpha\right)^{1/2}, \quad m \to -\infty, \end{aligned} \tag{3.109}$$

where constants Θ, R and K are defined in (3.97), (3.100) and (3.106), respectively.

3.2.7 Solution analysis

The calculation of the energetic characteristics of the fracture process are again based on the relation given in [85]. It was shown that the ratio between the local energy release rate and global energy release rate is:

$$\frac{G_0}{G} = R^2, \quad G_0 = \frac{c\epsilon_c^2}{2a} \tag{3.110}$$

where parameter R is defined in (3.100). The quantity $G_0 a$ is equal to the elastic energy released due to the breakage of one link between the oscillators at a crack tip whereas G demonstrate the bulk change of energy with a crack advance.

The effects caused by the mismatch in properties of lattices are in question. In addition, the effect of introduced interface is examined. For the demonstration of the results we, firstly, choose different values of springs c

at the interface (see Fig. 3.9) keeping the other parameters the same. The computations of the displacement fields require the prescribed values of v. The examples of function $\psi(\eta)$ and displacements for different values of μ_1 and μ_2 are shown in Fig. 3.11.

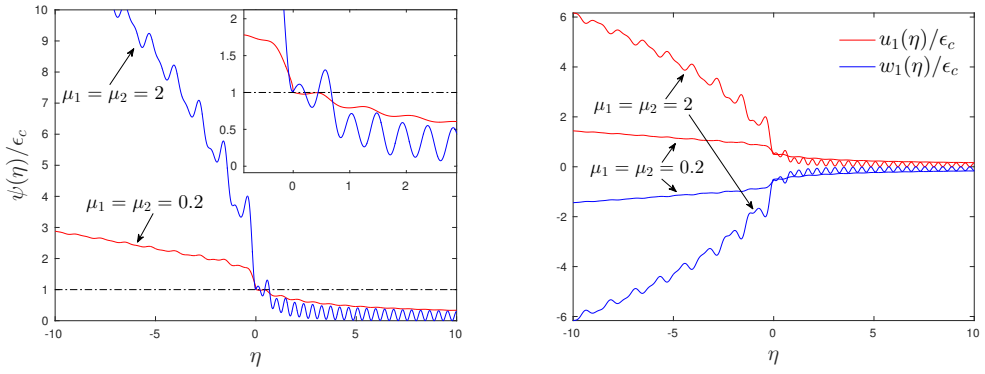

a) b)

Figure 3.11: Evaluation of results for the case of identical lattices $\beta_1^2/v_1^2 = \beta_2^2/v_2^2 = v_1^2/v_2^2 = 1$ but different properties of interfacial links at $v = 0.19v_c$ for : a) function $\psi(\eta)$, b) displacements along the interface.

After evaluation of the function $\psi(\eta)$ one can validate the second part of fracture criterion in (3.89). Fig. 3.11a) demonstrates the fault of this criterion in the cases $\mu = 2$ which makes this solution unphysical for $v = 0.19v_c$. At the same time the criterion (3.89) holds for the case $\mu = 0.2$. The displacement fields in Fig. 3.11b) are antisymmetric for chosen parameters and the increase of spring constants along a crack path leads to a larger crack opening.

One could wonder about the possible chance for a horizontal spring to break. The potential spot of spring failure along the interface within a top lattice is assigned $\eta_*^{(1)}$, while the complementary location for a bottom lattice

is $\eta_*^{(2)}$. In the occasion of these events the amount of energy that is released:

$$\begin{aligned} G_1 &= \frac{c_1}{2a}\left(u_1(\eta_*^{(1)}-1)-u_1(\eta_*^{(1)})\right), \\ G_2 &= \frac{c_2}{2a}\left(w_1(\eta_*^{(2)}-1)-w_1(\eta_*^{(2)})\right), \end{aligned} \tag{3.111}$$

where G_1 and G_2 refer to a top and bottom lattices respectively. Thus, in addition to fracture criterion (3.89) we impose an extra condition:

$$\frac{G_0}{G_j}=\frac{c}{c_j}, \quad j=1,2. \tag{3.112}$$

If the last condition is met at either $\eta_*^{(1)}$ for a top lattice or at $\eta_*^{(2)}$ for a bottom lattice, that will signal about spring breakage on a face, or both faces, of the main crack. Keeping the ratios of energy release rates $G_{1,2}/G_0$ coherent with the ratios of stiffnesses, we suppose that the critical value of the energy release rate is proportional to elastic properties. The last follows from the estimates of theoretical strength of material. The evaluated displacement fields are verified for both criteria (3.89) and (3.112).

The complete analysis is shown in Fig. 3.12 where the dependence of ratio G_0/G on crack speed is presented according to (3.110). In this figure admissible regimes are marked with thick lines, forbidden regimes – normal lines. In Fig. 3.12 material properties were chosen in such a way that the characteristic speeds of sounds in both lattices are the same ($v_1 = v_2$).

Results in Fig. 3.12a) signify that with the decrease of spring stiffness between lattices admissible regimes might appear at low crack velocities. The high values of crack speeds are accompanied by the failure of horizontal springs. Interestingly, at high values of interfacial spring constants admissible regimes vanish (see blue lines in Fig. 3.15). Moreover, there is a tendency of smaller values of G_0/G for bigger values of c which is seen in both figure. The last fact suggests the larger amount of energy is carried by elastic waves radiated by a crack tip when the stiffness of the interface increases.

Notice, that values of functions G_0/G for case $\mu_1 = \mu_2 = 1$ in Fig. 3.12a) and $\mu_1 = 4/3, \mu_2 = 2/3$ in Fig. 3.12b) are identical. However, the admissible

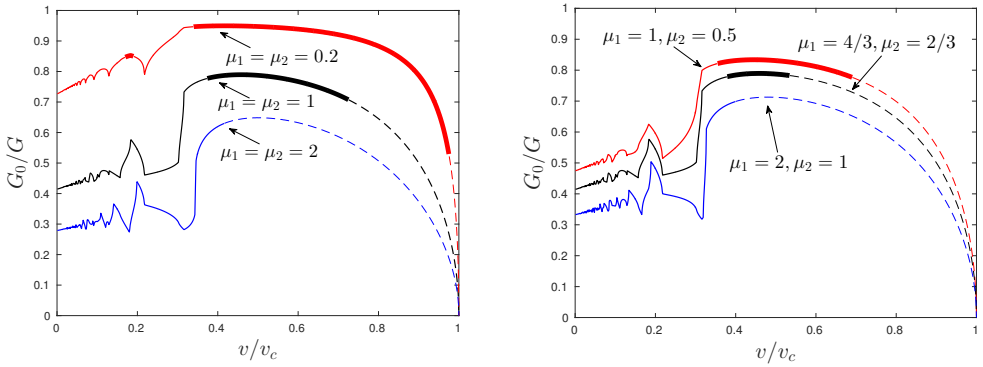

a) b)

Figure 3.12: Dependence of energy release rate ratio G_0/G on crack speed for case $v_1 = v_2$. Admissible regimes – thick lines, forbidden regimes – normal lines, breakage of horizontal links – dashed lines. The ratios of parameters $\beta_1^2/v_1^2 = \beta_2^2/v_2^2 = v_1^2/v_2^2 = 1$ and: a) identical values of μ_1 and μ_2, b) distinct values of μ_1 and μ_2.

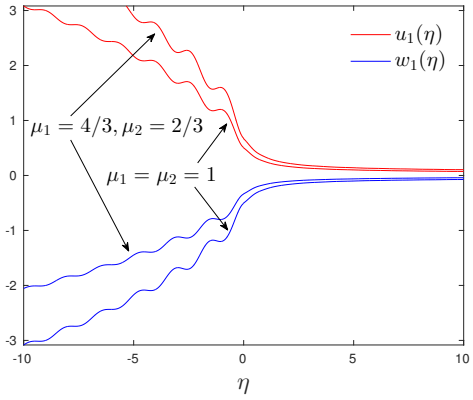

Figure 3.13: Displacement profiles along the interface for a case $\beta_1^2/v_1^2 = \beta_2^2/v_2^2 = v_1^2/v_2^2 = 1$ at $v = 0.5v_c$ and different values of parameters μ_1 and μ_2.

regimes occupy different ranges of crack speeds. More generally, such degeneration will appear for in the cases for which $\beta_1^2/v_1^2 = \beta_2^2/v_2^2 = v_1^2/v_2^2 = 1$

and $\mu_1 + \mu_2 = 2$ (see (3.94),(3.96) and (3.110)). This observation illustrates a necessity in examination of displacement fields for the investigation of possible steady-states. Indeed, the example of displacement fields at $v = 0.5v_c$ in Fig. 3.15b) for these two cases show the distinction in spite of the fact that values of G_0/G coincide. For such cases the verification of condition (3.112) becomes essential. Moreover, the displacements for different layers for the case $\mu = 4/3$ and $\mu = 2/3$ are shown in Fig. 3.14a). The evaluation of integrals in (3.108) is compared with the derived asymptotic expressions in (3.109). As in the case of the anisotropic lattice, we again observe the growth of the displacements matching macroscopically associated solution from the linear elastic theory.

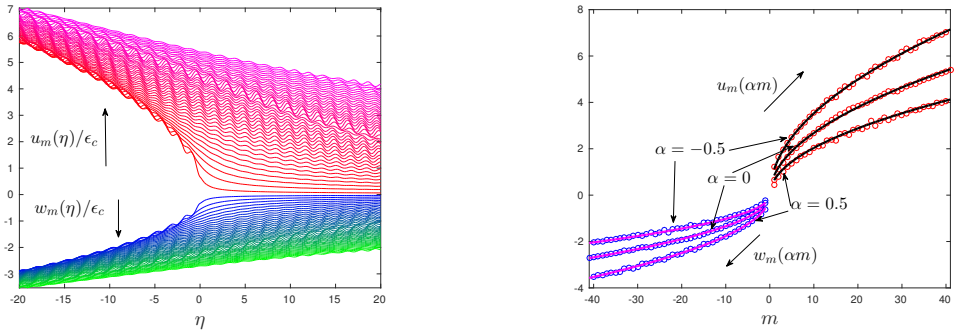

a) b)

Figure 3.14: Displacement profiles along the interface for a case $\beta_1^2/v_1^2 = \beta_2^2/v_2^2 = v_1^2/v_2^2 = 1$ at $v = 0.5v_c$ and $\mu_1 = 4/3, \mu_2 = 2/3$: a) for layers $|m| = 1...41$, b) along the rays $\eta = \alpha m$ for different m. Markers stand for the points evaluated by the integration in (3.108), solid lines are given by (3.109).

The other examples concern the material properties that result in different values of v_1 and v_2. There are three major differences in lattice parameters that we present: effects of different masses shown in Fig. 3.15a), a case of different stiffnesses inside the lattices is given in Fig. 3.15b), Fig. 3.15c)

presents settings corresponding to different masses and stiffnesses inside the lattices .

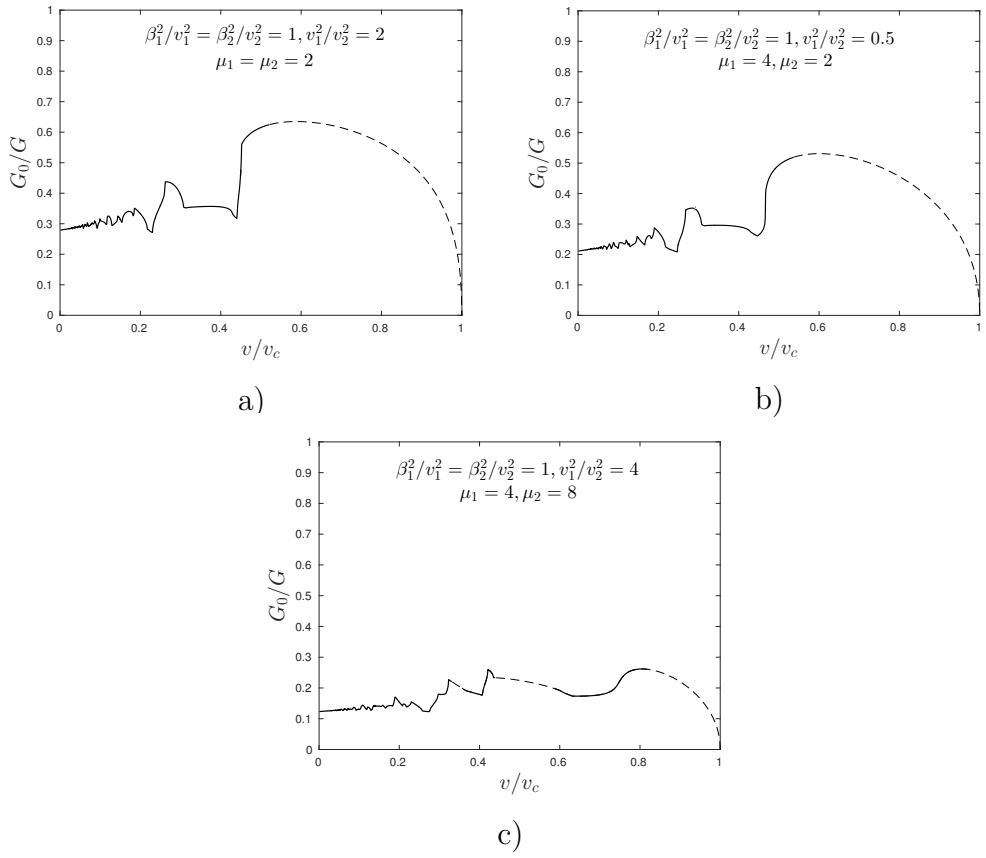

Figure 3.15: Dependence of energy release rate ratio G_0/G on crack speed for a case of different v_1 and v_2: a) different masses, b) different stiffnesses, c) different masses and stiffnesses. Admissible regimes – thick lines, forbidden regimes – normal lines, breakage of horizontal links – dashed lines.

In Fig. 3.15 we observe that choice of different parameters did not discover admissible regimes for high values of spring constants along the interface. It makes the stiffness of the interface one of the leading parameters in estimation of admissible regimes in bi-material systems if relations (3.112) takes place.

3.3 Discussion

In the present chapter we considered the problem of straight crack propagation in an square-cell lattices and admissible regimes were studied. The assumption of the straight crack paths allows to utilise the mathematical techniques and provide benchmark solutions. Although crack propagation may follow more complicated paths, the adopted assumption gives an upper bound for the energy release rate and demonstrates the peculiarities of the displacements that can be spotted in more difficult cases. The evaluation of displacement fields made it possible to validate the fracture condition not only along the crack path but also on the faces of the main crack. This resulted in the specification of forbidden and admissible regimes of crack propagation. Within the admissible regimes there exist cases when the horizontal springs on the crack faces snap. The failure of horizontal springs was discovered for the regimes with high values of energy release rate, suggesting that there are instabilities in steady-state crack movement at high velocities.

The first of the addressed problems in this chapter discusses a fracture process in an anisotropic lattice. Elastic properties of the lattice were chosen to be different in orthogonal directions. The effects of contrast in spring constants were reflected on the energy release rates. For instance, it was shown that the low values of elastic modulus in the horizontal direction with respect to the one in the vertical direction lead to the possibility of observing slow cracks. Moreover, we showed that for some values of material properties steady-state crack propagation is not detected at all. At the same time, the increase of elastic properties in the vertical direction is followed be the higher values of the energy release rate.

The calculation of displacement field was visualised for chosen settings. The illustrated example showed that steady-state crack propagation in a lattice provides the growth of displacement values in the vertical direction. The wave character of the displacements is presented at any layer of the

lattice. Furthermore, the computed results are compared with the derived asymptotic expressions and a good agreement between these calculations is observed.

In order to advance in the understanding of the effects of material properties on admissible regimes, fracture of a dissimilar lattice has been carried out. The interfacial crack between lattices with different is assumed to travel along a straight path. In the beginning, the bulk lattice with the interface of different elastic properties has been analysed. The results showed that one can find the settings of material parameters that provide the same values of the energy release rate. However, the consideration of the admissible regimes presents the difference in those cases. Moreover, the evaluated displacement fields revealed the difference in mentioned cases.

Finally, effort was made to discover admissible regimes for high values of interfacial stiffness. For that reason we chose to vary mismatch in material properties of the lattices. Unfortunately, it did not show possible steady-state regimes.

Chapter 4

Verification of fracture criteria

4.1 Dynamic fracture criteria

One of the major questions in the efficient prediction of fracture events is concerned with the choice of a proper fracture criterion. The simplest conventional condition, that can be proposed for the presented fracture problems of discrete systems with linear springs, can be stated in the following way. An elastic spring can be subjected to a quasi-static load and the ultimate elongation, u_s, followed by failure of a spring, is measured. Neglecting inertia effects, the conventional fracture criterion is, then, posed:

$$u = u_s. \tag{4.1}$$

Notice that in previous section everywhere we considered exactly this criterion. Although criterion (4.1) performs well for the small strain-rates of the spring, it can be insufficient for the study of a dynamic fracture. One of the ways to modify the corrections due to inertia effects is to impose a rate dependence of material properties, spring constants or u_s, for instance. However, the consideration of different fracture criteria, that grasp the specifics of rapid failure, can prevent from complications both in modelling and experiments. In such a way, this chapter deals with an investigation of the

incubation time criterion and the Tuler-Butcher criterion.

The former one suggests to consider a time averaged spring elongation, or the stress in linear elasticity, over a certain time interval. Such temporal parameter in called incubation time τ, an additional material property specified for rapid fracture processes. The criterion itself, written for the elastic bond in object, gives:

$$\frac{1}{\tau}\int_{t_f-\tau}^{t_f} u(t)\,dt = u_s, \tag{4.2}$$

which allows to determine fracture time t_f. Notice that u_s is still the threshold elongation of the spring when measured statically. This condition appeared to be efficient for modelling dynamic failure of solids [66, 97], cavitation [35] and electric breakdown [65].

One may propose damage accumulation as a cause of a spring breakage. This can be accounted by means of the Tuler-Butcher (TB) criterion firstly presented in [95]. In a TB material, critical elongation u_s, defined by a statical test, represents the elongation to be exceeded as:

$$\int_0^{t_f} H(u(t)-u_s)\left(\frac{u(t)}{u_s}-1\right)^2 dt = D \tag{4.3}$$

before the fracture occurs at $t = t_f$. $H(x)$ is the Heaviside step function which suggests in (4.3) that only the work of the overstretch $(u - u_s)$ contributes to damage. In the original formulation [95] the exponent two in (4.3) has been taken as a general power, but consideration of squared expression as presented here turns out to be reasonable according to experiments [8, 33, 98]. Additionally, such form of the criterion explains that a maximum work to be done by an external overload on the spring before it collapses. Looking at (4.3), it appears that, as for the incubation time criterion, TB materials can be regarded as one possible extension of ideal brittleness, which is promptly ascertainable by setting the accumulated energetic damage D to zero.

The specifics of each criteria can be highlighted by a simple example. Imagine a spring of some stiffness and static strength quantity u_s. The

spring is loaded with a gradual displacement of rate r, i.e. $u(t) = rt$. The examination of the fracture under condition (4.1) gives $t_f = u_s/r$. Passing the same type of load to the incubation time criterion in (4.2) predicts fracture time $t_f = u_s/r + \tau/2$ if $r < 2u_s\tau$ or $t_f = \sqrt{2u_s\tau/r}$, otherwise. Finally, the investigation of fracture time by the TB condition provides fracture to take place at $t_f = u_s/r + u_s\sqrt[3]{3D^2/r^2}$, according to (4.3). Clearly, both non-conventional criteria estimate the fracture time that exceeds the one achieved by a classical approach. Consequently, the elongation of a spring have to be bigger for a chosen type of load. Analogically to the solid fracture mechanics, the final value is usually considered to be rate dependent, as was mentioned before, and series of experiments are required to determine such dependence. This simple example shows that the presented criteria can easily grasp the rapid fracture processes by means introduced parameters, τ and D, which can be adjusted effortlessly.

4.2 Background

The illustration of various fracture criterion is performed for the simple chain attached to a rigid foundation demonstrated in fig. 4.1. In this particular case all the springs have stiffnesses c, the masses of oscillators are M and equilibrium distance between them is a. The applied force has a magnitude F and initially is located at position n_f. As before, crack speed v is limited by a critical value:

$$v < v_c, \quad v_c^2 = \frac{c}{M}a^2. \tag{4.4}$$

The normalisation of the speed parameters is again used:

$$\tilde{v} = \frac{v}{a}, \quad \tilde{v}_c = \frac{v_c}{a}, \tag{4.5}$$

and tildes are dropped for convenience. In other words, the crack tip equation is $n_*(t) = n_*(0) + vt$, where $n_*(0)$ is a distance between a crack tip and a force location at the beginning of the steady-state process. In the steady-state, the

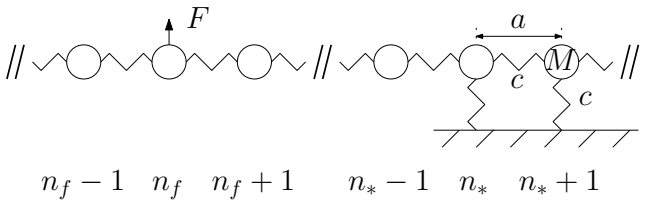

Figure 4.1: Chain of oscillators with equal masses M connected together and to the rigid foundation by linear springs of stiffness c. The crack position is defined by an oscillator with index n_*. The force has is F and n_f is its position. a is an equilibrium distance between the oscillators.

displacements of the oscillators are defined by function $u_n(t)$ are expressed through the function of a single variable $\eta = n - n_*(t)$:

$$u = u(\eta) \tag{4.6}$$

and is different for different values of v. The expressions for the evaluation of $u(\eta)$ are shown in (2.62). The solution of the problem also provided the relations for the ratio of energy release rates:

$$\frac{G_0}{G} = R^2(v), \quad G_0 = \frac{cu_c^2}{2a}, \tag{4.7}$$

as well as the dependence between loading parameters, material ones and a crack speed:

$$\frac{F}{F_0} = \frac{1}{R(v)}\sqrt{\frac{v_c + v}{v_c - v}} = \Pi(v), \quad F_0 = cu_c. \tag{4.8}$$

In the last equations parameter $R(v)$ is displayed in (2.57). In the previous chapters condition $u(0) = u_c$ held and u_c was treated, in terms of present analysis of fracture criteria, as u_s. The admissible regimes were determined through analysis of displacement field. For a certain crack speed the admissible regimes were defined to be if:

$$u(\eta) < u_c, \quad \eta > 0. \tag{4.9}$$

However, the solution in a steady-state reflects only the fact that under the given crack speed the displacement field is the one that was derived previously. In this chapter we deal with the case when, generally speaking, variable u_c can be rate dependant, i.e.:

$$u_c = u_c(v) \tag{4.10}$$

The last dependence is captured with the help of presented criteria (4.2) and (4.3), presumably knowing the value u_s found from a quasi-statical test. The application of these criteria for the analysis of considered problem is shown below.

4.2.1 Incubation time

A change of variable in Eq.(4.2) can be done to switch the integration in terms of η. The criterion is then reduces to:

$$\Gamma(v,\tau) = \frac{1}{v\tau}\int_0^{v\tau} \frac{u(\eta)}{u_c}\, d\eta = \frac{u_s}{u_c}. \tag{4.11}$$

The normalisation presented in the integral above is convenient because when the steady-state fracture process takes place this ratio does not depend on the applied criteria for a chosen v. As it was stressed out earlier, the dependence $u_c = u_c(v)$ is now easily derived by (4.11). The illustration of such criterion is demonstrated in Fig. 4.2. According to criterion (4.11), to find dependence u_s/u_c for a particular v one should calculate the shaded area, shown in Fig. 4.2, and divide it by τv.

Notice, that the displacement field depends on v which makes the performed analysis in chapter 2.1 helpful. Moreover, distinct results are expected for different values of τ. The admissible regimes in this case are those for which the following condition holds:

$$\Gamma(v,\tau) < \frac{1}{v\tau}\int_{\eta_*}^{\eta_*+v\tau} \frac{u(\eta)}{u_c}\, d\eta, \quad \forall \eta_* > 0. \tag{4.12}$$

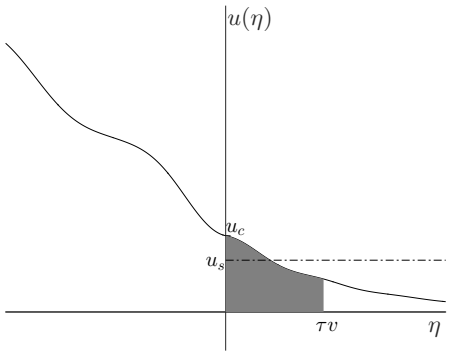

Figure 4.2: Illustration for the application of (4.11) for a case $v = 0.3v_c$ and $\tau = 3v_c$.

4.2.2 Tuler-Butcher

The TB criterion can be considered in a similar way. For our purposes, a change of variables in (4.3) leads to the expression:

$$\Lambda^2(v, D) = \int_0^\infty \frac{H(u(\eta) - u_s)}{vD} \frac{(u(\eta) - u_s)^2}{u_c^2} \, d\eta = \frac{u_s^2}{u_c^2}. \tag{4.13}$$

The demonstration of the last is shown in Fig. 4.3. In that figure one can observe the part of the displacement that should be taken into an account, according to the presents of the heaviside function in the integral. This example, as well as the previous one, shows the delay in fracture after the value u_s was reached. However, value u_c will take a different value. The analysis of admissible regimes in this case requires only to check if:

$$\Lambda(v, D) \leq 1. \tag{4.14}$$

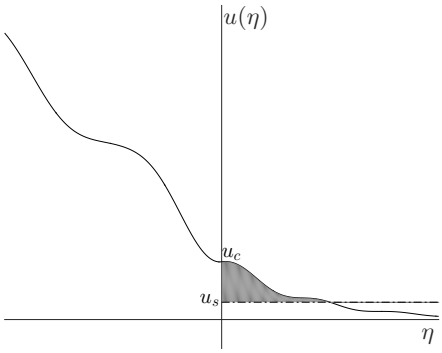

Figure 4.3: Illustration for the application of (4.3) for a case $v = 0.3v_c$ and $D = 0.3v_c$.

4.3 Analysis for a simple chain problem

All the results for various parameters τ and D are presented for their normalised quantities:

$$\tilde{\tau} = \tau v_c, \quad \tilde{D} = D v_c, \tag{4.15}$$

and tildes are then dropped for convenience. Firstly, one can notice that ratio G_0/G is independent from the various criteria. This ratio shows the amount of the elastic energy that is radiated by a moving crack tip. The considerations of different fracture conditions, however, affect the intervals of admissible regimes.

The effect of various fracture conditions in terms of energy release rate is reflected in Fig. 4.4 for several parameters to illustrate the distinctions. For instance, one can easily see that the intervals of admissible regimes cover bigger ranges when non-conventional criteria are taken into an account. Particularly, there is a monotonic tendency in increase of admissible regimes with an increase of τ. Also, new zones of admissibility appear in the low velocities region for increasing D, when TB condition is used. An immediate qualitative difference with the incubation time situation is that such admis-

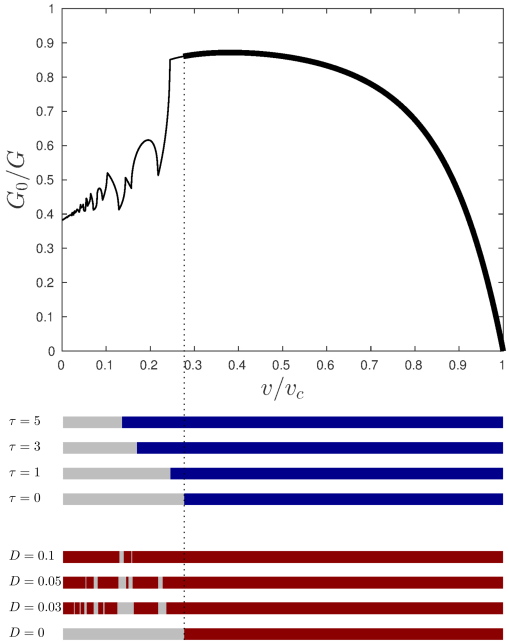

Figure 4.4: Energy release rate ratio G_0/G and admissible regimes for various model parameters and different fracture criteria. Thick lines (on the curve with criteria (4.1)), blue bars (for criteria (4.11)), red bars (for criteria (4.13)) indicate admissible regimes, thin lines(on the curve with criteria (4.1)) and grey bars stand for forbidden regimes.

sible intervals pop up small and scattered, but then, increasing D, expand gradually and merge until every subsonic crack speed can be obtained for D close to unity.

The examination of G_0/G covers the qualitative aspects of the problem. The quantitative changes, though, can be seen if one refers to the force dependences and study ratio u_s/u_c.

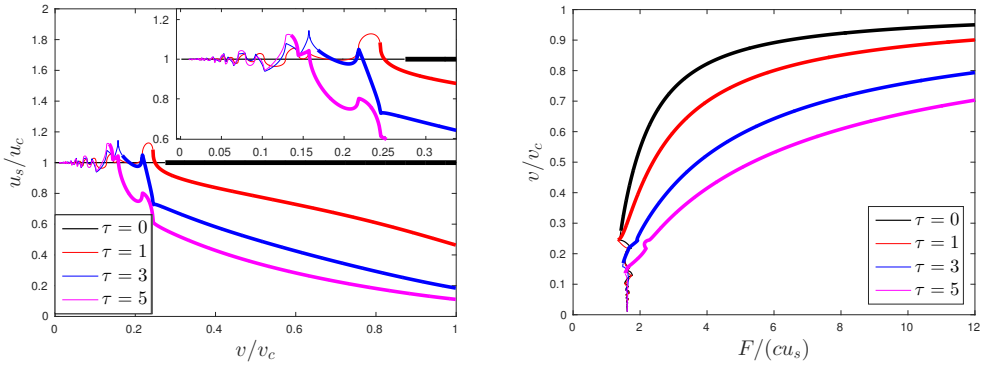

a) b)

Figure 4.5: Admissible (thick lines) and forbidden (normal lines) regimes of crack propagation different values of τ for a) dependence u_s/u_c according to (4.11). The insert shows the zoom of region of low crack speeds, b) normalised force $F/(cu_s)$ from (4.16).

4.3.1 Incubation time

Relation (4.11) allows us to compute the value of elongation of the spring at the crack tip at the moment of fracture. The force that leads to the particular speed can be predicted with the help of (4.8) and (4.11):

$$\frac{F}{cu_s} = \frac{\Pi(v)}{\Gamma(v,\tau)}, \tag{4.16}$$

where factor cu_s equals to the critical force found from a quasi-statical test.

The behaviour of the function $\Gamma(v,\tau)$, that is the way τ modifies the crack opening with respect rate independent one ($\tau \to 0$), is shown in Fig.4.5a). A linear elastic bond which exhibits a non-zero incubation time will in general allow bigger crack opening at the fracture moment. For low τ, though, oscillations of the ratio u_c/u_s around one occur at low velocities. The immediate effect on the force is plotted in Fig.4.5b). Given the result of the static test on the spring u_s, if the goal is, for instance, to detach the chain from a substrate with a certain velocity v, an incubation time criterion predicts that

the steady-state regime would be reached in general via a bigger force than one could expect if τ is neglected. The region where the relation between force and velocity is not bijective is stretched rightwards and the difference in velocities for the same force decreases steadily while raising the incubation time. Of course, the same can be summarized stating that a conventional failure criterion can be used only if the threshold stretch of the spring at the crack tip is dependent on the velocity of the phenomenon according to (4.11), the relation G/G_0 remaining untouched. Anyway, the minimum force in order to obtain propagation ($v/v_c \to 0$) is the same for every τ since in such limiting case incubation time and conventional criteria do not conflict (see (4.11)).

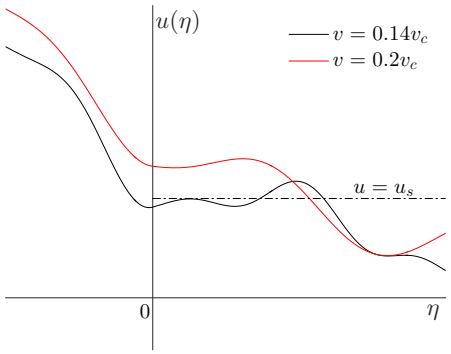

Figure 4.6: Crack opening for small velocities and high incubation times. With $\tau = 5$, the crack tip opening u_c at the admissible $v = 0.14v_c$ is predicted to be smaller than the static strength u_s. For comparison, $v = 0.2v_c$ shows the most common situation of $u_c > u_s$.

Another crucial effect of $\tau > 0$ on the crack propagation is that monotonically enlarges the regions of achievable steady-states as illustrated in Fig. 4.6. For instance, the speed $0.2v_c$, that is non-admissible for an ideally brittle material with equal u_s, can be reached with $\tau = 3$ and bigger.

4.3.2 Tuler-Butcher

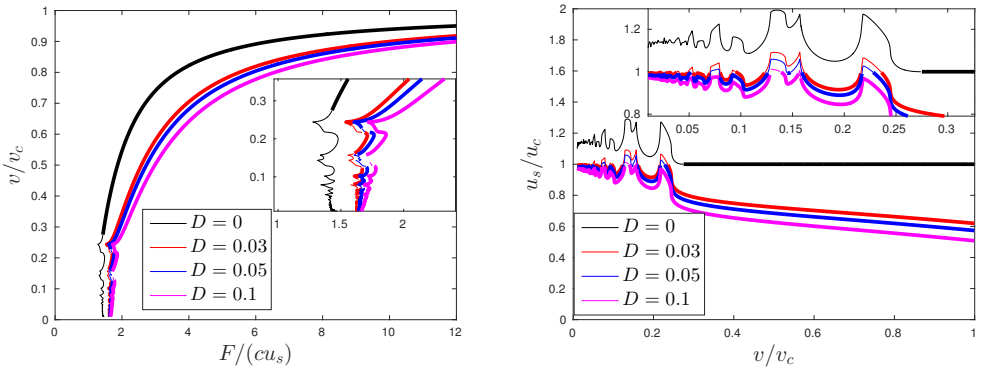

a) b)

Figure 4.7: Admissible (thick lines) and forbidden (normal lines) regimes of crack propagation different values of τ for a) dependence u_s/u_c according to (4.13). The insert shows the zoom of region of low crack speeds, b) normalised force $F/(cu_s)$ from (4.17).

By means of (4.13), one can retrieve the elongation of a spring at the crack tip associated to all the combinations of crack speed and D. As a consequence, keeping the force proportional to the material property u_s instead of the velocity dependent crack opening, (4.8) writes now

$$\frac{F}{cu_s} = \frac{\Pi(v)}{\Lambda(v, D)}. \tag{4.17}$$

The plots in Fig. 4.7 permit to visualize how a non-zero D affects the chain behaviour. As observed for incubation time condition, the immediate impact of TB damage accumulation results in augmented crack tip displacement at equal crack speed as an ideally brittle material showing equal static strength u_s at least in the range of medium/high v/v_c (see Fig. 4.7a)). The force to apply for getting a desired velocity is depicted in Fig. 4.7b). It is evident that the possibility for the material to bear a certain work of the overstretch

before breaking, given that the whole deformation profile is expanded by u_c/u_s, makes the chain detachment increasingly slower for same $F/(cu_s)$ and bigger D. A structure of TB criterion predicts the links to be dynamically tougher than u_s.

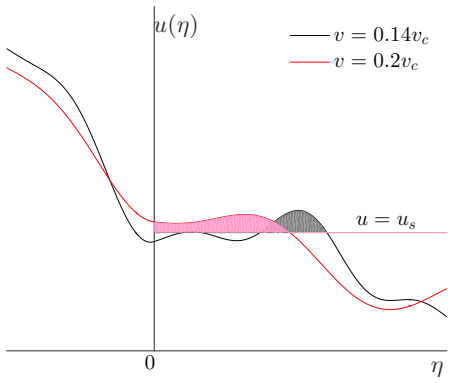

Figure 4.8: Crack opening at low velocities for small D. The profile $u(\eta)$ for two fracture speeds at $D = 0.03$ is shown. The shaded faces represent the areas where the integral (4.3) must be computed. The result for $v = 0.14v_c$ shows how $u_c < u_s$ means that the chain detaches ahead of $\eta = 0$ making that crack speed non-admissible.

Surprisingly and standing out from the incubation time findings, for $D \to 0$ and low fracture speed the complex structure does not respond like an ideally brittle one. Looking at Fig. 4.8, indeed, one can notice that the at low v, when $u(\eta)$ does not decrease monotonically, the criterion in (4.3) may return $u_c < u_s$. Nevertheless, those cases would mean that the chain breaks ahead of the crack tip and then marked as non-admissible in the steady-state propagation scenario. A point can be made therefore,that a theoretical limit for the crack opening is for a prediction by TB criterion $u_c \geq u_s$.

4.4 Discussion

The dynamic fracture propagation in discrete structures has been investigated in a considerable amount of possible scenarios (see references above) but the influence of failure criteria different from a threshold stress has not gained the attention that it deserves despite non-instantaneous criteria have already shown reliable in continuum mechanics (e.g. as recently discussed in [2]). As a first step to fill this gap, two time-dependent criteria have been analysed in details when applied to the dynamic fracture propagation of a chain of oscillators and they have been compared to the classical ideally brittle fracture. In both cases, enhanced admissibility have appeared at low crack speeds and mapped in Fig. 4.4. An increasing incubation time τ enlarges the admissibility continuously but never covers all the subsonic crack speeds. More than that, a TB criterion by a bigger D also creates completely new zones of achievable steady-states and it is predicted that all the subsonic range is possible if $D = 0.13$.

Speaking of the steady-state crack opening, the time-dependent criteria cause a delay in fracture after reaching the static strength of the bonds. This means that in most cases one should expect $u_c > u_s$ like it would happen when monotonically elongating a single spring. At low v, though, this is not the loading condition caused by a constant force applied on a complex structure. Ample and rapid oscillations ahead of the crack tip cause the delayed fracture to happen at $u_c < u_s$. While such propagation regimes are admissible at high τ for incubation time criterion, the same is not true for TB one (see Fig. 4.6 and Fig. 4.8). The mathematical form of the latter failure criterion indeed excludes such steady-states on the grounds that daughter cracks would jeopardize the steady-state assumption. Briefly, a theoretical limit has been found which states that under TB condition a dynamic fracture can propagate at constant speed only if $u_c \geq u_s$.

The velocity dependent energy release rate ratio G/G_0 is a solution which

is irrespective of the particular fracture criterion adopted. It is also valid regardless of the way the energy is introduced into the system. In the present work we use a constant force for the scope, but in case one prefers to do that in different ways, like for instance in [51] when dealing with lattices, possibly for facilitating experimental procedures, the relation for another loading condition would be needed. Such relation can be derived by adopting a criterion dependent ratio G/G_s where $G_s = ku_s^2/2$ can be obtained by functions like $\Gamma(v, \tau)$ or $\Lambda(v, D)$ defined as in (4.11) and (4.13).

To sum up, fracture criteria sensibly affect the dynamic propagation of cracks in discrete structures. The effects are particularly important both in terms of force – velocity relations and in new regimes of admissibility at low crack speeds. Once the solution of the dynamic problem has been retrieved in terms of energy release rate ratio and shapes of the displacement profiles as functions of the velocity, they are invariants and can promptly be used and adapted to the most suitable fracture criterion for the investigated problem. A possible outlook of this research can be the application of the approach to highly ordered bi-dimensional lattices (for instance crack propagation in graphene layers [94, 100]) or to the unbinding of long protein chains whose analysis has been made feasible by the improvements in the field of atomic force microscopy and for which the bonds strength has already shown to be eminently dependent on the strain rate [37, 52].

Conclusion

The work has been motivated by the experimental evidence of crack instabilities when a crack propagates inside a solid. Previously developed apparatus for studying such aspects of fracture mechanics has been extensively utilised. Here, the results from fracture problems are proposed for the detailed analysis.

One of the main achievements of the work demonstrates that macro-level behaviour during the fracture process, such as measurements of the established crack speed under a certain load applied to a solid with a predefined crack, can not carefully characterise the failure mechanisms. For that, a consideration of discrete solids has been performed and corresponding mathematical models was proposed. Formulations of the models lead to the Wiener-Hopf problem from which the final expressions for the solutions are retrieved. In spite of the fact that the obtained relations provide some relevant information of the fracture process, some of them are not easy to visualise. The gained quantities include the energy release rate and the numerical values of mechanical fields (displacements, stresses and strains). For achieving the complete set of final results, the evaluation of the solution of the problem was required, which was performed by means of developing and implementing robust numerical algorithms. The utilised methodology allowed to efficiently predict the possibility of cracks at constant speeds in discrete solids under certain loading conditions.

The advantages of accomplished work are reflected on the one-dimensional

discrete chain problems and fracture problems in square lattices. One-dimensional cases showed that the dynamic growth of cracks in discrete systems is supported by the radiation of elastic waves from a crack tip. Illustrated on chains with non-local interactions, distinct combinations of microlevel parameters, resulting in the same macroscopic properties, lead to different fracture scenarios in discrete solids. Moreover, it was possible to demonstrate the effects caused by a mismatch of material properties in bi-material structures. In the last case, one may observe supersonic cracks which are predicted by the model. The analysis of crack propagation in lattices reveals some new features. The obtained results showed the crack instabilities at high propagation speeds. Namely, at high speeds small cracks start to appear on the faces of the original moving crack. It was also highlighted by examples on dissimilar lattices that the energy release rate can have the same values for different settings and only through evaluation of displacements it is possible to distinguish such cases. In addition, the displacement field has been presented for a lattice problem which demonstrated a tendency of increase in values of displacements with the the distance from a crack path. Furthermore, the choice of different fracture criteria was questioned. Two non-conventional criteria predict different ranges of admissible regimes and different values of load, causing steady-state fracture.

The possible future development of the work can be done in the direction of multi-scale modelling of fracture. Many dynamical effects that happen at the macroscopic level can be well captured by different fracture conditions, for instance a delay of fracture in solids under loads with microsecond durations. However, such an approach does not bring the understanding of the phenomenon that happens inside the solid. I believe, that taking into an account micro structural characteristics and fracture processes at micro level can approach for an explanation of such effects of dynamic fracture mechanics. The results provided in this work can then serve to be a good starting point.

Appendix A

Numerical evaluation of integral transforms

A.1 Cauchy-type integral

A.1.1 General relations

Following from the presentation in (2.32) the following integral of an arbitrary function $f(x)$ has to be calculated:

$$\int_{-\infty}^{\infty} \frac{f(x)}{x-k} dx.$$

However, for the purposes of the particular problem the integration can be reduced if function $f(x)$ has certain properties. Two notations are introduced:

$$H_o(k) = \int_0^{\infty} \frac{x f_o(x)}{x^2 - k^2} dx, \quad H_e(k) = \int_0^{\infty} \frac{k f_e(x)}{x^2 - k^2} dx. \tag{A.1}$$

Here, $f_o(x)$ is an odd function, $f_e(x)$ is an even function, i.e.:

$$f_o(-x) = -f_o(x), \quad f_e(-x) = f_e(x).$$

For these functions their asymptotic behaviour should be determined. This can be supposed to be:

$$f_j(x) = \frac{f_\infty}{x^m} + O\left(\frac{1}{x^{m+2}}\right), \quad x \to \infty, \quad j = o, e. \tag{A.2}$$

Having (A.2) in mind, functions $H_j(k)$, $j = o, e$ may be approximated:

$$\begin{aligned} H_o(k) &\approx \int_0^A \frac{x f(x)}{x^2 - k^2}\, dx + f_\infty \int_A^\infty \frac{x}{(x^2 - k^2)x^m} dx, \\ H_e(k) &\approx \int_0^A \frac{k f_e(x)}{x^2 - k^2}\, dx + f_\infty \int_A^\infty \frac{k}{(x^2 - k^2)x^m} dx, \end{aligned} \tag{A.3}$$

where A is chosen in such a way that the relative error between function $f_j(x)$, $j = o, e$ and its asymptotic behaviour in (A.2) becomes significantly small. Last terms in (A.3) can be integrated analytically:

$$\begin{aligned} \int_A^\infty \frac{x}{(x^2 - k^2)x^m} dx &= \frac{1}{2}\left[\sum_{j=1}^{m-2} \frac{(-1)^j - 1}{(m-j-1)} \frac{1}{A^{m-j-1}} \frac{1}{k^{j+1}} + \log\left|\frac{A+k}{A-k}\right| \frac{1}{k^m}\right], \\ \int_A^\infty \frac{k}{(x^2 - k^2)x^m} dx &= \frac{1}{2}\left[\sum_{j=1}^{m-2} \frac{-1 - (-1)^j}{(m-j-1)} \frac{1}{A^{m-j-1}} \frac{1}{k^{j+1}} + \log\left|\frac{A+k}{A-k}\right| \frac{1}{k^m}\right]. \end{aligned} \tag{A.4}$$

As for the integration of the first terms in (A.3) the ensuing strategy is applied. The interval $[0, A]$ is divided into subintervals:

$$[0, A] = \bigcup_{i=1}^{n-1} [A_i, A_{i+1}].$$

On each subinterval function $f_j(x)$, $j = o, e$ is substituted with a polynomial of degree 3, i.e. we approximate function $f(x)$ with spline on the entire interval. We have:

$$f_j(x) \approx s_i(x) = a_i(x - A_i)^3 + b_i(x - A_i)^2 + c_i(x - A_i) + d_i, \quad x \in [A_i, A_{i+1}], \quad j = o, e. \tag{A.5}$$

Then, each term in (A.5) contribute to the integration. The notations for that are used:

$$
\begin{gathered}
I_n(a,b,c,k) = \int_a^b \frac{x(x-c)^n}{x^2-k^2}\,dx, \quad J_n(a,b,c,k) = \int_a^b \frac{(x-c)^n}{x^2-k^2}\,dx \\
I_0 = \frac{1}{2}\ln\left|\frac{b^2-k^2}{a^2-k^2}\right|,\; J_0 = \frac{1}{2k}\left(\ln\left|\frac{b-k}{a-k}\right| - \log\left|\frac{b+k}{a+k}\right|\right) \\
I_{n+1}(a,b,c,k) = \frac{1}{n}((b-c)^n - (a-c)^n) - cI_n(a,b,c,k) + k^2 J_n(a,b,c,k), \\
J_{n+1}(a,b,c,k) = I_n(a,b,c,k) - cJ_n(a,b,c,k).
\end{gathered}
\tag{A.6}
$$

Collecting all the intermediate steps in (A.3),(A.4),(A.5) and (A.6), the final expression for evaluation of $H_o(k)$ is obtained:

$$
\begin{aligned}
H_o(k) \approx \frac{f_\infty}{2}&\left[\sum_{j=1}^{m-2}\frac{(-1)^j-1}{(m-j-1)}\frac{1}{A^{m-j-1}}\frac{1}{k^{j+1}} + \log\left|\frac{A+k}{A-k}\right|\frac{1}{k^m}\right] \\
&+\sum_{j=1}^{n-1}\left[a_j I_3(A_j,A_{j+1},A_j,k) + b_j I_2(A_j,A_{j+1},A_j,k)\right. \\
&\left.+c_j I_1(A_j,A_{j+1},A_j,k) + d_j I_0(A_j,A_{j+1},A_j,k)\right].
\end{aligned}
\tag{A.7}
$$

In the same manner, the expression for $H_e(k)$ is:

$$
\begin{aligned}
H_e(k) \approx \frac{f_\infty}{2}&\left[\sum_{j=1}^{m-2}\frac{-1-(-1)^j}{(m-j-1)}\frac{1}{A^{m-j-1}}\frac{1}{k^{j+1}} + \ln\left|\frac{A+k}{A-k}\right|\frac{1}{k^m}\right] \\
&+k\sum_{j=1}^{n-1}\left[a_j J_3(A_j,A_{j+1},A_j,k) + b_j J_2(A_j,A_{j+1},A_j,k)\right. \\
&\left.+c_j J_1(A_j,A_{j+1},A_j,k) + d_j J_0(A_j,A_{j+1},A_j,k)\right].
\end{aligned}
\tag{A.8}
$$

Although expressions (A.7) and (A.8) are formally obtained there are several points to clarify. These expressions are suitable for the numerical implementation but there are several exceptional cases to be discussed.

A.1.2 Exceptions for numerical implementation of Cauchy-type integral

The attention is now focused on formulae (A.7) and (A.8).

1. $f_o(x) \sim f_\infty x^{-1}, \quad x \to \infty$.

   In case of odd function $f_o(x)$ in (A.1) and $m = 1$ in (A.4) the behaviour of function at infinity should be constructed differently. For this particular case the behaviour of function at zero should be also taken into an account. Then:

   $$f_0(x) = \frac{f_\infty}{x + f_0} + O\left(\frac{1}{x^3}\right), \quad x \to \infty,$$

   where $f_o \sim f_0 x^\alpha$, i.e. constant f_0 follows from the asymptotic behaviour of function $f_o(x)$ at zero. The estimate in (A.4) is changed accordingly:

   $$\int_A^\infty \frac{f_\infty}{x + f_0} \frac{x}{x^2 - k^2} dx = \frac{f_\infty}{2} \frac{k}{k^2 + \frac{f_\infty}{f_0}} \log\left|\frac{A + k}{A - k}\right| + R_o,$$

   $$R_o = \begin{cases} \frac{f_\infty \sqrt{\frac{f_\infty}{f_0}}}{k^2 + \frac{f_\infty}{f_0}} \left[\frac{\pi}{2} - \arctan \frac{A}{\sqrt{\frac{f_\infty}{f_0}}}\right], & \frac{f_\infty}{f_0} > 0, \\ \frac{f_\infty}{\sqrt{-\frac{f_\infty}{f_0}}} \frac{1}{k^2 + \frac{f_\infty}{f_0}} \log\left|\frac{A + \sqrt{-\frac{f_\infty}{f_0}}}{A - \sqrt{-\frac{f_\infty}{f_0}}}\right|, & \frac{f_\infty}{f_0} < 0. \end{cases}$$

2. $k = A$.

   As it is seen from the logarithmic terms (A.7) and (A.8) there appear computational problems and this cases should be treated differently. For simplicity, the choice of constant A can be changed. In the computer code constant A was increased by value 3 for all the points k that appeared to be closer then 3 to point A.

3. $k = 0$.

   It is easily seen for even function $f_e(x)$ that the corresponding function $H_e(k)$ in (A.1) is odd and consequently $H_e(0) = 0$. Otherwise, we

perform the integration on the first subinterval $[A_1, A_2]$ separately from the others. For this interval $A_1 = 0$ and:

$$f_o(x) \approx \alpha_1 x^3 + \alpha_2 x^2 + \alpha_3 x + \alpha_4, \quad x \in [0, A_2).$$

Function $f(x)$ is odd and, hence, $\alpha_4 = 0$. The integral over interval $[0, A_2]$ is calculated analytically:

$$\int_0^{A_2} \frac{x f_o(x)}{x^2}\, dx \approx \int_0^{A_2} \frac{\alpha_1 x^3 + \alpha_2 x^2 + \alpha_3 x}{x}\, dx = \frac{\alpha_1 A_2^3}{3} + \frac{\alpha_2 A_2^2}{2} + \alpha_3 A_2$$

The other integrations are performed by already derived relations.

4. $k = A_{j_0}$.

   If evaluation point of integral transform k coincides with one of the points where function f_j, $j = o, e$ is evaluated then there is again problem with logarithmic term. But now it appears in the coefficients in (A.6). Let us for a moment define nodes of intervals $[A_{j_0-1}, A_{j_0}]$ and $[A_{j_0}, A_{j_0+1}]$ as:

   $$a = A_{j_0-1},\ b = A_{j_0},\ c = A_{j_0+1}.$$

   Associated with these points splines are:

   $$f_j(x) \approx s_a(x) = \alpha_1 (x-a)^3 + \alpha_2 (x-a)^2 + \alpha_3 (x-a) + \alpha_4, \quad x \in [a, b],$$
   $$f_j(x) \approx s_b(x) = \beta_1 (x-b)^3 + \beta_2 (x-b)^2 + \beta_3 (x-b) + \beta_4, \quad x \in [b, c],$$
   $$j = o, e.$$

   Notice that $s_a(b) = s_b(b)$ which comes from the construction of spline construction. The integration over the interval $[a, c]$ is organised in by subtracting a singularity. More precisely, we subtract the value of function at singular point at the intervals $[a, b], [b, c]$ leaving integration

over the other subintervals the same. Thus, for odd function $f_o(x)$:

$$\int_a^b \frac{xs_a(x)}{x^2-b^2}\,dx + \int_b^c \frac{xs_b(x)}{x^2-b^2}\,dx$$

$$= \int_a^b \frac{x(s_a(x)-s_a(b))}{x^2-b^2}\,dx + \int_b^c \frac{x(s_b(x)-s_b(b))}{x^2-b^2}\,dx + s_b(b)\int_a^c \frac{x}{x^2-b^2}\,dx.$$

For function $f_e(x)$ we have:

$$\int_a^b \frac{ks_a(x)}{x^2-b^2}\,dx + \int_b^c \frac{ks_b(x)}{x^2-b^2}\,dx$$

$$= \int_a^b \frac{k(s_a(x)-s_a(b))}{x^2-b^2}\,dx + \int_b^c \frac{k(s_b(x)-s_b(b))}{x^2-b^2}\,dx + s_b(b)\int_a^c \frac{k}{x^2-b^2}\,dx.$$

For the next steps the notations are introduced. In the case of odd function $f_o(x)$:

$$I_1' = (c-b) + b\ln\left|\frac{2b}{c+b}\right|, \quad I_2' = \frac{1}{2}(c^2-b^2) - 2bI_1',$$

$$I_3' = \frac{1}{3}(c^3-b^3) - \frac{b}{2}(c^2-b^2) - 2bI_2',$$

$$J_1' = -\frac{1}{2}\ln|a^2-b^2|, \quad J_2' = (b-a) - b\ln\left|\frac{2b}{a+b}\right| + (b-a)J_1',$$

$$J_3' = \frac{(b-a)^2}{2} - b(b-a) + b(b+a)\ln\left|\frac{2b}{a+b}\right| + (b-a)J_2',$$

$$J_4' = \frac{(b-a)^3}{3} - \frac{1}{2}b(b-a)^2 + b(b^2-a^2) - b(b+a)^2\ln\left|\frac{2b}{a+b}\right| + (b-a)J_3',$$

$$F = \frac{1}{2}\ln\left|\frac{c^2-b^2}{a^2-b^2}\right|.$$

For the option of $f_e(x)$ the same coefficients are defined differently:

$$I_1' = \ln\left|\frac{c+b}{2b}\right|, \quad I_2' = (c-b) - 2bI_1',$$
$$I_3' = \frac{(c-b)^2}{2} - 2bI_2',$$
$$J_1' = -\frac{b}{2}\ln\left|\frac{a-b}{a+b}\right|, \quad J_2' = \ln\left|\frac{2b}{a+b}\right| + (b-a)J_1',$$
$$J_3' = (b-a) - (b+a)\ln\left|\frac{2b}{a+b}\right| + (b-a)J_2',$$
$$J_4' = \frac{(b-a)^2}{2} - (b^2-a^2) - (b+a)^2\ln\left|\frac{2b}{a+b}\right| + (b-a)J_3',$$
$$F = \frac{1}{2}\left(\ln\left|\frac{c-b}{c+b}\right| - \ln\left|\frac{a-b}{a+b}\right|\right).$$

The resulting integration for an odd function $f_o(x)$ is :

$$\int_a^c \frac{xf(x)}{x^2-b^2}\,dx \approx \int_a^b \frac{xs_a(x)}{x^2-b^2}\,dx + \int_b^c \frac{xs_b(x)}{x^2-b^2}\,dx$$
$$= \beta_1 I_3' + \beta_2 I_2' + \beta_3 I_1' + \alpha_1 J_4' + \alpha_2 J_3' + \alpha_3 J_2' + \alpha_4 J_1' + F.$$

The integral for even function $f_e(x)$:

$$\int_a^c \frac{kf(x)}{x^2-b^2}\,dx \approx \int_a^b \frac{bs_a(x)}{x^2-b^2}\,dx + \int_b^c \frac{bs_b(x)}{x^2-b^2}\,dx$$
$$= b(\beta_1 I_3' + \beta_2 I_2' + \beta_3 I_1' + \alpha_1 J_4' + \alpha_2 J_3' + \alpha_3 J_2' + \alpha_4 J_1' + F).$$

A.1.3 Benchmarks for Cauchy-type integral

Here we would like to present 2 particular examples to show the efficiency of proposed numerical algorithm. We consider following functions:

$$f_o(x) = \frac{x}{1+x^2}, \quad f_e(x) = \frac{1}{1+x^2}.$$

The analytical expressions for the functions in (A.1) are:

$$H_o^{(a)}(k) = \frac{\pi}{2}\frac{1}{1+k^2}, \quad H_e^{(a)}(k) = -\frac{\pi}{2}\frac{k}{1+k^2}.$$

The comparison is judged according to the relative error between analytical result and computed one. The error is defined as follows:

$$E_j(k) = \left| 1 - \frac{H_j(k)}{H_j^{(a)}(k)} \right|, \quad j = o, e,$$

where $H_j(k)$, $j = o, e$ express numerically evaluated integrals. Functions $f_j(x)$, $j = o, e$ are approximated by spline on the interval $[0, 60]$. The nodes of the interval are equally separated with the step $\Delta_h = 0.1$. The plots of relative error are displayed below for different cases of interval division. The values of k are chosen to be in interval $[0, 70]$ evenly distributed with a step Δ_h which kept to be untouched for different presented options. For the case $H_e(k)$ the first point $k = 0$ is omitted.

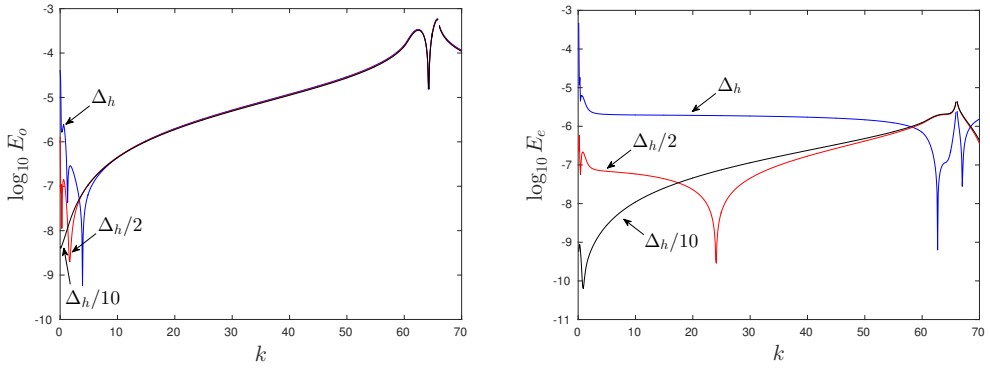

a) b)

Figure A.1: Relative error of integral evaluation: a) function $E_o(k)$, b) function $E_e(k)$.

These results show that the implemented algorithm is possible to provide reasonable results for the considered problems. These computations are used

for evaluation of functions $L_0^{\pm}(k)$ defined in (2.70) for which the required asymptotic behaviour is given in (2.76).

A.2 Numerical evaluation of Fourier transform

A.2.1 General relations

For the purposes of the research the following integral has to be evaluated:

$$F(y) = \int_0^{\infty} f(x) e^{ixy}\, dx. \tag{A.9}$$

The procedure is similar to the one proposed for the computation of Cauchy-type integral. Here, we would to include also the estimates of the function $f(x)$ at zero, as well as at infinity:

$$\begin{aligned} f(x) &= \frac{f_{\infty}^{(1)}}{x^{\alpha_1}} + \frac{f_{\infty}^{(2)}}{x^{\alpha_2}} + o\left(\frac{1}{x^{\alpha_2}}\right), \quad x \to \infty, \\ f(x) &= f_0^{(1)} x^{\beta_1} + f_0^{(2)} x^{\beta_2} + O\left(x^{\beta_2}\right), \quad x \to 0. \end{aligned} \tag{A.10}$$

Function $F(y)$ is then approximated as:

$$\begin{aligned} F(y) \approx \int_0^{\delta} \left(f_0^{(1)} x^{\beta_1} + f_0^{(2)} x^{\beta_2}\right) e^{ixy}\, dx + \int_{\delta}^{A} f(x) e^{ixy}\, dx \\ + \int_A^{\infty} \left(\frac{f_{\infty}^{(1)}}{x^{\alpha_1}} + \frac{f_{\infty}^{(2)}}{x^{\alpha_2}}\right) e^{ixy}\, dx. \end{aligned} \tag{A.11}$$

Constants δ, A are chosen in such a way that the relative error between the function and its asymptotic analogue is small enough. The analytical expression for the first integral gives:

$$\int_0^\delta \left(f_0^{(1)} x^{\beta_1} + f_0^{(2)} x^{\beta_2}\right) e^{ixy}\, dx = f_0^{(1)} I_\delta(\beta_1, y) + f_0^{(2)} I_\delta(\beta_2, y),$$

$$I_\delta(\beta, y) = \int_0^\delta x^\beta e^{ixy}\, dx \tag{A.12}$$

$$= \frac{i\delta^\beta}{y}\left[(-iy\delta)^{-\beta}\Gamma(\beta)\beta - (-iy\delta)^{-\beta}\Gamma(\beta, -iy\delta)\beta - e^{iy\delta}\right],$$

where $\Gamma(\beta), \Gamma(\beta, x)$ are gamma function and incomplete gamma function, respectively. The analytical integration of the last term in (A.11) reveals:

$$\int_A^\infty \left(\frac{f_\infty^{(1)}}{x^{\alpha_1}} + \frac{f_\infty^{(2)}}{x^{\alpha_2}}\right) e^{ixy}\, dx = f_\infty^{(1)} I_A(\alpha_1, y) + f_\infty^{(2)} I_A(\alpha_2, y),$$

$$I_A(\alpha, y) = \int_A^\infty \frac{e^{ixy}}{x^\alpha}\, dx$$

$$= \begin{cases} A^{1-\alpha}\left[\sqrt{\dfrac{\pi}{2|Ay|}}\left(1 - 2C\left(\sqrt{\dfrac{2|Ay|}{\pi}}\right)\right)\right. \\ \left. +i\sqrt{\dfrac{\pi}{2|Ay|^3}}(Ay)\left(1 - 2S\left(\sqrt{\dfrac{2|Ay|}{\pi}}\right)\right)\right], & \alpha = 0.5, \\ A^{1-\alpha}\left[\sqrt{2\pi|Ay|}\left(2S\left(\sqrt{\dfrac{2|Ay|}{\pi}}\right) - 1\right) + 2\cos(Ay)\right. \\ \left. +i\dfrac{Ay}{\sqrt{|Ay|}}\left(\sqrt{2\pi|Ay|}\left(1 - 2C\left(\sqrt{\dfrac{2|Ay|}{\pi}}\right)\right) + 2\sin|Ay|\right)\right], & \alpha = 1.5, \\ A^{1-\alpha}E_\alpha(-iAy), \quad \text{otherwise.} \end{cases} \tag{A.13}$$

where $E_\alpha(x)$ – exponential integral, $S(x), C(x)$ – Fresnel integrals. The reason for the writing it down in different cases is to save the computational time while function evaluations. The evaluation of already implemented special functions for rational α is time-consuming.

The intermediate interval of integration $[\delta, A]$ is divided into subinterval on which the function is represented by a spline:

$$[\delta, A] = \bigcup_{j=1}^{n-1} [A_j, A_{j+1}],$$

$$f(x) \approx s_j(x) = a_j(x - A_j)^3 + b_j(x - A_j)^2 + c_j(x - A_j) + d_j, \quad x \in [A_j, A_{j+1}]. \tag{A.14}$$

The integration of the interpolated function (A.14) in over an interval $[A_j, A_{j+1}]$ is performed analytically:

$$\begin{aligned}
\int_{A_j}^{A_{j+1}} s_j(x) e^{ixy} &= a_j I_3(A_j, A_{j+1}, A_j, y) + b_j I_2(A_j, A_{j+1}, A_j, y) \\
&\quad + c_j I_1(A_j, A_{j+1}, A_j, y) + d_j I_0(A_j, A_{j+1}, A_j, y), \\
I_n(a, b, c, y) = \int_a^b (x - c)^n e^{ixy} &= \frac{(b - c)^n e^{iby} - (a - c)^n e^{iay}}{iy} \\
&\quad - \frac{n}{iy} I_{n-1}(a, b, c, y), \\
I_0(a, b, c, y) &= \frac{e^{iby} - e^{iay}}{iy}.
\end{aligned} \tag{A.15}$$

Combination of (A.12), (A.13) and (A.15) reveals the final expression for $F(y)$ in (A.9):

$$\begin{aligned}
F(y) \approx\ & f_0^{(1)} I_\delta(\beta_1, y) + f_0^{(2)} I_\delta(\beta_2, y) + f_\infty^{(1)} I_A(\alpha_1, y) + f_\infty^{(2)} I_A(\alpha_2, y) \\
& + \sum_{j=1}^{n-1} \left[a_j I_3(A_j, A_{j+1}, A_j, y) + b_j I_2(A_j, A_{j+1}, A_j, y) \right. \\
& \left. + c_j I_1(A_j, A_{j+1}, A_j, y) + d_j I_0(A_j, A_{j+1}, A_j, y) \right].
\end{aligned} \tag{A.16}$$

The final expression in (A.16) was implemented and used for the computations for the solution of the problem displayed in (2.91). Notice that for that presentation all the singularities were subtracted. Thus, these terms should be considered when the asymptotic behaviour at infinity is estimated. In the computations value $\delta = 0$ was set as the singularity at zero was subtracted.

There is one exceptional case which comes from (A.14) of the integral estimation. Notice that for small values of y there can appear a computational difficulty. That is why the Taylor expansion of the integrals in (A.14) was used for $|(b-a)y| < 10^{-3}$.

A.2.2 Benchmark for Fourier transform

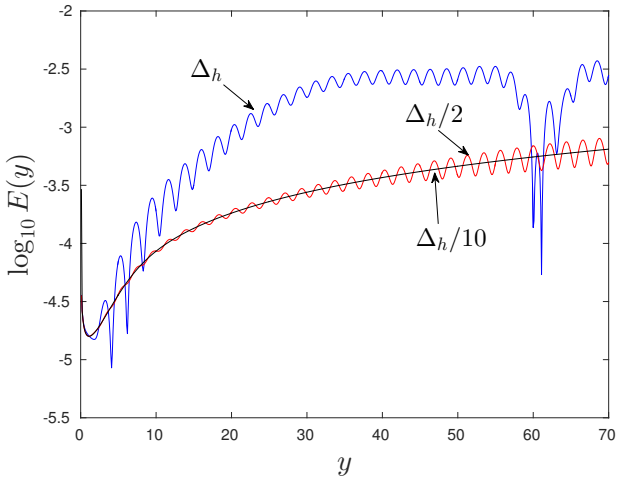

Figure A.2: Relative error of the Fourier transform evaluation.

For the verification of the implemented procedure function $f(x)$ was chosen to be:

$$f(x) = \frac{x}{x^2+1}.$$

The analytical expression of the integral transform is:

$$F^{(a)}(y) = \int_0^\infty f(x)e^{ixy}dx = -\frac{1}{2}\left[e^{-y}\overline{\mathrm{Ei}(y)} + e^{y}\mathrm{Ei}(-y)\right] + \frac{\pi i}{2}e^{-y}, \quad y > 0,$$

where $\mathrm{Ei}(y)$ is the exponential integral function. For the investigation of the numerical algorithm interval $[0, 60]$ was divided by a constant step $\Delta_h = 0.1$. The interval for y was chosen to be $[0.1, 70]$ with the step Δ_h. The other

options for interval divisions have been also considered while the interval of y remained the same. The relative error between the numerical and analytical results is presented as:

$$E(y) = \left| 1 - \frac{F(y)}{F^{(a)}(y)} \right| .$$

The plot of relative error is displayed in Fig. A.2.The presented numerical algorithm is used for the evaluation Fourier transform in (2.91) for functions $\hat{U}^{\pm}(k)$.

Bibliography

[1] F. F. Abraham, R. Walkup, H. Gao, M. Duchaineau, T. D. De La Rubia, and M. Seager. Simulating materials failure by using up to one billion atoms and the world's fastest computer: Brittle fracture. *Proceedings of the National Academy of Sciences*, 99(9):5777–5782, 2002.

[2] L. M. Alves and R. F. R. M. Lobo. The possibility to predict crack patterns on dynamic fracture. *International Journal of Fracture*, pages 1–23, 2017.

[3] M. Ayzenberg-Stepanenko, G. Mishuris, and L. Slepyan. Brittle fracture in a periodic structure with internal potential energy. spontaneous crack propagation. In *Proc. R. Soc. A*, volume 470, page 20140121. The Royal Society, 2014.

[4] B. Baker. Dynamic stresses created by a moving crack. *Journal of Applied Mechanics*, 29(3):449–458, 1962.

[5] C. Behn and M. Marder. The transition from subsonic to supersonic cracks. *Philosophical Transactions of the Royal Society of London A: Mathematical, Physical and Engineering Sciences*, 373(2038):20140122, 2015.

[6] N. Bernstein, J. R. Kermode, and G. Csanyi. Hybrid atomistic simulation methods for materials systems. *Reports on Progress in Physics*, 72(2):026501, 2009.

[7] D. Bonamy and K. Ravi-Chandar. Dynamic crack response to a localized shear pulse perturbation in brittle amorphous materials: on crack surface roughening. *International Journal of Fracture*, 134(1):1–22, 2005.

[8] M. Boustie and F. Cottet. Experimental and numerical study of laser induced spallation into aluminum and copper targets. *Journal of applied physics*, 69(11):7533–7538, 1991.

[9] K. B. Broberg. The propagation of a brittle crack. *Arkiv for Fysik*, 18(10):159–192, 1960.

[10] K. B. Broberg. *Cracks and fracture*. Academic Press, 1999.

[11] D. Broek. *Elementary engineering fracture mechanics*. Springer Science & Business Media, 2012.

[12] M. Brun, A. B. Movchan, and L. I. Slepyan. Transition wave in a supported heavy beam. *Journal of the Mechanics and Physics of Solids*, 61(10):2067–2085, 2013.

[13] M. J. Buehler, F. F. Abraham, and H. Gao. Hyperelasticity governs dynamic fracture at a critical length scale. *Nature*, 426(6963):141–146, 2003.

[14] M. J. Buehler and H. Gao. Modeling dynamic fracture using large-scale atomistic simulations. *Dynamic Fracture Mechanics*, page 1, 2006.

[15] G. Carta, M. Brun, and A. Movchan. Dynamic response and localization in strongly damaged waveguides. In *Proc. R. Soc. A*, volume 470, page 20140136. The Royal Society, 2014.

[16] G. P. Cherepanov. Crack propagation in continuous media: Pmm vol. 31, no. 3, 1967, pp. 476–488. *Journal of Applied Mathematics and Mechanics*, 31(3):503–512, 1967.

[17] A. Cherkaev, A. Kouznetsov, and A. Panchenko. Still states of bistable lattices, compatibility, and phase transition. *Continuum Mechanics and Thermodynamics*, 22(6-8):421–444, 2010.

[18] D. Coker, A. Rosakis, and A. Needleman. Dynamic crack growth along a polymer composite–homalite interface. *Journal of the Mechanics and Physics of Solids*, 51(3):425–460, 2003.

[19] D. Colquitt, M. Nieves, I. Jones, N. Movchan, and A. Movchan. Trapping of a crack advancing through an elastic lattice. *International Journal of Engineering Science*, 61:129–141, 2012.

[20] B. Cotterell and J. Rice. Slightly curved or kinked cracks. *International Journal of Fracture*, 16(2):155–169, 1980.

[21] T. Cramer, A. Wanner, and P. Gumbsch. Energy dissipation and path instabilities in dynamic fracture of silicon single crystals. *Physical Review Letters*, 85(4):788, 2000.

[22] M. Di Paola, A. Pirrotta, and M. Zingales. Mechanically-based approach to non-local elasticity: variational principles. *International journal of solids and structures*, 47(5):539–548, 2010.

[23] J. Fineberg, S. P. Gross, M. Marder, and H. L. Swinney. Instability in dynamic fracture. *Physical Review Letters*, 67(4):457, 1991.

[24] J. Fineberg and M. Marder. Instability in dynamic fracture. *Physics Reports*, 313(1):1–108, 1999.

[25] L. Freund. Crack propagation in an elastic solid subjected to general loading—i. constant rate of extension. *Journal of the Mechanics and Physics of Solids*, 20(3):129–140, 1972.

[26] L. Freund. Crack propagation in an elastic solid subjected to general loading—ii. non-uniform rate of extension. *Journal of the Mechanics and Physics of Solids*, 20(3):141–152, 1972.

[27] L. B. Freund. *Dynamic fracture mechanics*. Cambridge university press, 1998.

[28] F. D. Gakhov. *Boundary Value Problems: International Series of Monographs in Pure and Applied Mathematics*, volume 85. Elsevier, 2014.

[29] H. Gao, Y. Huang, and F. F. Abraham. Continuum and atomistic studies of intersonic crack propagation. *Journal of the Mechanics and Physics of Solids*, 49(9):2113–2132, 2001.

[30] N. J. Glassmaker, A. Jagota, C.-Y. Hui, W. L. Noderer, and M. K. Chaudhury. Biologically inspired crack trapping for enhanced adhesion. *Proceedings of the National Academy of Sciences*, 104(26):10786–10791, 2007.

[31] N. Gorbushin and G. Mishuris. Analysis of dynamic failure of the discrete chain structure with non-local interactions. *Mathematical Methods in the Applied Sciences*, 2016.

[32] N. Gorbushin and G. Mishuris. Dynamic crack propagation along the interface with non-local interactions. *Journal of the European Ceramic Society*, 36(9):2241–2244, 2016.

[33] D. E. Grady. Length scales and size distributions in dynamic fragmentation. *International Journal of Fracture*, 163(1):85–99, 2010.

[34] A. A. Griffith. The phenomena of rupture and flow in solids. *Philosophical transactions of the royal society of london. Series A, containing papers of a mathematical or physical character*, 221:163–198, 1921.

[35] A. Gruzdkov and Y. V. Petrov. Cavitation breakup of low-and high-viscosity liquids. *Technical Physics*, 53(3):291–295, 2008.

[36] J. A. Hauch, D. Holland, M. Marder, and H. L. Swinney. Dynamic fracture in single crystal silicon. *Physical Review Letters*, 82(19):3823, 1999.

[37] P. Hinterdorfer and Y. F. Dufrêne. Detection and localization of single molecular recognition events using atomic force microscopy. *Nature methods*, 3(5):347–355, 2006.

[38] D. Holland and M. Marder. Ideal brittle fracture of silicon studied with molecular dynamics. *Physical Review Letters*, 80(4):746, 1998.

[39] C. Hsieh and R. Thomson. Lattice theory of fracture and crack creep. *Journal of Applied Physics*, 44(5):2051–2063, 1973.

[40] D. Hull. Influence of stress intensity and crack speed on fracture surface topography: mirror to mist to macroscopic bifurcation. *Journal of materials science*, 31(17):4483–4492, 1996.

[41] G. R. Irwin. Analysis of stresses and strains near the end of a crack traversing a plate. *Applied Mechanics*, 24:361–364, 1957.

[42] A. Ivankovic, N. Murphy, and S. Hillmansen. *Evolution of dynamic fractures in PMMA: experimental and numerical investigations*. WIT Press/Computational Mechanics, 2004.

[43] D. A. Kessler and H. Levine. Steady-state cracks in viscoelastic lattice models. *Physical Review E*, 59(5):5154, 1999.

[44] H. Kikuchi, R. K. Kalia, A. Nakano, P. Vashishta, P. S. Branicio, and F. Shimojo. Brittle dynamic fracture of crystalline cubic silicon carbide (3c-sic) via molecular dynamics simulation. *Journal of applied physics*, 98(10):103524, 2005.

[45] A. V. Kisil. The relationship between a strip Wiener–Hopf problem and a line Riemann–Hilbert problem. *IMA Journal of Applied Mathematics*, page hxv007, 2015.

[46] B. Kostrov. Unsteady propagation of longitudinal shear cracks. *Journal of applied Mathematics and Mechanics*, 30(6):1241–1248, 1966.

[47] S. Kulakhmetova, V. Saraikin, and L. Slepyan. Plane problem of a crack in a lattice. *Mechanics of Solids*, 19:101–108, 1984.

[48] F. Lipperman, M. Ryvkin, and M. B. Fuchs. Nucleation of cracks in two-dimensional periodic cellular materials. *Computational Mechanics*, 39(2):127–139, 2007.

[49] X. Liu and M. Marder. The energy of a steady-state crack in a strip. *Journal of the Mechanics and Physics of Solids*, 39(7):947–961, 1991.

[50] M. Marder, C.-H. Chen, and T. Patzek. Simple models of the hydrofracture process. *Physical Review E*, 92(6):062408, 2015.

[51] M. Marder and S. Gross. Origin of crack tip instabilities. *Journal of the Mechanics and Physics of Solids*, 43(1):1–48, 1995.

[52] R. Merkel, P. Nassoy, A. Leung, K. Ritchie, and E. Evans. Energy landscapes of receptor–ligand bonds explored with dynamic force spectroscopy. *Nature*, 397(6714):50–53, 1999.

[53] G. Mishuris, A. Movchan, and D. Bigoni. Dynamics of a fault steadily propagating within a structural interface. *Multiscale Modeling & Simulation*, 10(3):936–953, 2012.

[54] G. Mishuris, A. Movchan, and L. Slepyan. Dynamical extraction of a single chain from a discrete lattice. *Journal of the Mechanics and Physics of Solids*, 56(12):487–495, 2007.

[55] G. Mishuris, A. Movchan, and L. Slepyan. Waves and fracture in an inhomogeneous lattice structure. *Waves in Random and Complex Media*, 17:409–428, 2007.

[56] G. Mishuris, A. Movchan, and L. Slepyan. Dynamics of a bridged crack in a discrete lattice. *Quarterly Journal of Mechanics and Applied Mathematics*, 61(2):151–160, 2008.

[57] G. Mishuris, A. Movchan, and L. Slepyan. Localised knife waves in a structured interface. *Journal of the Mechanics and Physics of Solids*, 57(12):1958–1979, 2009.

[58] G. Mishuris and L. Slepyan. Brittle fracture in a periodic structure with internal potential energy. *Proceedings of the Royal Society A: Mathematical, Physical and Engineering Sciences*, 470(2165):20130821, 2014.

[59] M. Nieves, G. Mishuris, and L. Slepyan. Analysis of dynamic damage propagation in discrete beam structures. *International Journal of Solids and Structures*, 97–98:699–713, 2016.

[60] M. Nieves, A. Movchan, I. Jones, and G. Mishuris. Propagation of Slepyan's crack in a non-uniform elastic lattice. *Journal of the Mechanics and Physics of Solids*, 61(6):1464–1488, 2013.

[61] B. Noble. Methods based on the wiener-hopf technique for the solution of pdes. 1958.

[62] V. Oppenheim Alan, S. Willsky Alan, and S. H. Nawab. Signals and systems, 1997.

[63] A. Parisi and R. C. Ball. Role of surface waves on the relation between crack speed and the work of fracture. *Physical Review B*, 66(16):165432, 2002.

[64] L. Pechenik, H. Levine, and D. A. Kessler. Steady-state mode I cracks in a viscoelastic triangular lattice. *Journal of the Mechanics and Physics of Solids*, 50(3):583–613, 2002.

[65] Y. V. Petrov. Incubation time criterion and the pulsed strength of continua: fracture, cavitation, and electrical breakdown. In *Doklady Physics*, volume 49, pages 246–249. Springer, 2004.

[66] Y. V. Petrov and A. Utkin. Dependence of the dynamic strength on loading rate. *Materials Science*, 25(2):153–156, 1989.

[67] A. Piccolroaz, G. Mishuris, and A. Movchan. Symmetric and skew-symmetric weight functions in 2d perturbation models for semi-infinite interfacial cracks. *Journal of the Mechanics and Physics of Solids*, 57(9):1657–1682, 2009.

[68] D. Polyzos and D. I. Fotiadis. Derivation of mindlin's first and second strain gradient elastic theory via simple lattice and continuum models. *International Journal of Solids and Structures*, 49(3):470–480, 2012.

[69] K. Ravi-Chandar. *Dynamic fracture*. Elsevier, 2004.

[70] K. Ravi-Chandar and W. Knauss. An experimental investigation into dynamic fracture: Iii. on steady-state crack propagation and crack branching. *International Journal of Fracture*, 26(2):141–154, 1984.

[71] J. R. Rice, Y. Ben-Zion, and K.-S. Klm. Three-dimensional perturbation solution for a dynamic planar crack moving unsteadily in a model elastic solid. *Journal of the Mechanics and Physics of Solids*, 42(5):813–843, 1994.

[72] J. R. Rice et al. A path independent integral and the approximate analysis of strain concentration by notches and cracks. ASME, 1968.

[73] A. Rosakis, O. Samudrala, and D. Coker. Cracks faster than the shear wave speed. *Science*, 284(5418):1337–1340, 1999.

[74] A. J. Rosakis. Intersonic shear cracks and fault ruptures. *Advances in Physics*, 51(4):1189–1257, 2002.

[75] P. Rosenau. Dynamics of dense lattices. *Physical Review B*, 36(11):5868, 1987.

[76] C. L. Rountree, R. K. Kalia, E. Lidorikis, A. Nakano, L. Van Brutzel, and P. Vashishta. Atomistic aspects of crack propagation in brittle materials: Multimillion atom molecular dynamics simulations. *Annual Review of Materials Research*, 32(1):377–400, 2002.

[77] M. Ryvkin and L. Slepyan. Crack in a 2d beam lattice: analytical solutions for two bending modes. *Journal of the Mechanics and Physics of Solids*, 58(6):902–917, 2010.

[78] B. L. Sharma. On energy balance and the structure of radiated waves in kinetics of crystalline defects. *Journal of the Mechanics and Physics of Solids*, 96:88–120, 2016.

[79] E. Sharon, G. Cohen, and J. Fineberg. Propagating solitary waves along a rapidly moving crack front. *Nature*, 410(6824):68–71, 2001.

[80] E. Sharon and J. Fineberg. Confirming the continuum theory of dynamic brittle fracture for fast cracks. *Nature*, 397(6717):333–335, 1999.

[81] E. Sharon, S. P. Gross, and J. Fineberg. Energy dissipation in dynamic fracture. *Physical review letters*, 76(12):2117, 1996.

[82] L. Slepyan, M. Ayzenberg-Stepanenko, and G. Mishuris. Forerunning mode transition in a continuous waveguide. *Journal of the Mechanics and Physics of Solids*, 78:32–45, 2015.

[83] L. Slepyan, A. Cherkaev, and E. Cherkaev. Transition waves in bistable structures. II. analytical solution: wave speed and energy dissipation. *Journal of the Mechanics and Physics of Solids*, 53(2):407–436, 2005.

[84] L. Slepyan, G. Mishuris, and A. Movchan. Crack in a lattice waveguide. *International Journal of Fracture*, 162(1-2):91–106, 2010.

[85] L. I. Slepyan. *Models and phenomena in fracture mechanics*. Springer Science & Business Media, 2012.

[86] L. I. Slepyan and L. V. Troyankina. Fracture wave in a chain structure. *Journal of Applied Mechanics and Technical Physics*, 25(6):921–927, 1984.

[87] J. Spence, Y. Huang, and O. Sankey. Lattice trapping and surface reconstruction for silicon cleavage on (111). ab-initio quantum molecular dynamics calculations. *Acta metallurgica et materialia*, 41(10):2815–2824, 1993.

[88] A. S. J. Suiker, A. V. Metrikine, and R. De Borst. Comparison of wave propagation characteristics of the cosserat continuum model and corresponding discrete lattice models. *International Journal of Solids and Structures*, 38(9):1563–1583, 2001.

[89] R. Thomson. Physics of fracture. *Solid state physics*, 39:1–129, 1986.

[90] R. Thomson, C. Hsieh, and V. Rana. Lattice trapping of fracture cracks. *Journal of Applied Physics*, 42(8):3154–3160, 1971.

[91] E. Trofimov and A. Vainchtein. Shocks versus kinks in a discrete model of displacive phase transitions. *Continuum Mechanics and Thermodynamics*, 22(5):317–344, 2010.

[92] L. Truskinovsky and A. Vainchtein. Kinetics of martensitic phase transitions: lattice model. *SIAM Journal on Applied Mathematics*, 66(2):533–553, 2005.

[93] L. Truskinovsky and A. Vainchtein. Quasicontinuum models of dynamic phase transitions. *Continuum Mechanics and Thermodynamics*, 18(1-2):1–21, 2006.

[94] J.-L. Tsai, S.-H. Tzeng, and Y.-J. Tzou. Characterizing the fracture parameters of a graphene sheet using atomistic simulation and continuum mechanics. *International Journal of Solids and Structures*, 47(3):503–509, 2010.

[95] F. R. Tuler and B. M. Butcher. A criterion for the time dependence of dynamic fracture. *International Journal of Fracture Mechanics*, 4(4):431–437, 1968.

[96] S. Vajpayee, R. Long, L. Shen, A. Jagota, and C.-Y. Hui. Effect of rate on adhesion and static friction of a film-terminated fibrillar interface. *Langmuir*, 25(5):2765–2771, 2009.

[97] G. Volkov, Y. V. Petrov, and A. Utkin. On some principal features of data processing of spall fracture tests. *Physics of the Solid State*, 59(2):310–315, 2017.

[98] S. Wei, F. Qun-bo, W. Fu-chi, and M. Zhuang. Modeling of microcrack growth during thermal shock based on microstructural images of thermal barrier coatings. *Computational Materials Science*, 46(3):600–602, 2009.

[99] J. Willis and A. Movchan. Dynamic weight functions for a moving crack. i. mode i loading. *Journal of the Mechanics and Physics of Solids*, 43(3):319–341, 1995.

[100] J. Xiao, J. Staniszewski, and J. Gillespie. Fracture and progressive failure of defective graphene sheets and carbon nanotubes. *Composite structures*, 88(4):602–609, 2009.

[101] X.-P. Xu and A. Needleman. Numerical simulations of fast crack growth in brittle solids. *Journal of the Mechanics and Physics of Solids*, 42(9):1397–1434, 1994.

[102] E. H. Yoffe. The moving griffith crack. *The London, Edinburgh, and Dublin Philosophical Magazine and Journal of Science*, 42(330):739–750, 1951.